EWG-IE 27TH Annual Meeting

European Working Group on Internal Erosion in Embankment Dams, Levees and Dikes, and their Foundations

Vancouver, Canada

18-21 June 2019

THE UNIVERSITY OF BRITISH COLUMBIA

DEPARTMENT OF CIVIL ENGINEERING

BC Hydro
Power smart

NSERC
CRSNG

Book of Abstracts

27th EWG-IE

June 18-21, 2019

Vancouver, Canada

This book of abstracts contains papers presented at the 27th Annual Meeting of the European Working Group on Internal Erosion (EWG-IE), from 18 to 21 June 2019, Vancouver, British Columbia, Canada. The workshop meeting was hosted by the University of British Columbia (UBC) and co-chaired by Dr. Jonathan Fannin (UBC) and Dr. Desmond Hartford (BC Hydro). The technical programme was organized in consultation with Dr. Stephane Bonelli (EWG-IE Chair).

Jonathan Fannin, Ph.D., P.Eng

University of British Columbia, Vancouver, Canada

Co-Chair, 27th EWG-IE

Scientific Committee

Stephane Bonelli, France, EWG-IE Chair

Elizabeth Bowman, England

Jonathan Fannin, Canada, Co-Chair, 27th EWG-IE Meeting

Desmond Hartford, Canada, Co-Chair, 27th EWG-IE Meeting

Didier Marot, France

Catherine O'Sullivan, England

Jaromir Riha, Czech Republic

Bryant Robbins, USA

Donatella Sterpi, Italy

Akihiro Takahashi, Japan

Vera van Beek, Netherlands

Local Organization Team

Suzana Espindola, Publications

Daniela Hajdukovic, Communications

Sheeraz Marfatia, Business Operations

Helen Yau, Registration

Claire Wei, Catering

Table of Contents

EWG-1 Applying New and Old Knowledge to Explain Internal Erosion Events

R. Bridle

UK Member, ICOLD Technical Committee on Embankment Dams
Editor and part-author, ICOLD Bulletin 164 on Internal Erosion
Dam Safety Ltd
rodney.bridle@damsafety.co.uk
www.damsafety.co.uk

Upward global backward erosion

Upward global backward erosion, like horizontal backward erosion, initiates when flowlines and equipotentials congregate at a free outlet creating hydraulic forces ('gradients') sufficient to detach particles and initiate the formation of a backward erosion pipe going upwards through susceptible soils (see van Beek et al, 2014). The erosion pipe may break through to the surface forming a sinkhole. The upward backward erosion process is aided by gravity, and seems very tenacious. The erosion pipe may travel rapidly to the surface, but the rate varies in different soils and depends on sufficient supplies of water from the aquifer around the erosion pipe to sustain the process. Having a 'free' outlet at its base is vital, if the free discharge of water and eroded particles is restricted the process cannot continue. The case histories below show the relevance of upward backward erosion to dam safety engineering.

Very slow upward backward erosion in clay soils at Lluest Wen dam

At Lluest Wen, a 24 m high dam completed in 1896, upward backward erosion occurred through the puddle clay core (ICOLD, 2016). Subsidence was observed in 1912 and remediated by grouting. In 1969 a sinkhole broke through on to the dam crest. The clay particles eroded by upward backward erosion had discharged slowly through a crack 5-10 mm wide, ultimately increasing to 50 mm wide, through the wall of the brick culvert which passed through the base of the core. Clay debris had been found, but its significance was not appreciated. Bridle (2018) showed that the critical gradient to cause upward backward erosion was about 20, matching the gradient applied downwards in the 24 m high dam.

Medium paced horizontal and upward backward erosion in glacial and fine soils at Shikwamkwa dam

ICOLD (2016) also reports on Shikwamkwa dam, a 35 m high zoned earthfill embankment completed in 1958 with a fine soil core on glacial soil foundations. Soon after construction, backward erosion sand boils appeared downstream. On investigation sinkholes were found in the upstream fine soil blanket, installed to decrease the hydraulic gradient through the foundations below the dam, and in one case in the upstream shoulder of the dam. Numerous attempts at control, prediction and remediation were unsuccessful, leading to the replacement of the dam in 2003. The new dam, 300 m downstream, is a zoned earthfill embankment with a plastic concrete cut-off to a maximum depth of 65 m to bedrock through the foundation.

Very rapid upward backward erosion through the foundation sediments in the reservoir floor at Lar dam

ICOLD (2016) reports on sinkholes in the reservoir basin of Lar dam in Iran. Three existed before the dam was constructed and three new conical sinkholes formed rapidly when water level rose as impounding started. The foundation sediments are several thousand metres deep, through some fine but much coarse-grained soil, above karstic limestone through which large caverns provide 'free' outlets for water draining down from the sediments above. The conical sinkholes suggested that they had formed above a single upward backward erosion pipe initiated at outlets in the karst caverns below the very deep coarse-grained sediments. The anomaly is that these coarse grained soils seem susceptible to suffusion, but the speed at which the sinkholes formed when gradients rose during impounding suggests upward backward erosion occurred, possibly through the fine fraction between the coarser particles.

Applying the Sellmeijer 2D chart to upward backward erosion

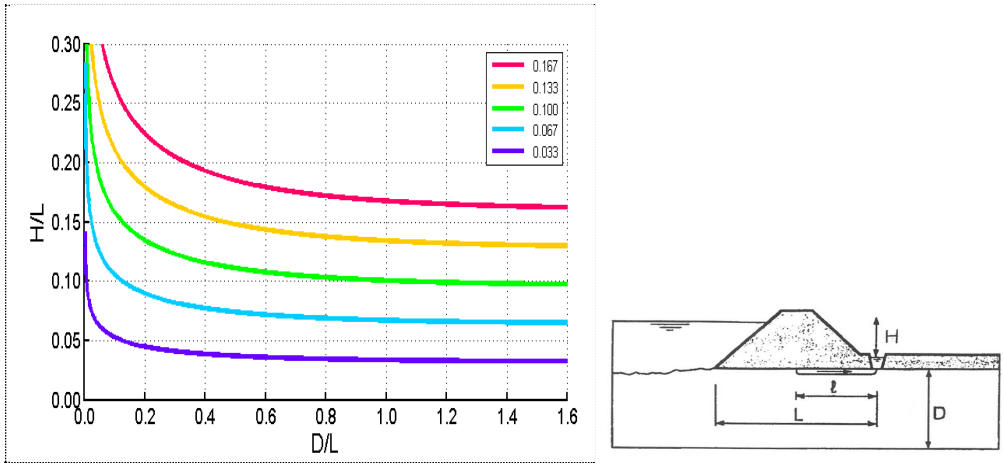

Figure 1. Showing critical gradients that would lead to failure by 2D horizontal backward erosion failure to 'free outlet' at downstream toe for increasingly resistant foundation sands. Inset defines H, L and D. (Figure 20 [4.4 in preprints] ICOLD Bulletin 164, Volume 1, ICOLD 2017, courtesy of Drs Hans Sellmeijer and Vera van Beek).

ICOLD (2017) provides Figure 1, the Sellmeijer 2D chart (and formulae) (Sellmeijer et al, 2011) as a means of checking whether water-retaining embankments on sandy foundations will fail by backward erosion and piping. From Figure 1 it can be seen that for H/L greater than about 0.20 on deep sand foundation aquifers (D/L>0.4), 2D backward erosion (to a free outlet at the toe) will cause failure even in the most resistant of foundation sands. In (vertical) upward backward erosion, the orientation of the dimensions is turned through 90°. The water depth (H) is slightly greater that the length (depth of foundation), H/L ≈ 1; the aquifer is a vertical cylinder, of substantial diameter, making D/L large (>1.0, say). Consequently, backward erosion pipes can be expected to form, provided that there is a free outlet to good drainage at its downstream end (bottom in vertical backward erosion). At Lar, the karst caverns provide the free outlet. At Shikwamkwa, the horizontal backward erosion pipes apparently provided a sufficient outlet to allow upward backward erosion to proceed. At Lluest Wen, the small quantities of seepage from the low permeability clay core discharged into the crack at gradients high enough to detach clay particles, initiating the slow upward backward erosion process.

Horizontal and upward backward erosion in possibly suffusive soils

The Lar sediments and the Shikwamkwa foundation soils may have been gap-graded and potentially suffusive, and it seems that the backward erosion pipes in those cases may have developed through the potentially suffusive fines in the pores between the coarse-grained matrix. Douglas et al (2016) carried out downward flow permeameter experiments to investigate global upward backward erosion and suffusion. Suffusive soils lost fines from the top of the samples, fines were lost from the bottom of samples where upward global backward erosion occurred. This may be explained by considering the erosion processes. Suffusion initiates when the hydraulic forces imposed by downward flow drive suffusive fine particles downwards. As fines are cleared from the upper part of the sample the hydraulic gradient increases across the remaining gap-graded lower part of the sample, the upper eroding fines move faster, joining those below, filling pore spaces, reducing pore velocity and restricting the progress of the suffusion, in some cases potentially halting it. Backward erosion commences where equipotentials congregate at outlets and impose sufficient forces to initiate erosion which continues at the tip of the erosion pipe as it progresses upwards. The effects of outlets of various configurations and sizes at the base of the permeameter were tested. High hydraulic gradients were needed to cause upward backward erosion where there were many small diameter outlets, possibly because the aquifers providing water to each of the outlets were too small to initiate erosion. Few larger outlets resulted in sinkhole formation at lower gradients, possibly because the larger aquifers around the few outlets and the few erosion pipes as they progressed upwards generated higher erosive forces.

A 'short-cut' to use the 2D Sellmeijer method to estimate critical gradients for 3D backward erosion

2D backward erosion occurs when there is a free outlet – a ditch or no confining layer - all along the downstream toe of the embankment. 3D backward erosion occurs through holes in 'confining' layers – fine low permeability soils –

at the toe and downstream of the embankment. Sand boils often form during 3D backward erosion. Van Beek et al (2015) showed that 3D backward erosion occurs at *very approximately half* (≈ 0.5) the Sellmeijer 2D gradient, thus providing an approximate means of assessing whether 3D backward erosion could lead to failure. At AV Watkins dam, where a serious local backward erosion incident occurred, the approximation showed that 3D backward erosion may have occurred in the 1.6 m deep fine sand layer immediately under the embankment not, as had been thought previously, in the deeper layers below the hardpan layer under the upper fine sand. More is said about this in Bridle (2019).

References

Bridle, R. 2019. ICOLD Bulletin 164 on internal erosion - how to estimate the loads causing internal erosion failures in earth dams and levees. *Paper submitted to ICOLD Symposium Ottawa June 12*

Bridle, R. 2018. An update on ICOLD Bulletin 164 on internal erosion. *Proc ICSE 9, Ninth International Conference on Scour and Erosion, Scour and Erosion IX - Keh-Chia (Ed.), Taylor & Francis Group, London*, ISBN 978-0-367-07467-8, 81-90

Douglas, K.J., Fell, R., Peirson, W.L. & Studholme, H. 2016. *Experimental investigation of global backward erosion and suffusion. UNICIV Report No R-465* ISBN 0-7334-3719-2 ISSN 0077-880X

ICOLD 2017. *Bulletin 164 Internal erosion of existing dams, levees and dikes, and their foundations. Volume 1: Internal erosion processes and engineering assessment*. Paris: International Commission on Large Dams. (Publication of final preprint in English and French issued on 19 February 2015, first preprint issued in English, 22 January 2013)

ICOLD 2016. *Bulletin 164 Internal erosion of existing dams, levees and dikes, and their foundations. Volume 2: Case histories, investigations, testing, remediation and surveillance*. Paris: International Commission on Large Dams. Final preprint in English only, issued 6 May 2016 from: http://www.icold-cigb.org.

Sellmeijer, J.B., Lopez De La Cruz, J., van Beek, V.M. & Knoeff, J.G. 2011. Fine tuning of the backward erosion piping model through small scale, medium scale and IJKdijk experiments. *European Journal of Environmental and Civil Engineering, Volume 15, Issue* 8, 1139-1154.

Van Beek, V.M., van Essen, H.M., Vandenboer, K. & Bezuijen, A. 2015. Developments in modelling of backward erosion piping. *Geotechnique* 65*,* No.9, 740-754

Van Beek, V.M., Bezuijen, A., Sellmeijer, J.B. & Barends, F.B.J. 2014. Initiation of backward erosion piping in uniform sands. *Geotechnique* 64*,* No.12, 927-941.

EWG-1 Applying New and Old Knowledge to Explain Internal Erosion Events

Your Notes:

EWG-2 The Failure of the Hubalov Weir Due to Piping

J. Riha

Faculty of Civil Engineering, Brno University of Technology, Veveri 95, 602 00 Brno, Czech Republic
E-mail: riha.j@fce.vutbr.cz

Key Words: weir collapse, small hydropower plant, seepage, piping

Introduction

The Hubalov weir is located in the north of the Czech Republic at the Jizera River that is the right bank tributary of the Elbe River. The purpose of the weir is river slope stabilization and generation of hydropower. The hydraulic structure consists of 93.6 m long and 10.3 m weir body. The height of the weir is 1.56 m. At the right bank, the weir is equipped with the gated sluice. This serves for flushing down the gravel deposited in front of the inlet to the small hydropower plant (HPP) located at the right bank of the Jizera river (Fig. 1). Due to the minor significance and low potential consequences in case of weir collapse it has been classified as a hydraulic structure of the category IV, ie. the lowest consequence class with only limited extent of surveillance and measurements.

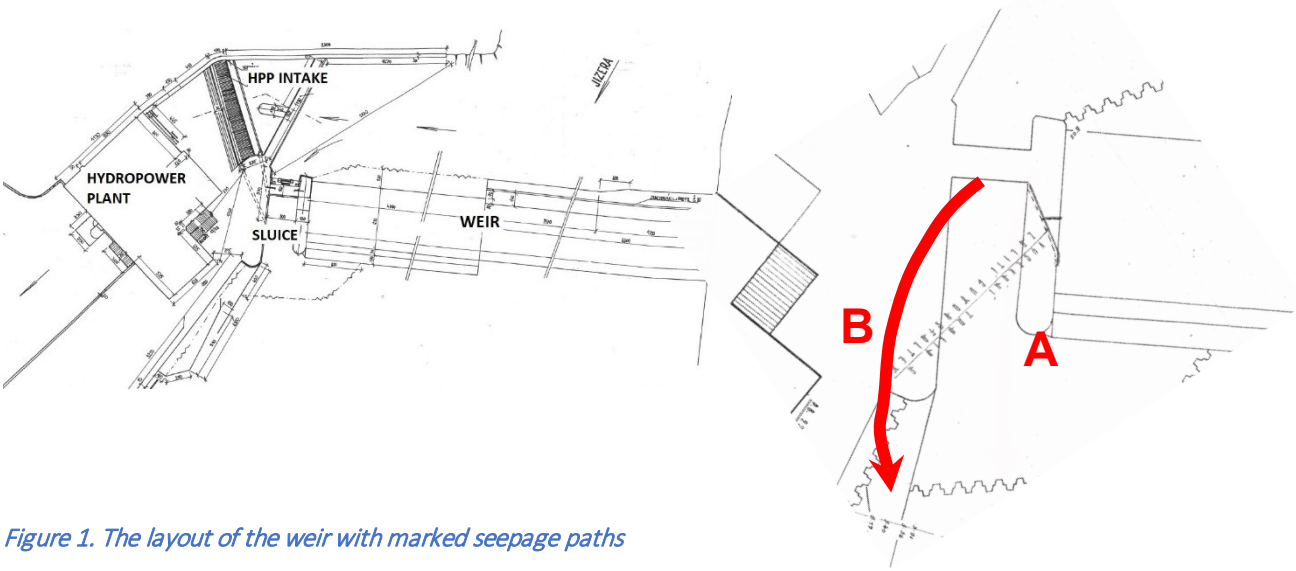

Figure 1. The layout of the weir with marked seepage paths

The collapse of the weir

On 11 June 2018, the Hubalov weir collapsed close to the right abutment at the vicinity of the small hydropower plant. The documentation indicates that the damage started downstream behind the right-bank massive pier between the sluice and the hydropower plant. The collapse continued by gradual subsidence of the right pier by approximately 1.8 m. Intensive vortex developed fast in front of the sluice gates, which indicated intensive flow below the sluice. At the same time, gates and the footbridge over the sluice inclined and collapsed. This propagated to the left sluice pier, which inclined towards the sluice and separated from the weir body. To the stability of the left pier contributed the sheet pile supporting its lower part. It sunk about 0.7 m following the left pier (Fig. 2).

The causes of the weir collapse

The collapse was caused by internal erosion of permeable sandy gravels. Two potential seepage paths (A, B in Fig. 1 right) were identified, one below the sluice gate and the second one between the sluice and the HPP. The local defect started probably behind the right sluice pier where flushed out material caused subsidence of the platform in front of the hydropower plant. At the continuation phase, subsidence of the right pier caused a collapse of the bottom slab of the sluice and total collapse of the structure. Contributing factors were deficiencies upstream of the sluice like open contraction joints and cracks in the intake bed and a fact that upstream sheet pile wall was not extended to the sluice

and HPP plant intake. Other factors were the absence of the stilling basin below the sluice, the fact that wooden piles, vibrations coming from the turbines and high head during the dry period, supported foundation slabs. Poor knowledge about true geological conditions at the site was also crucial.

Figure 2. The upstream view on the collapsed sluice walls

The development of the local seepage paths below the concrete structures supported by wooden piles was hardly to be identified. The seepage was also possible via not-sealed contraction joints between right sluice pier and the HPP and damaged bottom pavement in front of the sluice and HPP intake. Taking into account the first subsidence of the HPP platform, the more probable is the development of the seepage path B. Further, on the right sluice pier started to subside and incline and ripped off the bottom slab of the sluice. Thus, extremely short seepage path developed below the sluice gates, which resulted in bursting out the slab and the scour cca 1.7 m deep. This phase took about 15 – 20´.

The collapse was caused by the combination of following unfavourable factors:

- Structural deficiencies at the upstream intake channel to the HPP, which enabled seepage into the subbase via not sealed contraction joints, cracks and defects in the intake bed.
- Upstream sheet pile wall was not extended to the sluice and HPP intake.
- The absence of the stilling basin, scouring the riverbed downstream of the weir and the stilling basin. The stabilizing riprap did not improve this situation and did not extend the seepage path.
- Former demolition and construction works might contribute to the seepage behind the right sluice wall.
- The effective stress in the sand gravel soil below the foundation slabs supported by wooden piles was practically zero; the material lost its resistance against internal erosion. Certain role may be attributed to vibrations coming from the turbines.
- The dry period resulted in historically highest head, i.e. difference between upstream and downstream water levels at the weir.

Acknowledgement

This paper has been prepared under project TH04030087 Tools for optimization of the management of levee systems and FAST-S-19-5714 Probabilistic assessment of the soil instability due to seepage in earth structures and their foundations

EWG-2 The Failure of the Hubalov Weir Due to Piping

Your Notes:

EWG-3 Assessment of Internal Erosion of Zoned Embankment Dams with Widely Graded Materials

L. Yan; M. Li; C. Anderlini
BC Hydro

Abstract

After discovery and remediation of sinkholes in one of its large embankment dams, BC Hydro, like many other major dam owners, continues to face the challenges of assessing seepage-induced internal erosion and related dam safety risks of embankment dams. In particular, BC Hydro owns and operates many large embankment dams comprising coarse widely graded core and filter materials, thus appropriate assessment of internal erosion of existing dams is critical in assessing their health and safety risks. This presentation summarizes BC Hydro's practice, experience and future direction in assessing internal erosion of zoned embankment dams.

BC Hydro's Approach

Internal erosion initiates when hydraulic forces exceed the resistant forces of soil particles within an embankment dam or its foundation. Internal erosion may be arrested if the adjoining material provides adequate filtering function that prevents loss of base materials while allows passing of seepage flow. Many of BC Hydro's zoned embankment dams consist of impervious core and downstream zones built of glacial till materials, which are widely graded with silt-sand-gravel and some oversize particles. These widely graded materials may be prone to internal instability and/or segregation, and often do not meet modern filter criteria (USBR, 2011). To evaluate internal erosion in zoned embankment dams, BC Hydro current practice has been focusing on assessment of material susceptibility to internal stability and filter compatibility. The following approach is being undertaken:

- Comprehensive and detailed review of construction records;
- Desktop studies of as-constructed material gradations;
- Performing conventional small scale filter tests; and
- Moving towards filter testing of large particle size gradation samples

Detailed Construction Record Review – Embankment Fill and Foundation Characterization

As a dam owner, in order to thoroughly understand seepage performance of an existing dam, it is important to carry out a comprehensive and detailed review of all available construction records. This includes compilation and review of technical specifications, record drawings, quality control and record tests of fill placement (gradations, density, etc.), construction photos, construction sequences and placement equipment and methods, foundation excavation and treatments, foundation seepage cutoff wall construction, etc. Detailed and comprehensive review of design and construction record data helps understand the original design intent as well as the as-constructed conditions to evaluate if the materials meet the modern design criteria. Attention is given to compiling and reviewing available daily construction records/correspondences to detect any unusual construction methods and problems, e.g. material variations, fill placement sequence, winter construction, etc. The result of such data compilation and review is Embankment Fill and Foundation Characterization Report to provide solid basis for subsequent dam performance assessments. Use of 3D CAD and GIS models facilitates the data compilation and analysis, and the development of 3D seepage/stress analysis models for the dam. All material susceptibility to internal stability and filter compatibility analysis results for each pertinent and available construction data is also incorporated into the GIS model to account for spatial distribution/variability so as to look for potential location(s) of internal erosion.

Desktop Analysis of As-constructed Gradations

Desk study is performed on the dam fill materials and its foundation materials using the existing empirical methods based on the construction data. Attention is given to the applicability of the methods since most methods are not applicable to all soil types. The methods are considered only suitable for the soils types that were used in the research to develop the empirical methods. The desk study generally includes the assessment of (1) internal stability, (2) vulnerability to segregation, (3) potential to crack and to hold a crack under seepage flow, and (4) filter compatibility. In the filter compatibility assessment, for the filter materials deemed susceptible to internal instability and segregation,

the filter gradations are adjusted by removing some fine fractions of the originally filter gradations to account for internal instability and segregation (Foster, 2007, Li et al., 2014, ICOLD, 2017)

Recognizing the wide range of particle size gradation curves, ICOLD (2017) recommends using the finest base soil gradation, the average soil gradation, and the coarsest base soil gradation in the filter compatibility assessment. It has been found that these three material gradations do not necessarily represent the upper and lower filter requirements, especially for the base materials which fall into two different base soil categories. A statistical approach to account for the variability of gradations is recommended (Li et al. 2009 and Fannin et al. 2017) to inform the range of filter requirements. In this approach, all of the material gradations from construction quality control and record tests are digitized into a spreadsheet and statistical analyses are performed using the Visual Basic for Applications (VBA) code.

Conventional Filter Tests

Following the desk study, laboratory tests are carried out on select samples to verify the applicability of the methods used in the desk study. Attention is given to the selection of representative gradations, sample preparations, testing conditions, and test result interpretations. The conventional laboratory tests include the following:

- Internal Stability Tests in 280 mm diameter rigid wall permeameter cell for materials up to 1.5" particle size;
- Continuing Erosion Filter (CEF) Tests in 280 mm diameter rigid wall permeameter cell for materials up to 1.5" particle size; and
- Sand Castle Tests of filter specimens about 150 mm in diameter and 120 mm in height for assessing filter crack holding potential.

Because of the small scale laboratory testing device relative to the range of full material particle sizes of the dam fills, various degrees of gradation scalping are required for these filter tests. This has precluded testing of the actual full range in gradation of the coarse widely graded fill materials in the dams and has raised questions on the applicability of the test results and assessment criteria. With respect to assessment of the filter crack holding potential, some field Sand Castle Tests were carried out in-situ in test pits. However, the results of the both the laboratory and in-situ tests are difficult to interpret because these tests are non-standard and have not yet been related to actual dam performance under seepage flow nor in large scale testing under boundary and seepage conditions similar to in-situ.

Development of Large Scale Laboratory Testing Facility

Current assessment of internal erosion of zoned dams is largely based on empirical methods. Appropriate empirical methods need to be selected for the fill materials in question, and laboratory testing is required to verify the application of the empirical methods. In view of the above limitations with the small scale lab testing, BC Hydro is currently working with its subsidiary Powertech Labs Inc. to develop an advanced, state-of-the-art laboratory testing facility. This facility will allow BC Hydro to carry out large scale laboratory testing to characterize the filtering and drainage functionality of widely-graded dam fill materials that exist in BC Hydro's dams. Currently, two sizes (300 mm and 500 mm diameter) of rigid wall permeameter cells are being fabricated to permit testing of both internal instability and CEF testing of materials up to 3" maximum particle size, with a potential to develop a 900 mm diameter cell to test materials up to 6" particle size. A large scale hydraulic flume is also being developed to assess filter performance of various materials under horizontal seepage with cracked conditions.

References

Fannin, R.J., Li, M. and Anderlini, C. (2017), "Evaluation of internal erosion scenarios in an embankment dam", 37th Annual USSD Conference, Anaheim, CA, April.

Foster, M.A. (2007), "Application of No, Excessive and Continuing Erosion Criteria to Existing Dams, In Internal Erosion of Dams and their Foundations", Editors: R Fell, J-J Fry, and Taylor Francis, 103–114.

ICOLD (2017), "Internal erosion of existing dams, levees and dikes, and their foundations", Bulletin 164.

Li, M., Fannin, R.J. and Garner, S.J. (2009), "Application of a new criterion for assessing the susceptibility to internal erosion", CDA 2009 Annual Conference, Whistler, BC, Canada, October.

Li, M., Fannin, R.J. and Anderlini, C. (2014), "Assessing performance of a potentially internally unstable filter", CDA 2014 Annual Conference, Banff, Alberta, Canada, October.

EWG-3 Assessment of Internal Erosion of Zoned Embankment Dams with Widely Graded Materials

Your Notes:

EWG-4 The Suffusion Defect at the Surface Asphaltic Lining

M. Rudolfová
ČEZ, a. s., Hydropower plants, Prof. Vl. Lista 329, Štěchovice, Czech Republic,
E-mail: mirka.rudolfova@cez.cz
J. Říha
Faculty of Civil Engineering, Brno University of Technology, Veveří 95, Brno, Czech Republic,
E-mail: riha.j@fce.vutbr.cz
M. Špano
Faculty of Civil Engineering, Brno University of Technology, Veveří 95, Brno, Czech Republic,

Introduction

The pump storage hydropower plant is located in the north-east of the Czech Republic in the altitude 1350 m above SWL. The sealing of the upper reservoir is surface asphaltic lining (Fig. 1). The scheme was commissioned in 1996 and from that time is in full operation.

The surface asphaltic lining at the upper reservoir of the pump strorage hydropower scheme is composed from overlying mastic coating, 80 mm thick dense layer and the binder layer composed by porous asphaltic concrete (AC) of variable thickness from 40 to 80 mm (Fig. 2). The designed base material underlying the binder layer was 200 ± 50 mm thick supporting (drainage) layer with grains ranging in size from 16 to 90 mm. The interface between the drainage layer and the dam body had to be transition (screed) layer from aggregates with grains ranging from 0 to 250 mm. The screed is of variable thickness and is smoothing uneven surface of the upstream slope of the perimetral rockfill dam. The rockfil dam consists of crushed stone with grains up to 800 mm.

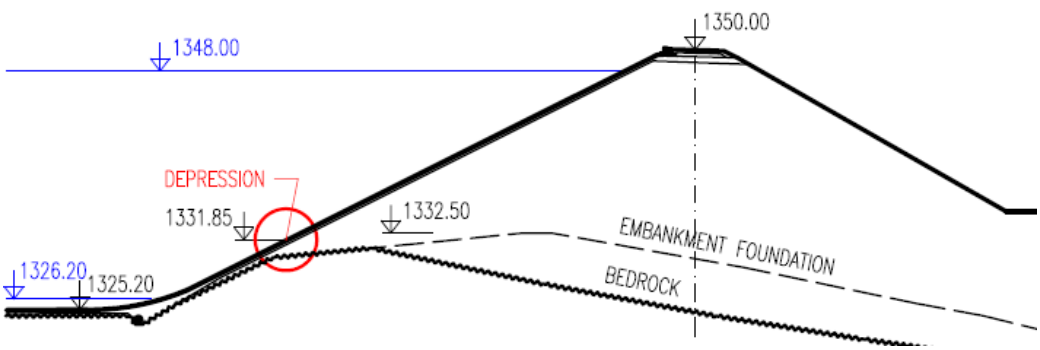

Figure 1. Cross section of the perimetral dam

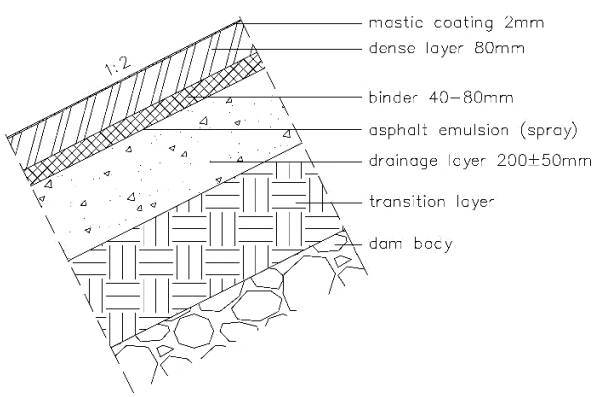

Figure 2. Composition of the asphalt concrete lining

The depression at the lining

In the year 2018, the small depression was identified at the surface of asphaltic lining at the upper reservoir of the scheme. After dismantling the asphaltic surface the sinkhole appeared in the underlying layers indicating the suffusion of loose materials below the lining (Fig. 3). The backward analysis of filter criteria of the soils underlying the lining including the dam material indicated full compliance with general recommendations on the gradation.

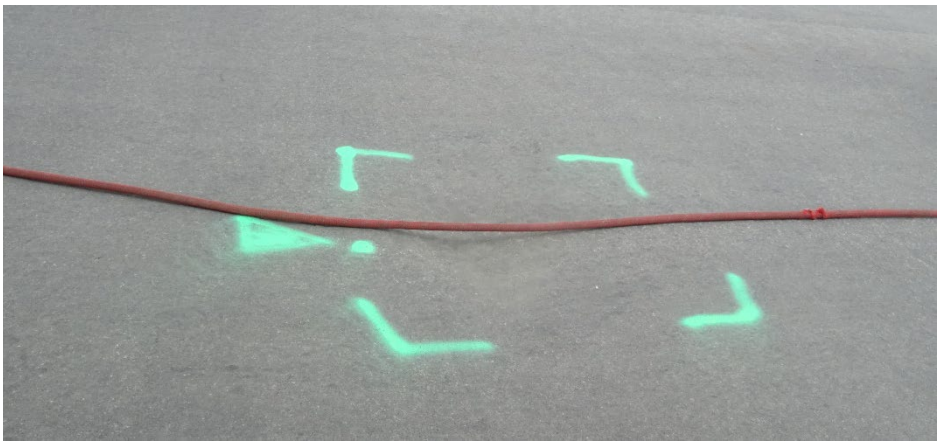

Figure 3. The depression at the AC lining

Figure 4. The sinkhole in the base materials below the AC lining

Analysis and discussion

More detailed analysis of the documentation during the construction and the findings from numerous boreholes to the lining have shown significant variability in the thickness of base layers and variability (nonhomogeneity) in grain size of materials used. Thus even if the filter criteria have been fulfilled for the soil properties documented during construction, the defect was attributed to the great variability and nonhomogeneity of the soils dam body and soil layers below the asphaltic lining. The sinkhole probably propagated into the local greater voids in the rockfill dam body. This should be taken into account when assessing suffusion criteria at the contact with coarse highly nonhomogeneous materials. Another, until now not completely calrified issue is the occurrence of satuated, probably confined zone below the lining. Another issue is the occurrence of saturated confined zone below the lining. Data records documenting the first impoundment of the reservoir have shown that in the sinkhole location there was large horizontal crack of the asphaltic lining in 1996, which probably caused intensive seepage to the dam body.

Acknowledgement

This study has been prepared under the project TH04020154 Optimization of the construction, repairs and performance of asphaltic concrete linigs.

EWG-4 The Suffusion Defect at the Surface Asphaltic Lining

Your Notes:

EWG-5 Cleveland Dam, Vancouver: Terzaghi's Recommendations on Seepage Control and Mitigation of Internal Erosion

J. Fannin, Ph.D., P.Eng.
Dept. of Civil Engineering, Univ. of British Columbia, 6250 Applied Science Lane, Vancouver BC, Canada
E-mail: jonathan.fannin@ubc.ca

Introduction

The Cleveland Dam is a 91 m high concrete gravity dam, on the Capilano River, North Vancouver. It impounds the Capilano Reservoir (Figure 1), a source of drinking water for the City of Vancouver. The left (east) abutment of Cleveland Dam comprises a thick sequence of interbedded glacial deposits. In 1957, Karl Terzaghi was retained by the Commissioner of the Greater Vancouver Water District, "*to investigate the complex drainage conditions extant at the left abutment… and make recommendations as to what additional measures seem appropriate*". In the years 1958 to 1961, Vancouver-based geotechnical consultants C.F. Ripley and Associates prepared a "*Compilation of data re. downstream slope of east abutment, Cleveland Dam, for Dr. Terzaghi*". To inform his understanding of the stability of the east abutment, Terzaghi drew upon extensive observations by Dr. Victor Dolmage, a Vancouver-based consulting geologist working on the subsoil exploration of the damsite. In 1961, Terzaghi reported on his conclusions and recommendations.

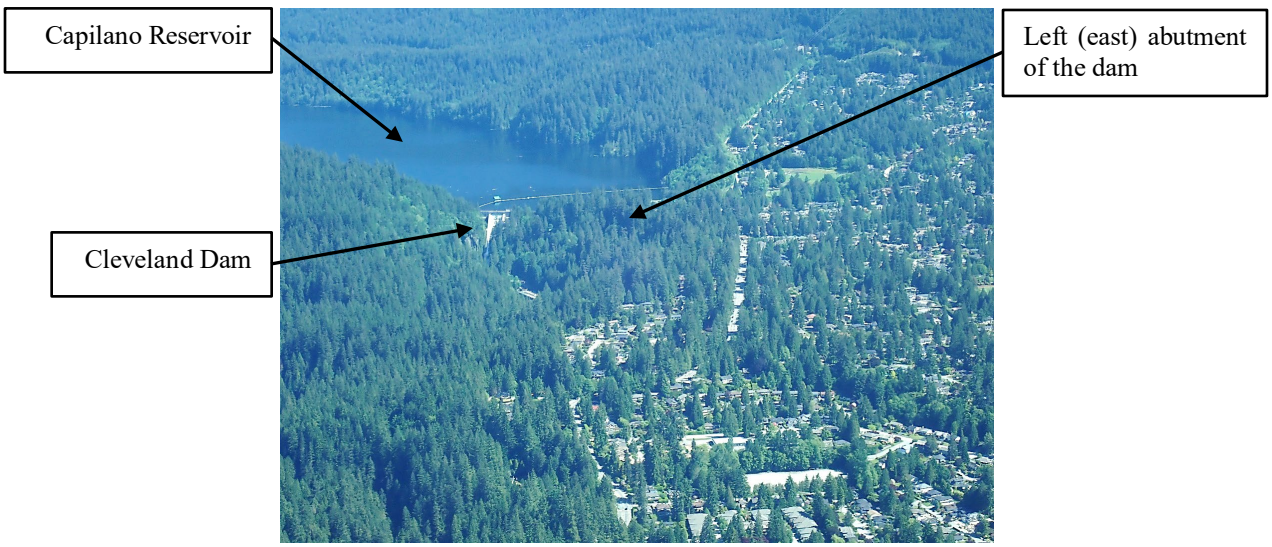

Figure 1. Cleveland Dam and left (east) abutment [Photo. J.Fannin]

Glacial Geology of the Damsite

Cleveland Dam was built in a narrow rock canyon (Figure 2), believed incised after the last glaciation. The deposits of the east abutment, which Dolmage had identified to contain "*at least three till sheets separated from each other by glacial river and lake sediments*", are attributed to infill of an ancestral pre-glacial channel of the Capilano River. In the vicinity of the east abutment, the bedrock surface is "*locally covered with a layer of very hard till T_s, and till sheet T_3 rests directly on the till T_s or on bedrock*". Terzaghi believed the "*extremely uneven character of its upper surface suggests that much of the sheet has been removed by erosion*", before a silt stratum S_1 was "*probably deposited in an inter-glacial lake*". The overlying T_1 stratum, an "*ill-defined and locally composite layer*", was identified as "*a till, or till-like material*". The formation of the G_1 stratum found above it, "*a fluvio-glacial deposit with a lenticular pattern of stratification*", was attributed to repeated advance-retreat movements of ice. Terzaghi believed that "*whenever the ice front retreated the till sheet formed during the preceding advance was partly removed by erosion and replaced by fluvio-glacial sediments or glacial lake deposits*", yielding a discontinuous pattern of stratification

that is characterised by "*steep and sharp boundaries between undisturbed silt and adjacent sand and gravel*". The G_1 stratum, termed the upper aquifer, was found to extend without discontunity from the left abutment of the dam to exposures on the east slope of the present valley downstream from the left abutment. It is overlain by a very dense and hard till stratum T_o. The formation of the uppermost G_o blanket of clean sand, gravel, cobble and boulders "*may have been glacio-fluvial initially, with later re-sorting as a marine beach*".

Cleveland Dam: Provisions for Seepage Control

The dam rests on bedrock that was cleared of river sediments, prior to the start of construction in 1952. On both ends of the gravity section, abutment core walls increase the seepage path length in the glacial sediments above bedrock surface. Bedrock beneath the gravity section and core walls was grouted. The design also incorporated a grout curtain extending into the east abutment, and an impervious blanket on the east slope of the reservoir, both of which were constructed in 1953-54.

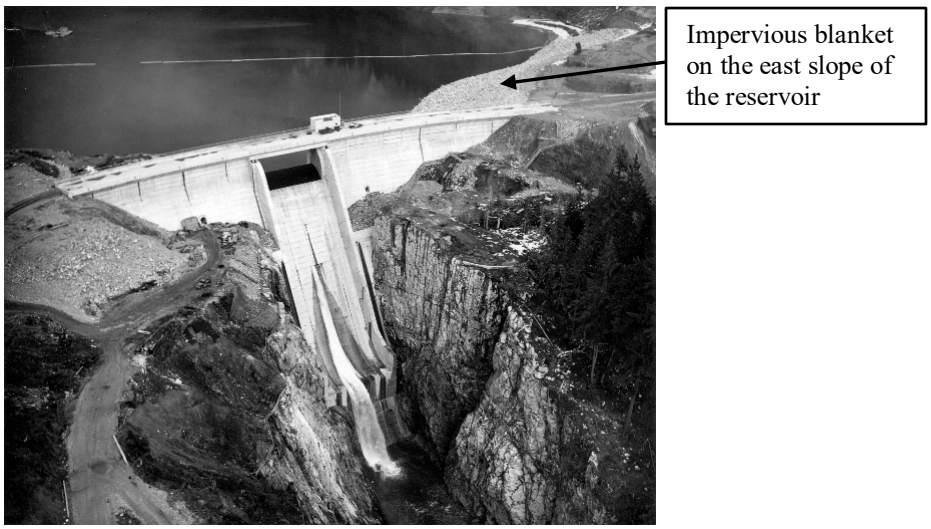

Figure 2. Vancouver City Archives CVA 275-20: Cleveland Dam [Photo. W. Draycott]

First-filling of the reservoir commenced in December 1954. It was recognised that impounding the reservoir might comprise the stability of the east slope of the valley downstream from the dam. Given the complex pattern of stratification in the east abutment, as a precautionary measure, three drainage tunnels were excavated into the slope (in 1954-55). Supplemental drainage provisions on the slope downstream of the dam included weighted filter blankets (in 1955) over groundwater seeps exhibiting discharge of eroded silt, bleeder wells (in 1955), and a drainage shaft (in 1957). On the matter of the weighted filter blankets, it should be noted that concepts for filter design, as first proposed and patented by Terzaghi in 1922-24, and the companion empirical (D_{15}) filter rules for soil retention and permeability that were first published by Terzaghi in 1939 (see Fannin, 2008), had only just been extended for application to widely-graded base soils in a 1955 publication of the USBR.

Terzaghi's Conclusions and Recommendations

The pattern of seepage through the east abutment was primarily established with reference to periodic readings of piezometric level at observation wells, and a comparison of these field data with a series of idealised flow net diagrams. Terzaghi's conclusions and recommendations addressed (i) the efficacy of the grout curtain, the impervious blanket, and the drainage tunnels, for purposes of seepage control, and (ii) the mitigation of internal erosion within the glacial deposits of the east abutment of the dam, believed induced by filling of the reservoir.

References

Terzaghi, K. (1961). On stability conditions at East Abument of Cleveland Dam, G.V.W.D., British Columbia. Consulting report, 88p.

Fannin, R.J. (2001). Karl Terzaghi: from theory to practice in geotechnical filter design. ASCE J. Geotech. & Geoenv. Engng., 134: 267-276.

EWG-5 Cleveland Dam, Vancouver: Terzaghi's Recommendations on Seepage Control and Mitigation of Internal Erosion

Your Notes:

EWG-6 Centrifuge Modeling for Visualization of Backward Erosion Piping Progression

K. Horikoshi; S. Noda; A. Takizawa; A. Takahashi
Tokyo Institute of Technology, Japan

Key Words: centrifuge modelling, backward piping erosion

The backward erosion piping in foundation ground under the levee is known to be one of the causes of failure of the levee system. To investigate the backward erosion piping progression, authors conducted a series of physical model seepage test in a centrifuge model (Koito *et al.* 2016, Takahashi *et al.* 2017, Takizawa *et al.* 2018).

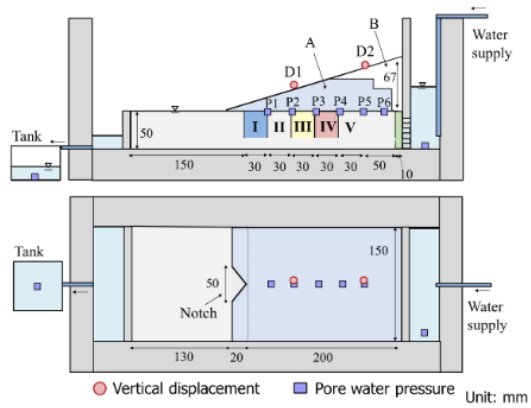

Figure 1. Model setup

In this paper, our previous experimental works on the backward erosion piping progression are reexamined by using visual information. Model levee in the previous experimental works is shown in Figure 1. In the tests, only the slope on the protected side is modelled. For the upper layer, less permeable Silica No.8 (hydraulic conductivity = 4.4×10^{-5} m/s) is used, while the lower layer is made of Silica No. 5 (hydraulic conductivity = 1.0×10^{-3} m/s). The expected hydraulic condition is that the river water seeps through not the embankment but the foundation ground when the flood water level rises. Seepage test is conducted in a centrifugal acceleration field of 50G.

Firstly, visual observation made in physical model seepage tests with embankment made of Kaolin clay is discussed. Figure 2 shows observations of sand volcanoes that appear near the toe of slopes on the protected side in Case 3 in Takizawa et al. 2018 as an example. To visually observe the sand volcanoes of the foundation ground, the coloured sands are placed as shown in Fig. 1. From observations, coloured sand from Area I is ejected from the notch on the toe of the slope, which is regarded as an initiation of the pipe formation. (Fig.2(a)) The major sand volcanoes point moves with increase of the flood water level and the coloured sand from Area II is observed at "1" in Fig. 2(b). When the seepage stage moves on to the next, progression of the pipe resumes and continues for a certain period of time under the constant average hydraulic gradient (Fig.2(c-d)). From Fig. 2(d), the coloured sand from Area I is observed after ejection from Area IV. Based on the above observations, the pipping initiate near the toe of slopes at shortest distance between the upstream and downstream. However, the temporal forward progression from Area IV to Area I in Fig. 2(d) indicates that pipe does not necessarily propagate along the shortest seepage path. Observed multiple erosion patterns on the foundation surface after the test in Fig. 3 (b) also lead to the same conclusion.

Figure 4 shows the pipe visible from side observation window in Case 3 in Takizawa et al. 2018 as an example. The pipe (a)forms, (b)clogs,(c) resumes, (d) extends to the flood-side with expansion of a pipe diameter (e)clogs and (f) resumes and extends. This clogging is caused by local collapse of the expanded pipe due to overburden pressure.

In order to discuss the three-dimensional progression of the backward erosion piping, secondly, results obtained from a physical model seepage tests with embankment made of transparent material are presented. This transparent embankment is made by coagulated water by an agar. It enables the opportunity to observe piping progression as shown in Fig. 5. Same as clay, it also reproduces local collapse of expanded pipes. From observations of piping progression through the transparent embankment, it is confirmed that piping progression is not straight but meandering and branching.

Finally, hypothetical three-dimensional piping progression is concluded based on results of a series of tests as follows: In progression process of the backward erosion piping, a pipe extends to the flood-side with expansion of a pipe diameter. Local collapse of the pipe due to overburden pressure induced by the embankment leads to meandering and branching of pipe.

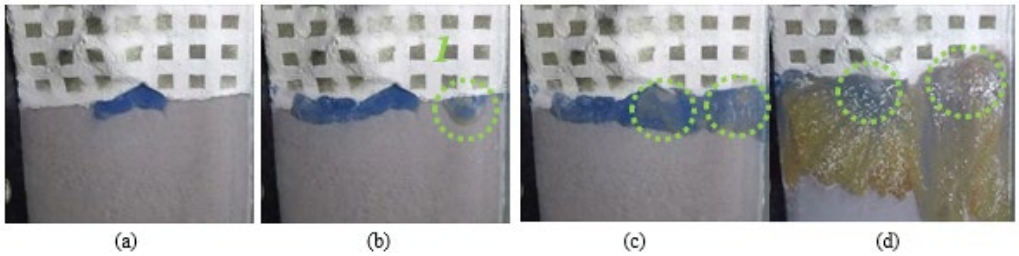

Figure 2. Observation of pipe progression

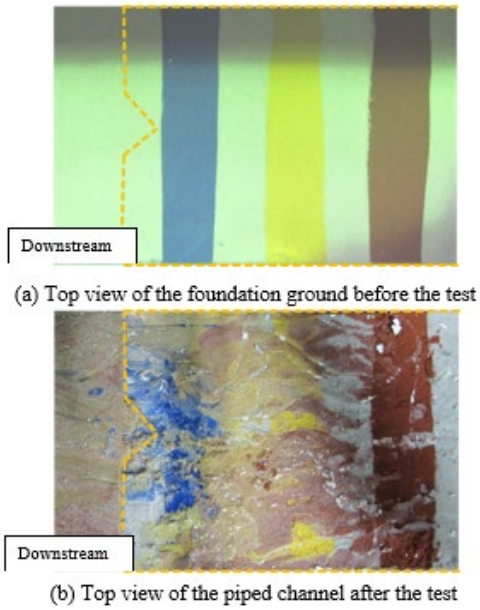

Figure 3. Top view of the foundation ground

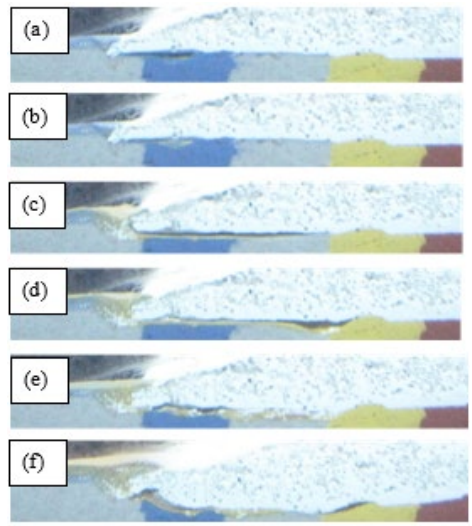

Figure 4. Observation of pipe progression from side observation window

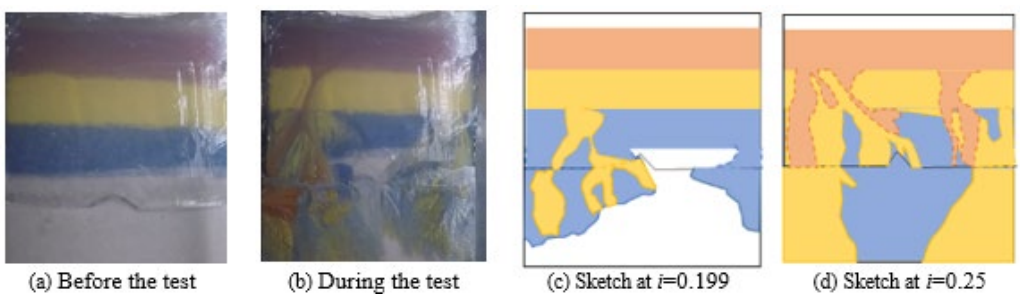

Figure 5. Top view and sketch of the foundation ground

References

Koito, Horikoshi, & Takahashi, (2016). Physical modelling of backward erosion piping in foundation beneath levee. *Proc. 8th International Conference on Scour and Erosion, Oxford*, 445-451.

Takahashi, A., Horikoshi, K. & Maruyama, T., (2017) : Physical modelling of backward erosion piping in levee foundation subjected to repeated flooding, Book of Abstracts for *25th Meeting European Working Group on Internal Erosion in Embankment Dams & their Foundations*, pp. 4-5, 2017.

Takizawa, A., Horikoshi, K. & Takahashi, A., (2018) : Physical modelling of backward erosion piping in layered levee foundation, *Proceedings of the 9th International Conference on Scour and Erosion*, pp. 33-38.

EWG-6 Centrifuge Modeling for Visualization of Backward Erosion Piping Progression

Your Notes:

EWG-7 A New Design and Testing of A Small-Scale Experimental Device of Backward Erosion Piping

J. Riha
Faculty of Civil Engineering, Brno University of Technology, Veveri 95, 602 00 Brno, Czech Republic
E-mail: riha.j@fce.vutbr.cz

L. Petrula
Faculty of Civil Engineering, Brno University of Technology, Veveri 95, 602 00 Brno, Czech Republic
E-mail: petrula.l@fce.vutbr.cz

Keywords: backward erosion piping, seepage, hydraulic conductivity, critical hydraulic gradient.

Introduction

The backward erosion piping (BEP) is driven by the seepage forces acting on the soil grains at the upstream end of the seepage path. To simplify the assessment of BEP occurrence, authors compare the value of average hydraulic gradient with its critical value obtained using empirical data (Bligh, 1910; Lane, 1935). The more detailed model of BEP for uniform sands was proposed by Sellmeijer (1988) and later by Van Beek (2015). A new device of circular cross-section where hydraulic gradients along the sample can be observed as well as the erosion progression was presented by Robbins et al. (2018). However, the impact of the local critical hydraulic gradient in the soil on the backward erosion piping was not fully studied yet. In the paper, a newly developed small-scale BEP testing device is presented.

The new testing device, procedure and material

A testing device consists of two major parts: the testing box and the sedimentation cone. The testing box is of rectangular cross-section of dimensions 0.12 × 0.12 m with the length 0.35 m. At the inlet section, 70 mm thick layer of gravel protected by the sieve is installed to homogenize flow into the sandy sample (length about 0.22 m). In the downstream front wall, there is hole of diameter 12 mm through which the water with eroded material flows out of the testing box. Through this hole, a predefined 0.1 m long "pipe" was created underneath the top cover of the box. Along the predefined pipe and expected path of its progression, 17 piezometers with spacing 20 mm were installed in the top cover of the device so the hydraulic gradient along the seepage path may be observed. Downstream of the box, the sedimentation cone was attached. Here the downstream boundary condition is fixed and eroded amount may be observed. Both the testing box and the sedimentation cone are made of transparent perplex glass. The device is connected to the vertically movable tank defining variable upstream boundary conditions (Fig. 1).

The testing procedure consisted of sample preparation, the phase in which no erosion occurred and the phase of erosion. Firstly, tested soil (sand with known characteristics) was placed in the device, the sedimentation cone was connected and the sample was saturated with water. The sample was subjected to seepage with fixed downstream and variable upstream boundary condition given by the elevation of movable tank. The tank was gradually raised and piezometric heads along the sample were measured. At the initial phase the critical hydraulic gradient was not exceeded and the erosion did not occur. After exceeding a certain critical elevation of the tank, erosion occurred. Eroded material and the pipe dimensions were observed during this phase by the camera. Finally, after intensive erosion, a total failure occurred and the experiment was finished.

Interim results

The results from the experiments were piezometric heads along the sample, hydraulic conductivity of the soil and an estimate of eroded amount in time. Based on the piezometric heads in the last step when the sample was still stable the critical hydraulic gradient was identified. After summarizing results from the set of experiments the critical hydraulic gradient and its relation to other characteristics will be set.

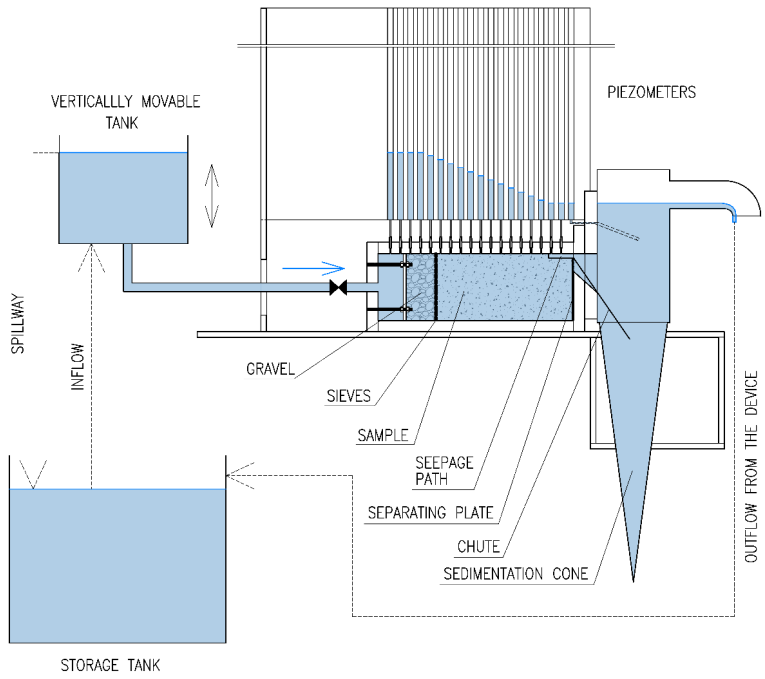

Figure 1. Testing device

Conclusion

The device for the testing of backward erosion piping was described in brief. It is intended to run several sets of experiments with different materials and variable soil porosity. From the results the threshold and erosion parameters will be derived, i.e. critical hydraulic gradient, critical shear stress and soil erodibility. To simulate the BEP process numerical model will be developed and calibrated using the experimental data.

References

BEEK, V. V. *Backward erosion piping: Initiation and Progression*. Masters Thesis. 2015. Technical University of Delft, Netherland.

BLIGH, W. G. Dams Barrages and Weirs on Porous Foundations. *Engineering News*, 1910, 64.26: 708-710.

LANE, E. W. (1935) Security from Under-Seepage Masonry Dams on Earth Foundations, *Transactions of the American Society of Civil Engineers*, 1935, 100.1: 1235-1272.

ROBBINS, B. A., VAN BEEK, V. M., LÓPEZ SOTO, J. F., MONTALVO BARTOLOMEI, A. M., MURPHY, J. 2018. A novel laboratory test for backward erosion piping. *International Journal of Physical Modelling in Geotechnics*, vol. 18, no. 5, pp. 266–279,

ROBBINS, B. A., GRIFFITHS, D. V. 2018. Modelling of Backward Erosion Piping in Two- and Three- Dimensional Domains. In *Internal Erosion in Earthdams, Dikes and Levees: Proceedings of EWG-IE 26th Annual Meeting 2018*. Springer Nature Switzerland, Cham, Switzerland, pp. 149-158.

SELLMEIJER, J. B. *On the mechanism of piping under impervious structures*, Ph.D. Thesis, Delft, Netherland, 1988.

This study is part of the projects TH04030087 Tools for optimization of the management of levee systems and FAST-J-19- 5744 Hydraulic and transport conditions in the seepage path.

EWG-7 A New Design and Testing of A Small-Scale Experimental Device of Backward Erosion Piping

Your Notes:

EWG-8 Large-Scale Test of a Coarse Sand Barrier as a Measure Against Backward Erosion Piping

E. Rosenbrand; V. van Beek; U. Förster; B. van der Kolk; A. Wiersma; J. Terwindt; D. Peters; S. Akrami; A. Koelewijn; K. van Gerven; L. Voogt; Adam Bezuijen

A novel remediation technique against backward erosion piping is being investigated in a multi-scale experimental program. The coarse sand barrier (CSB) is a trench containing densified coarse sand that is placed below an embankment dam or levee in order to prevent the upstream progression of a pipe. The effectiveness of the measure is based on the larger resistance of the densified coarse sand in the barrier against piping erosion, and on the low hydraulic load in the barrier resulting from the conductivity contrast between barrier and background material. This method was investigated in laboratory experiments on a small-scale (aquifer depth 0.10 m) and a medium-scale (aquifer depth 0.40 m) and was found promising. In order to increase the confidence in the potential of the measure for application in the field, two experiments at a larger scale (aquifer depth 3 m) were conducted. This contribution presents the analysis of the piping process of the first large-scale experiment based on measurements during the test and excavation of the sample after the test.

Experiment

The samples were prepared in an experimental facility at Deltares, the Delta Flume. The sand body is trapezoidal, 5 m wide, 34.1 m long at the top, 18 m long at the bottom, and 3 m thick. The sand body was densified and covered by a blanket of compacted clay, except for the inflow area and outflow area (a transverse ditch of 0.5 m wide). The barrier is 0.5 m deep in the sand body, penetrates ca. 0.2 m into the blanket layer and is 0.3 m thick. A plan view of the sample is shown in Figure 1.

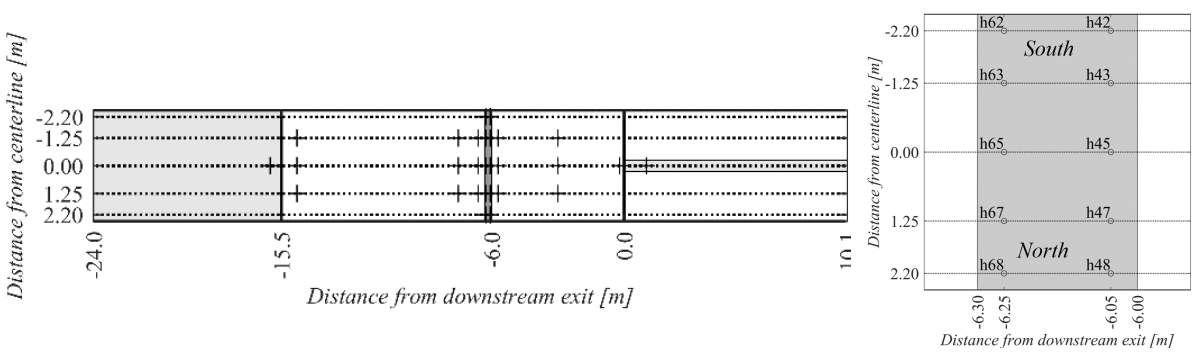

Figure 1. l.h.s: plan view of the top of the sample, the dark grey area indicates the location of the barrier, the light grey areas indicate the inflow area (from -24 m to -15.5 m) and the outflow area at the ditch (from 0 m to 10.1 m), the white area is covered by the blanket. Crosses indicate locations of PPT's; r.h.s.: close-up of the barrier, transducer row h6# is at the upstream side of the barrier, h4# is on the downstream side of the barrier.

The sand body was instrumented with pore pressure transducers (PPTs) and buoyant tracers. Visual observations and discharge measurements were recorded periodically. During the test leakage occurred and the upstream water level was lowered for repairs during the test and also prior to achieving a clear breakthrough of the pipe through the barrier. Excavations were performed after the test.

Analysis of piping progress

During laboratory experiments, the piping process occurred below a transparent cover (Akrami et al. 2019). Those tests show that the head measured inside the barrier, and the gradient over the barrier, as computed from measurements on the upstream and downstream side inside the barrier, provide a good indication of the pipe reaching the barrier,

and of progression of the pipe inside the barrier. For the large-scale test, the measured heads in row h6# on the upstream side inside the barrier, the applied upstream head, and the computed gradients during the test are shown in Figure 2. These are combined with observations during the test and observations from excavation to infer how the piping process took place.

Sand boils were observed on both the north and south side inside the ditch indicating the formation of pipes. The first pipe appears to arrive at the barrier close to side #2 (the south side): all heads in the barrier fall, and the gradient at side #2 rises. The rise at side #3 shortly afterwards suggests progression of the pipe parallel to the barrier in the background sand over a limited distance. The gradient in side #2 continues to increase sharply indicating erosion continues downstream. There is a gap in the data, during which the upstream head is maintained at 4 m, and subsequently lowered for repairs. At the reduced head drop, the head indicated by h62 is ca. 5 cm higher than the head indicated by the other transducers in row 6#. This suggests that this transducer has settled by ca. 5 cm during the data gap. This suggests that erosion of the barrier created a void into which the transducer sank during the repair activities. From then the measurements of h62, and the computed gradient at side #2 are not representative.

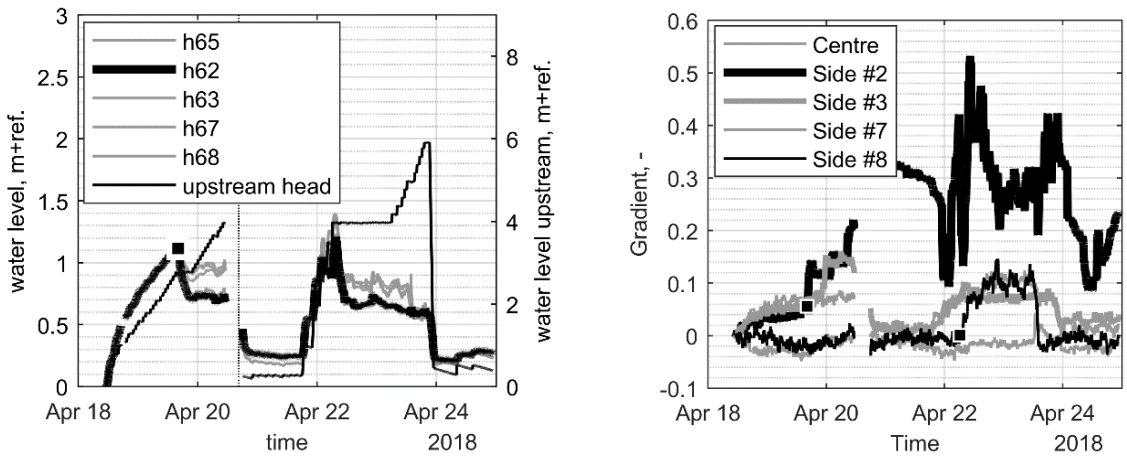

Figure 2. l.h.s.: head measured relative to the surface of the sand body in the row of transducers on the upstream side of the barrier (left hand axis) and upstream water level (right hand axis). Data is missing from 20-04, 11:10 to 18:00, but the upstream water level was maintained at 4 m until 16:30 (vertical line), then the upstream water level was reduced for repairs against leakage; r.h.s.: computed gradient over transducer pairs inside the barrier. Squares indicate times at which a pipe appears to have reached the barrier in the vicinity of h#2 and h#8.

Excavations support this interpretation, these show that a large pipe formed on the south side of the ditch and progressed to the south side of the barrier. This pipe cut into the cover layer, and was filled with barrier material. In front of the barrier, a ca. 0.4 m wide area was eroded on the south side of the model. Above the barrier itself, the cover layer had subsided over a width of ca. 0.5 m. At this location, a thin layer of fine sand was found on top of the barrier. The origin of this sand was not adequately explained. If the pipe had progressed through the barrier, a larger amount of sand would be expected. However, it cannot be ruled out that the pipe did breach the barrier, as the upstream water level was being lowered in the period that the erosion occurred. The subsidence of the blanket into the barrier may then have prevented further erosion at this location.

When the upstream water level was raised again, sand boils on both sides of the ditch were activated, but the erosion activity on the north side of the model appeared dominant. A pipe appears to reach the barrier around side #8 on 22-04 causing the gradient to increase. Gradients at side #7 and #8 start to fall on 23-04 at 12:30. This might indicate progression of the pipe in the barrier, but excavations indicate that the barrier was intact on the north side. Leakage was observed in the north side of the model at that time. Excavations revealed several pipes on the north side of the model at the ditch, these spread out into a delta towards the barrier. These pipes were much smaller than on the south side. That would be expected, as flow initially concentrated to the south pipe in the barrier, and later was distributed over several pipes. A larger pipe in the south side would also provide more space for eroded barrier material, which

would account for the greater extent of damage that occurred on the south side of the model. This test indicates that the pipe did not progress parallel to the entire barrier prior to damage of the barrier, which is different from the laboratory tests. In the laboratory tests, the barrier was level with the sand body, and pipe progression into the barrier is considered to be governed by the local horizontal gradient in the barrier. In the current test, the barrier penetrates into the cover layer, therefore the barrier can crumble into the pipe downstream to a much greater extent. It appears that in this case the progression of the erosion front in the barrier is also limited by the space and transport capacity of the pipe downstream of the barrier. Settlement of the clay layer may also have hindered the continuation of the process in this experiment.

The second large-scale test was conducted with a barrier that was level with the sand body, where the resistance of the barrier would be controlled by the same mechanism as in the laboratory tests. However, results from this first test are important with regards to practical application, as the installation of a barrier that is level with the background sand is more challenging than the installation of a barrier that penetrates into the cover layer.

References

Förster, U. et al (2019), A coarse sand barrier as an alternative preventive measure against backward erosion piping. Proceedings of the XVII ECSMGE, Reykjavik.

Akrami et al. (2019), Analysis of pipe progression during backward erosion piping in the presence of a coarse sand barrier. Proceedings of EWG-IE 27th Annual Meeting, Vancouver.

EWG-8 Large-Scale Test of a Coarse Sand Barrier as a Measure Against Backward Erosion Piping

Your Notes:

EWG-9 Hydraulic Losses through Sand Boils: Measurements and Theory

B. Robbins
U.S. Army Corps of Engineers, 3909 Halls Ferry Road, Vicksburg, MS, USA
I. Stephens
U.S. Bureau of Reclamation, Montrose, CO, USA
V. van Beek; A. Koelewijn
Deltares, Boussinesqweg 1, 2629 HV Delft, The Netherlands
A. Bezuijen
Deltares, Boussinesqweg 1, 2629 HV Delft, The Netherlands
Department of Civil Engineering, Ghent University, Ghent, Belgium

Extended Abstract:

Levees and dykes are often built on alluvial and deltaic foundations that consist of granular soils covered by more cohesive, fine grained deposits. This common foundation condition is highly susceptible to backward erosion piping (BEP), an internal erosion mechanism by which shallow erosion channels progress through the sand foundation under the cohesive cover layer. The probability of failure due to BEP is commonly assessed by comparing the head loss across a structure to critical values obtained from predictive methods. The total head loss at the critical pipe length can be divided into head loss occurring across the intact soil upstream of the pipe, head loss occurring in the erosion pipe, and head loss occurring over the sand boil and cover layer. While much focus has been given to the first two sources of head loss, very little attention has been given to the head loss over the sand boil and cover layer.

In 2016, high water levels were observed along the Mississippi River in the United States and the Waal River in the Netherlands. The high water levels caused sand boils to activate at both locations such that the head losses occurring over the sand boil and cover layer could be measured. Measurements of the pressure profile along the sand boil throat were made by inserting small standpipes down the sand boil throat as shown in Figure 1. The standpipe was lowered down the sand boil throat in intervals, with a measurement of the excess head (relative to the water surface above the boil) taken at each depth once the water level in the standpipe had stabilized. The measured pressure profiles, shown as excess head relative to the water surface, for each location are shown in Figure 2. In addition to measurements of the pressure profile, the flow rate, sand boil dimensions, and flow velocities in the sand boil throat were also measured. Samples of the sand in the sand boils were obtained for determining particle size distributions of the eroded material. For complete details on the measurements made, the interested reader is referred to Robbins et al. (2019).

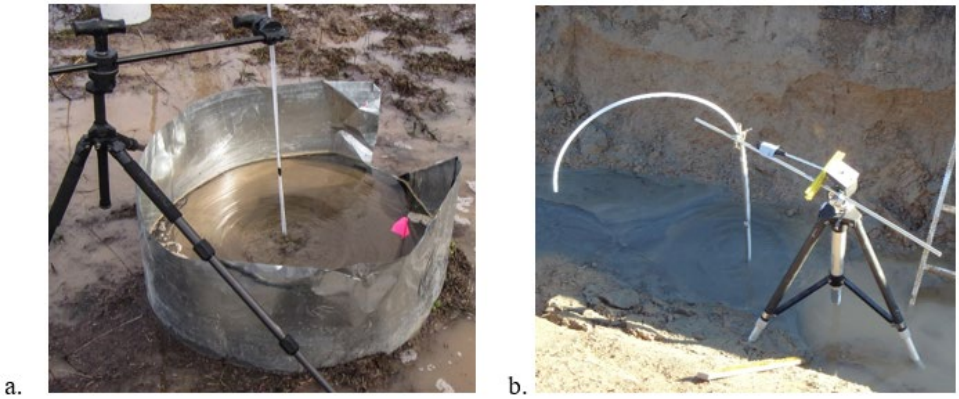

Figure 1. Photographs of head loss measurements in sand boils located along (a) the Mississippi River in the United States and (b) the Waal River in the Netherlands.

Interestingly, the head loss profiles observed in the two boils (Figure 2) were completely different. The Mississippi River sand boil had a well-defined cone in which a heavy suspension of sand was actively "boiling". As seen in Figure 2, this upper boiling sand zone caused approximately 8-9 cm of head loss, below which no additional losses were observed in the sand boil. To the contrary, the Waal River sand boil appeared to have a near constant pressure gradient from the ground surface to a depth of roughly 0.8 m. While quite different trends were observed, it was found that a physical explanation for the observed pressure profiles was provided by considering the relationship between flow velocity and suspension porosity. Baldock et al. (2004) presents a relation between the porosity of a fluid suspension under steady state conditions and the flow velocity, particle diameter, and particle density. Using these concepts, a simple hydraulic theory was developed to predict the head loss profile in the sand boils. As shown in Figure 2, the developed theory closely predicted the measured trends observed in the field. For complete details on the theoretical formulation, refer to Robbins et al. (2019).

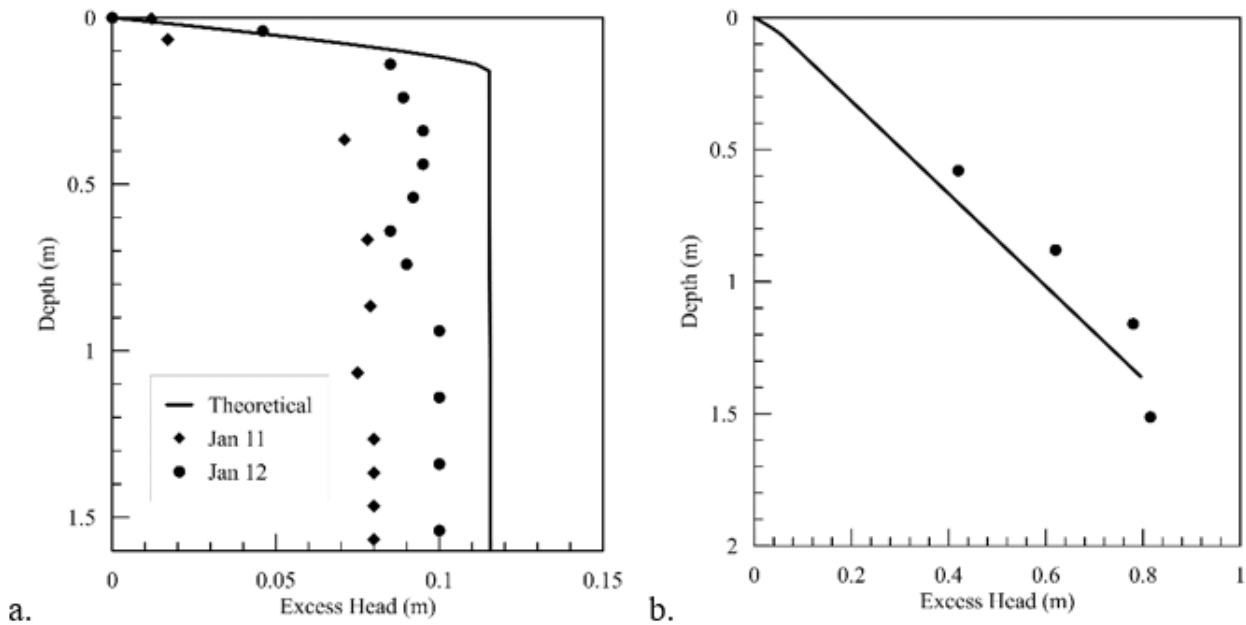

Figure 2. Measured and predicted head profiles for (a) Mississippi River and (b) Waal River sand boils.

The results of this study illustrate that the head loss across a sand boil (and associated cover layer) is a function of the flow velocity through the boil and the properties (diameter and density) of the sand grains being transported. A simple hydraulic theory was found to favourably predict the trends in the head loss profiles observed in the field. By coupling the hydraulic theory for sand boil head losses to numerical models for predicting BEP, the risk of embankment failure due to BEP can be more accurately assessed.

References

Baldock, T.E., Tomkins, M.R., Nielsen, P. & Hughes, M.G. (2004). Settling velocity of sediments at high concentrations. Coastal Engineering 51, No. 1, 91–100.

Robbins, B.A., Stephens, I.J., Van Beek, V.M., Koelewijn, A.R., & Bezuijen, A. (2019). Field measurements of sand boil hydraulics. Géotechnique. https://doi.org/10.1680/jgeot.18.P.151. (ahead of print)

EWG-9 Hydraulic losses through sand boils: Measurements and theory

Your Notes:

EWG-10 Analysis of Pipe Progression during Backward Erosion Piping in the Presence of a Coarse Sand Barrier

S. Akrami; A. Bezuijen; V. van Beek; E. Rosenbrand; U. Förster; A. Koelewijn

Introduction

The coarse sand barrier (CSB) is considered as a promising measure to prevent failure of embankments due to backward erosion piping. In this method, a trench consisting of coarse sand is placed below the blanket layer at the downstream side of the embankment, across the possible path of the pipe to prevent development of a pipe. A pipe can progress upstream until it encounters the CSB, which prevents further progression of the pipe unless a significantly higher head drop (compared to the case without CSB) is applied. This results in a much higher safety level for the levee. The increased strength is due to the barrier's higher resistance against erosion, and the relatively high hydraulic conductivity contrast between the barrier and the background material leading to a reduction of the hydraulic load in the barrier. The feasibility of this method has been investigated in a three-phase experimental programme at Deltares consisting of small-, medium- and large-scale experiments, confirming this method as a highly effective piping inhibiting measure. This contribution presents the results of one phase of this research, the medium-scale experiments, during which several laboratory experiments were conducted. In this paper, the piping process and observations on the pipe progression in presence of a CSB are presented and analyzed to get a better insight in the principle of pipe progression with respect to different barrier materials.

Experimental study

The medium-scale experiments have been conducted in a box with inner dimensions of 1.753 m length, 0.881 m width, 0.403 m depth, seepage length of 1.385 m, exit hole diameter of 0.082 m and barrier thickness of 0.300 m. Dimensions of sand body and exit hole of the medium-scale set-up are approximately four times larger than the small-scale set-up. A detailed description of the small-scale apparatus is given in Bezuijen et al. (2018). The test procedure during small- and medium-scale experiments is the same as is described by Bezuijen et al. (2018), and Van Beek et al. (2015). During the medium-scale tests, a constant head drop is applied for 5 minutes or longer. In case of sand transport, the head is kept constant until the transport stops for several minutes, after which the head is increased again. Flow rate is measured for each head increment and head measurements are recorded, using pore pressure transducers. During these experiments, different combinations of fine sand and barrier materials are tested to investigate the effect of hydraulic conductivity contrast, amongst other factors. Due to the transparent cover layer of the set-up, the piping process can be observed. In this paper results of four medium-scale experiments are presented with combinations of Baskarp fine (B15) or Baskarp coarse (B25) sand (with d_{50} of 0.151 and 0.228 mm respectively and C_u of 1.6) as a background sand and compound materials GZB1 or GZB 2 (with d_{50} of 1.402 and 0.886 mm, and C_u of 3.7 and 2.2 respectively) as a CSB with high relative density.

Results

The observations of the experiments were similar for the four experiments. When a head difference is created, flow is concentrated towards the exit hole, resulting in local fluidization and formation of an erosion lens. Subsequently several pipes formed at the exit hole. However, for the pipe progression from the exit hole to the barrier, further head increments are required. The common procedure of backward erosion piping will continue by progression of the pipe towards upstream leading to failure. Once the pipe reaches the CSB, the flow towards the pipe is insufficient to cause the pipe to grow into the barrier due to the more stable situation. The high flow rates and lower erosion resistance in the background sand next to the pipe, compared to that of the barrier, result in pipe formation parallel to the CSB, along the entire width of the CSB. This formed a T-shape pipe as also observed in small-scale experiments with a CSB, described by Bezuijen et al. (2018). This transverse development of the pipe causes the flow to be redistributed, reducing the load on the barrier. Therefore, flow is conveyed through the barrier towards the T-shape pipe to exit through the central pipe which causes converge of flow to the centre of the model. This results in the largest depth, just downstream of the CSB in the centre of the model. Due to the collection of water to exit through the central pipe, major crumbling of the barrier at that location and some crumbling along the entire width is observed.

As the head is increased in time, the pipe enters the barrier and lengthens through the barrier in several noteworthy steps, which will be defined here, see Figure 1. After the pipe reaches the barrier and progresses along the barrier, it enters the barrier at the damage step, which is defined as the point at which one or more pipes are observed to grow few cm into the barrier. However, formation of largest depth downstream of the CSB and extensive crumbling of the barrier affected a large area inside the barrier, making the damage point difficult to register. At the next step (short growth), one or more pipes grow several cm but do not progress beyond halfway through the barrier. In some tests, after the short growth, there is another significant growth step (medium growth), which still does not cause the pipe to lengthen past halfway through the barrier. There is also lengthening of pipes in smaller amounts that is not considered as a step. At the next step (long growth), one of the pipes progressed beyond halfway through the barrier but stops before the upstream barrier interface. After this step, the pipe progressed nearby the upstream interface of the barrier and typically grew parallel to the upstream interface, inside the barrier (lateral growth/pre-failure in barrier). Subsequently, further head increase can cause the pipe to progress through the upstream interface leading to breaching of the barrier interface (failure). It should be noticed that these steps are only recognizable in the observations, and the results of pore-water pressure transducers only demonstrate when the pipe reaches the barrier, long growth and failure steps, which are therefore defined as the most significant progression steps.

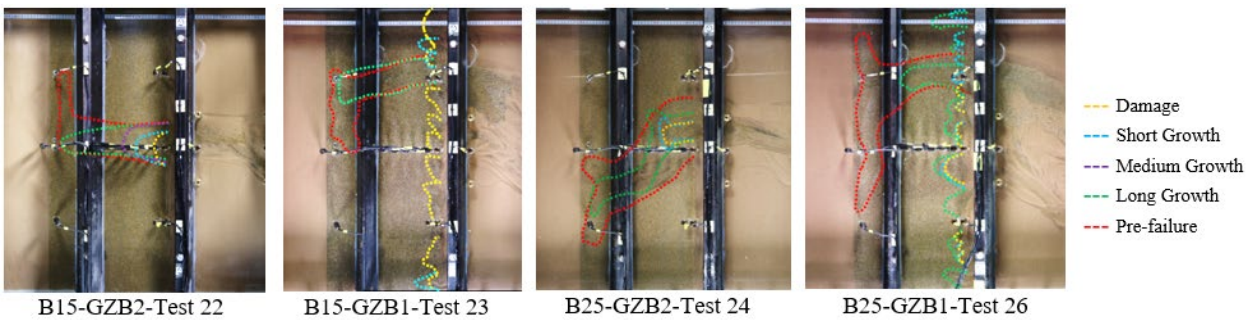

Figure 1. Pipe progression in different experiments for the various defined steps

Discussion and Conclusions

The observed process of pipe formation and progression in the barrier is sketched in different tests as shown in Figure 1. Transverse development of the pipe at the barrier interface in the background sand downstream was observed in all the experiments prior to damage. In the experiments with a stronger barrier, GZB 1, several pipes tend to form and progress inside the barrier, whereas, with a weaker barrier, GZB 2, typically one dominant pipe enters the barrier and progresses. For the experiments with B15, in all the progression steps after short growth, the pipe width is observed to be constant during lengthening of the pipe. While, in the tests with B25, widening and lengthening of the pipe occurred at the same time. Moreover, the occurrence of a long growth and subsequent pipe progression parallel to the upstream interface of the barrier inside the barrier occurred in all the experiments. As a consequence, the steps in the observations illustrate that the largest resistance to erosion can be found when the pipe has progressed into the barrier. In addition, the observations assist the numerical modelling of the experiments for the development of a prediction model.

References

Bezuijen A, Rosenbrand E, Van Beek VM, Vandenboer K (2018) Experiments for a coarse sand barrier as a measure against backward erosion piping. International conference on physical modelling in geotechnics. 17-20 July 2018. University of London, London.

Van Beek, V.M. (2015). Backward Erosion Piping Initiation and Progression. Ph.D. thesis. TU Delft, Delft.

EWG-10 Analysis of Pipe Progression during Backward Erosion Piping in the Presence of a Coarse Sand Barrier

Your Notes:

EWG-11 3D Numerical Simulation of Backward Erosion Piping Tube Experiments

V. M. van Beek; A. Noordman; B. A. Robbins; D. V. Griffiths

Backward erosion piping (BEP) is an internal erosion mechanism, driven by the detachment of particles at the pipe tip and erosion of the particles along the pipe walls and bottom. This erosion mechanism was extensively studied in (Robbins et al., 2018), who describe horizontal tube experiments in which the head loss along the erosion pipe was measured during pipe formation. This study investigates the ability of numerical models to predict the head loss in the erosion pipe in a 3D situation by simulating the tube experiments using DgFlow (Van Esch et al., 2013), a finite element (FE) program in which the groundwater flow is coupled to the pipe flow using line elements, and using the 3D finite element program described in Robbins and Griffiths (2018), in which backward erosion is simulated by changing soil elements to pipe elements.

Experiments

Horizontal tube experiments, described in Robbins et al. (2018) and Van Beek et al. (2019) were conducted to investigate the local critical gradient at the pipe tip, causing pipe progression, and the critical shear stress in the pipe, which controls the dimensions of the pipe. During the experiments, the head was measured along the top of the tube using pore pressure transducers spaced 10 cm apart. Van Beek et al. (2019) describe the critical shear stress in the pipe, obtained from measurements in a selection of experiments for which the pipe had progressed partially through the sample. The critical shear stresses from the tube experiments were found to be in adequate agreement with the Shields curve. For simulation of the experiments, a selection of 4 experiments was used. The selection contains experiments on two different sand types (3C, 4B and 4C on 40/70 sand, with d50 of 300 µm, and 8B on 20/40 sand with d50 of 600 µm), conducted with two tube sizes (B – 76.2 mm and C – 152.4 mm in diameter). For more information about the selected experiments, the interested reader is referred to Robbins et al. (2018) and Van Beek et al. (2019).

Numerical simulations

Since the critical shear stress of the sand dictates the dimensions of the erosion pipe, and therefore its resistance to flow, it is an important parameter in backward erosion piping modelling. Although the critical shear stress can be derived from the Shields curve, it has not yet been verified that numerical models using laminar flow equations for the erosion pipe yield reasonable hydraulic solutions when using typical critical shear stresses for sands. In this study, the tube experiments have been modelled in two different FE programs to investigate whether use of the measured critical shear stress in the model results in the correct representation of the hydraulic losses in the erosion pipe. The used programs are DgFlow (Van Esch et al, 2013), a finite element program in which the groundwater flow is coupled to the pipe flow using line elements, and the 3D finite element program described in Robbins and Griffiths (2018), in which backward erosion is simulated by changing hexahedral soil elements to pipe elements. Both of the programs represent the erosion pipe as viscous, laminar flow in wide and shallow pipes (2D flow). The difference in approach for representing the pipe has consequences for the way the flow through the pipe is translated to the exerted shear stress: since line elements have no width, a width-to-depth ratio needs to be specified for DgFlow, whereas for the program by Robbins and Griffiths (2018) the width of the elements is controlled by the mesh size. The number of elements to be opened simultaneously is an input value to this program, and influences the width to depth ratio.

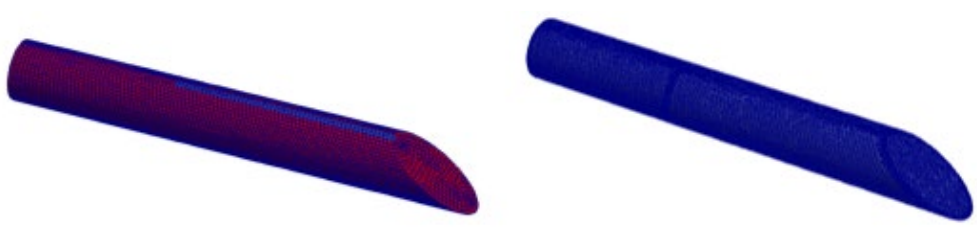

Figure 1. Tube as simulated for the FEM model by Robbins and Griffiths (2018), with pipe elements in blue (left) and tube simulated for DgFlow (right).

In the simulations with DgFlow the width to depth ratio of the pipe was varied (4, 8, 12 and 20), while the mesh size was kept constant at 0.01 m. In the simulations with the model by Robbins and Griffiths (2018), the element size and number of elements used to represent the erosion pipe were varied (0.01 and 0.005 m, and 1, 2, 4 respectively). The width-to-depth ratio was calculated afterwards as the ratio of the combined width of the parallel elements representing the erosion pipe and the average pipe depth along the entire pipe profile. Figure 1 shows examples of the simulated tubes in the two programs.

Analysis of head profiles

The head profiles along the top of the tube were retrieved from the numerical calculations and compared to the measurements from the experiments. Figure 2 (left) shows the head profile for experiment 3C. For all experiments both the measured and computed head along the length of the pipe was fairly linear. Therefore, for comparison of the head profiles, the average measured and calculated pipe gradients were compared by plotting the ratio of the two gradients to the width-to-depth ratio (Figure 2 - right). The figure illustrates that the calculated pipe gradients are lower when the model by Robbins and Griffiths is used. This can be due to the larger inflow area in general and the (relative) increase of surface area with increase of width-to-depth ratio. The larger inflow area allows for more flow through the pipe, resulting in larger pipe depths and therefore lower pipe gradients. For both models, the ratio of pipe gradients is relatively higher for the 20/40 sand than for the 40/70 sand, implying that for the 20/40 sand a lower width-to-depth ratio would be more appropriate than for the 40/70 sand. Since the 20/40 sand is coarser than the 40/70 sand, the pipe could be restrained by the size of the tube resulting in lower *w/a* ratios.

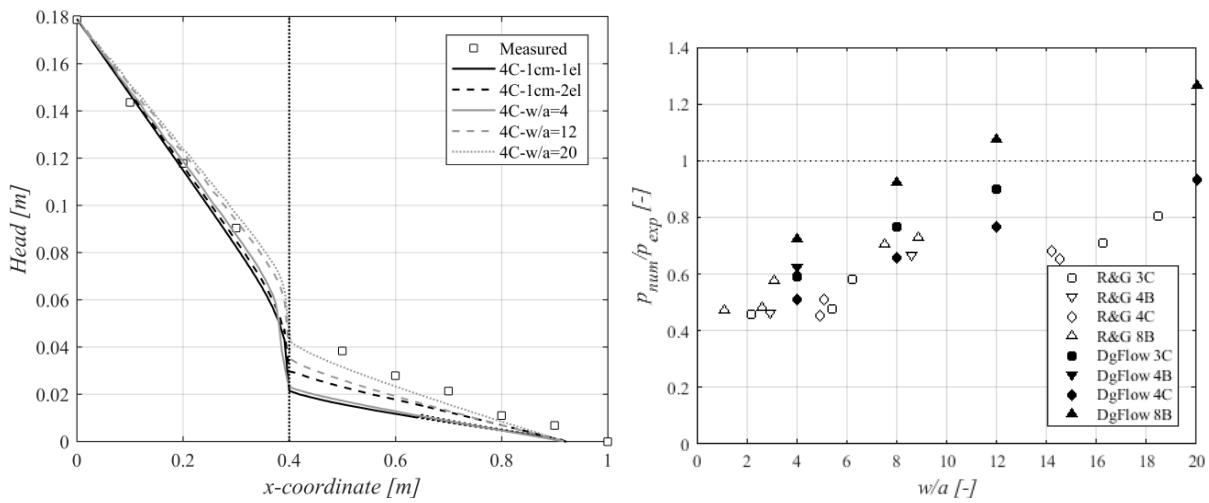

Figure 2: Left: Examples of measured and calculated head profiles, using the Robbins and Griffiths (2018) model (black lines) and DgFlow (grey lines). The dotted black vertical line indicates the position of the pipe tip. Right: ratio of average numerical and measured pipe gradients plotted to the (average) width-depth-ratios. The dotted horizontal line indicates the line of perfect match.

Conclusions

When applying a critical shear stress in 3D backward erosion piping modelling for the estimation of head loss in the erosion pipe, it must be realized that the width-to-depth ratio has a significant effect on the result. The simulation of tube experiments illustrates that this ratio may both depend on the model assumptions and possibly the soil type. More research is required to quantify this effect more precisely such that guidelines for modeling BEP in practice can be developed.

References

Robbins, B.A., Van Beek, V.M., Lopez, J.F., Montalvo Bartolomei, A.M., Murphy, J., (2018). A novel laboratory test for backward erosion piping. *Int. J. Phys. Model. Geotech*. doi:doi/10.1680/jphmg.17.00016.

Robbins, B. A., and Griffiths, D. V. (2018). Modelling of Backward Erosion Piping in Two-and Three-Dimensional Domains. In *European Working Group on Internal Erosion*. Springer, Cham. 149-158.

Van Beek, V.M., Robbins, B.A., Hoffmans, G.J.C.M. Bezuijen, A., Van Rijn, L.C. (2019). Use of incipient motion data for backward erosion piping models. *Int. J. Sediment Research*. doi: doi.org/10.1016/j.ijsrc.2019.03.001.

Van Esch, J.M., Sellmeijer, J.B., and Stolle, D. (2013). Modeling transient groundwater flow and piping under dikes and dams. In *3rd International Symposium on Computational Geomechanics (ComGeo III)* (p. 9).

EWG-11 3D Numerical Simulation of Backward Erosion Piping Tube Experiments

Your Notes:

EWG-12 Application of the Random Finite Element Method to Backward Erosion Piping

B.A. Robbins
U.S. Army Engineer Research and Development Center, Vicksburg, MS 39180
D.V. Griffiths
Dept. of Civil and Environmental Engineering, Colorado School of Mines, Golden, CO, U.S.A.
G.A. Fenton
Dept. of Engineering Mathematics, Dalhousie University, Halifax, NS, Canada

Extended Abstract

Backward erosion piping (BEP) is an internal erosion mechanism that poses significant risks to earth embankments and has been shown experimentally to be highly sensitive to spatial variations in soil properties. In this study, a numerical approach for analysing BEP is presented using the Random Finite Element Method (RFEM), which is able to account for the influence of statistically described input parameters and spatial variability on important output design parameters in geotechnical engineering. The RFEM combines finite element and random field theory, followed by Monte-Carlo simulations. In this study, a two dimensional finite element (FE) model for simulating BEP was used to analyze pipe progression through cross-correlated and spatially correlated random fields of hydraulic conductivity and critical gradient for pipe progression. The FE model simulates pipe progression in plan view by modelling steady state groundwater flow through the soil and laminar pipe flow through the erosion pipe that develops. The pipe progresses when a critical hydraulic gradient in front of the pipe elements is exceeded. For complete details on the BEP model, the interested reader is referred to Robbins and Griffiths (2018).

To examine the influence of soil variability on the piping process, the progression of an erosion pipe through a square domain with side lengths L=10m was simulated as shown in Figure 1a. The domain boundaries at y=0 and y=10 are impervious. The boundary at x=10 is fixed to a constant head of h=0, while the head applied at the x=0 boundary is gradually increased until the pipe progresses through the domain (Figure 1b). The erosion pipe was initiated at the downstream boundary (x=10) by either switching the center element to a pipe element (as shown in Figure 1a) or by allowing the pipe to initiate anywhere along the downstream boundary. The latter case was found to yield higher probabilities of piping failure.

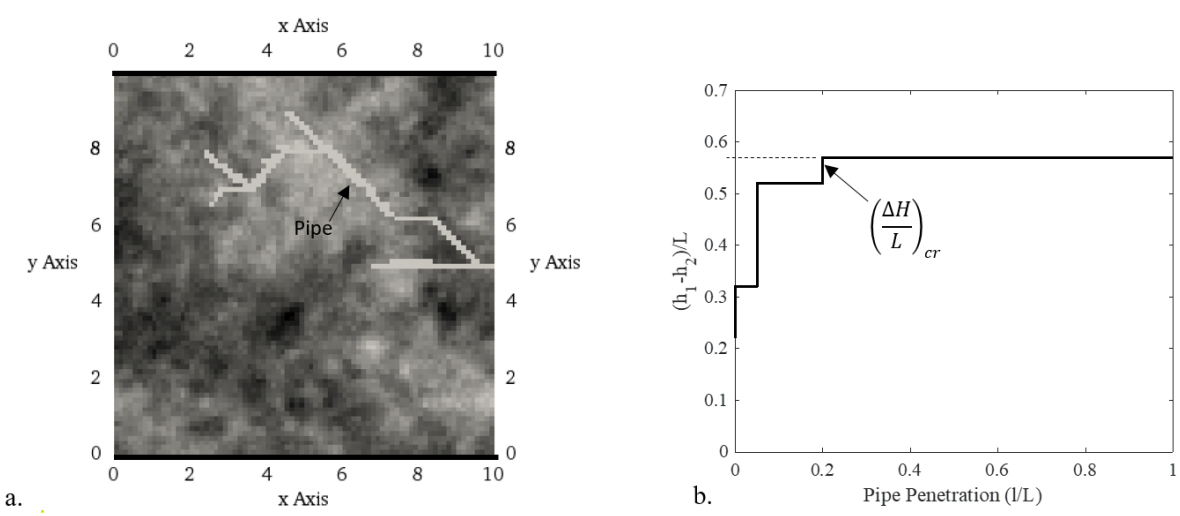

Figure 1. Results from a single realization showing (a) the erosion pipe path through the random field and (b) the required differential head to propagate the pipe various lengths through the domain.

For each analyses, the upstream head was increased until the erosion pipe progressed completely through the domain as shown in Figure 1b. The largest head required was taken as the critical head, which was used to calculate the critical average hydraulic gradient at failure for each realization. Monte Carlo analyses were then conducted to generate distributions of the critical hydraulic gradient for piping failure across the 10m test problem.

In this initial study, the influence of variable hydraulic conductivity of the soil on the piping process was of primary interest. Random fields of hydraulic conductivity were generated with various coefficients of variation and spatial correlation lengths. Typical results (with the only variable being hydraulic conductivity) are illustrated in Figure 2. As shown, the probability of pipe progression increases as the coefficient of variation of the hydraulic conductivity decreases. Furthermore, for a given coefficient of variation, it is readily seen that the probability of failure increases as the correlation length increases. In addition to studying the influence of variable hydraulic conductivity, limited simulations were run with random fields of the critical gradient for pipe progression. The critical gradient was assumed to be normally distributed with a mean value of i_{cr}=0.3 and a standard deviation of 0.05. Analyses were run with the critical gradient and hydraulic conductivity uncorrelated, perfectly correlated, and perfectly negatively correlated. For the limited cases assessed, the variation in the hydraulic conductivity was found to be the dominant variable. Additional analyses are currently being conducted to assess the impact of the critical gradient variability for a broader range of values.

In general, the results of this study illustrate that variations in hydraulic conductivity can have a substantial influence on BEP analyses results. As such, the use of predictive tools assuming uniform soil properties may be overly conservative. Additional studies are currently being undertaken to better understand the influence of soil variability on BEP analysis.

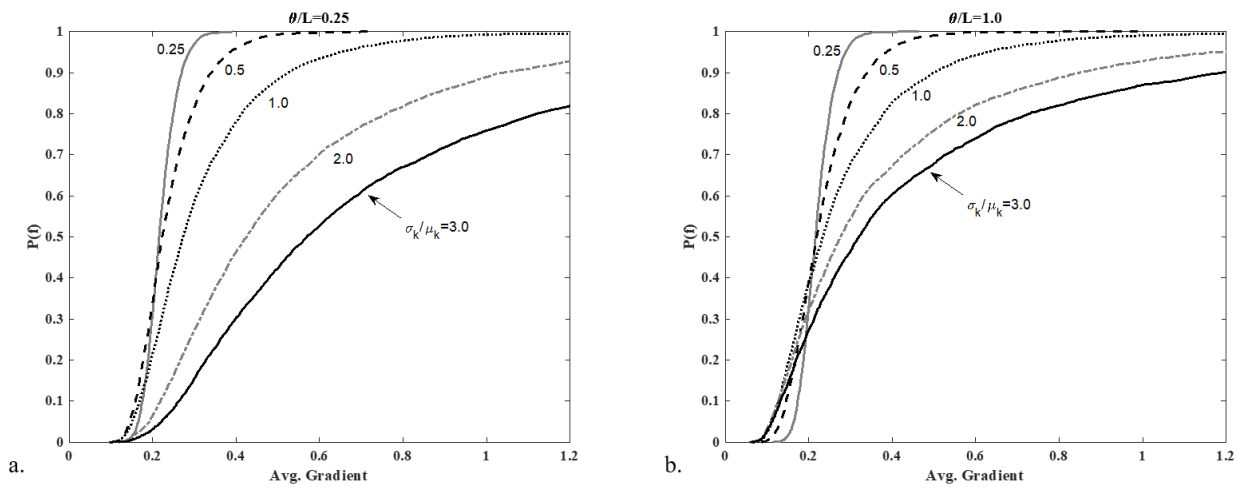

Figure 2. Monte Carlo simulation results illustrating the influence of spatial variation (coefficient of variation and correlation length) in hydraulic conductivity on BEP failure probabilities using the RFEM.

References

Robbins, B. A., and Griffiths, D. V. (2018). Modelling of Backward Erosion Piping in Two-and Three-Dimensional Domains. In *European Working Group on Internal Erosion*. Springer, Cham. 149-158.

EWG-12 Application of the Random Finite Element Method to Backward Erosion Piping

Your Notes:

EWG-13 The Hole Erosion Test: State of the Art, State of Practise and Open Questions

S. Bonelli

Irstea, Aix Marseille Univ, RECOVER. 3275 route Cézanne, 13182 Aix-en-Provence, France
E-mail: stephane.bonelli@irstea.fr

Abstract

The Hole Erosion Test (HET) was developed by Wan and Fell to measure the erosion properties of soils [10, 20]. The experience acquired on several hundred tests on several soils in several countries for 20 years has confirmed what an excellent tool this test can be for quantifying the rate of concentrated leak erosion in a soil, and for finding the critical shear stress corresponding to initiation of erosion. This presentation provides a review of this internal erosion test, which is now part of geotechnical laboratory testing as well as the triaxial or oedometric test. It does not claim to be exhaustive because of the growing interest in this iconic test at the international level.

We first present some salient aspects of the principle of the hole erosion test, in particular the different methods of preparation of intact or remoulded specimens, and the control by pressure drop or by flow rate [2, 8, 11, 19, 20].

The main lines of the interpretation methodology are recalled [2, 8, 19, 20], including the determination of the friction coefficient [8], and the head loss [8, 13, 16]. This methodology is based on a simplification of the turbulent flow equations of a two-phase fluid with erosion of the wall [4, 5, 7, 10, 11, 12]. This test was modeled by continuous model CFD type [7, 10, 14] or discrete DEM / fluid type [3, 17], which gives it a solid consistency in terms of validation of simplifying assumptions.

The fact that the same equations that are used for the test interpretation and for the analysis of an earth dike or an earth dam is a crucial feature [6, 8]. It follows of that a key result: the failure time of a water retaining structure is due to the erosion index, and not to the height of the structure (Figure 1, [8]).

Some examples of test results are presented, in particular a parametric study conducted by Irstea in 2015 on a large dam project (put into service since). Some open questions are finally addressed, among which the most intriguing: how to compare the results obtained with the Hole Erosion Test and the Jet Erosion test [9, 15, 17, 18] ?

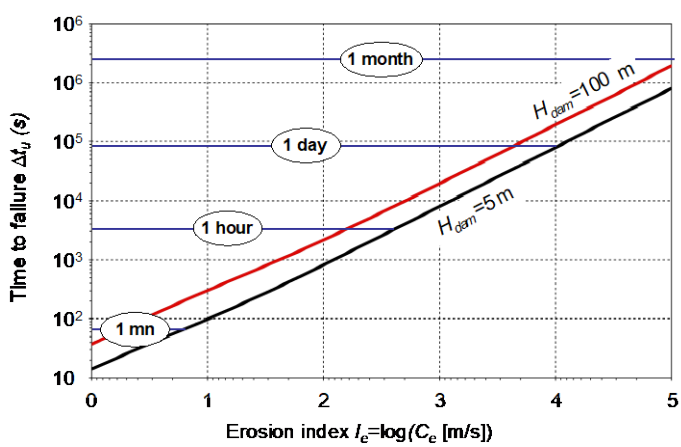

Figure 1. Time to failure as a function of the erosion index for two dam heights [8].

References

[1] Benahmed N., Bonelli S. (2012) Investigating concentrated leak erosion behaviour of cohesive soils by performing Hole Erosion Tests, *European Journal of Environmental and Civil Engineering*, Vol 16, N°1, pp. 43-58.

[2] Benahmed N., Chevalier C., Bonelli S., Chapter 5 - Concentrated leak erosion, in *Erosion of geomaterials*, Wiley/ISTE , p. 155-186, 2012.

[3] Benseghier Z., Cuéllar P., Luu L.-H., Delenne J.-Y. , Bonelli S., Philippe P. (2019), Relevance of the free jet model for the soil erosion by impinging jets, *ASCE Journal of Hydraulic Engineering*, accepted.

[4] Bonelli S., Brivois O., Borghi R., Benahmed N. (2006). On the modelling of piping erosion, *Comptes Rendus de Mécanique*, Vol. 8-9, n° 334, pp. 555-559.

[5] Bonelli S., Brivois O. (2008) The scaling law in the hole erosion test with a constant pressure drop, *International Journal for Numerical and Analytical Methods in Geomechanics*, Vol. 32, pp. 1573-1595.

[6] Bonelli S., Benahmed N. (2011) Piping flow erosion in water retaining structures, *International Journal of Hydropower and Dams,* Vol. 18, n°3, pp. 94-98.

[7] Bonelli S., Golay F., Mercier F., Chapter 6 - On the modelling of interface erosion, in *Erosion of geomaterials*, Wiley/ISTE , p. 187-222, 2012.

[8] Bonelli S., Fell N., Benahmed N., Chapter 4 - Concentrated leak erosion, in *Erosion of Geomechanics Applied to Dams and Levees*, Wiley/ISTE , p. 271-342, 2013.

[9] Fell R., Hanson G., Herrier G., Marot D., Wahl T., Chapter 5 - Relationship between the Erosion Properties of Soils and Other Parameters, in *Erosion of Geomechanics Applied to Dams and Levees*, Wiley/ISTE , p. 343-381, 2013.

[10] Golay F., Lachouette D., Bonelli S., Seppecher P. (2011) Numerical modelling of interfacial soil erosion with viscous incompressible flows, *Computer Methods in Applied Mechanics and Engineering*, Vol. 200, pp. 383-391.

[11] Haghighi I., Chevalier C., Duc M., Guédon S., Reiffsteck P. (2013), Improvement of Hole Erosion Test and Results on Reference Soils, *Journal of Geotechnical and Geoenvironmental Engineering*, 139(2):330-339.

[12] Lachouette D., Golay F., Bonelli S. (2008) One-dimensionnal modeling of piping flow erosion, *Comptes Rendus de Mécanique*, Vol. 336, pp. 731-736.

[13] Lüthi M., Fannin R.J., Millar R.G. (2012), A modified Hole Erosion Test (HET-P) device. *Geotechnical Testing Journal* 35(4): 1–5.

[14] Mercier F., Golay F., Bonelli S., Anselmet F., Borghi R., Philippe P. (2015), Numerical modelling of concentrated leak erosion during Hole Erosion Tests, *Acta Geotechnica*, Volume 10, Issue 3, pp 319-332.

[15] Regazzoni P.-L., Marot D. A comparative analysis of interface erosion tests, *Natural Hazards*, Springer Verlag, 2013, 67 (2), pp.937-950.

[16] Riha J., Jandora J. (2013), Pressure conditions in the hole erosion test, *Canadian Geotechnical Journal* 52(1):114-119

[17] Sibille L., Lominé F., Poullain P., Sail Y., Marot D. (2015), Internal erosion in granular media: direct numerical simulations and energy interpretation. *Hydrological Processes*, Wiley, 29 (9), pp.2149-2163.

[18] Wahl, T.L., Regazzoni, P.-L., and Erdogan, Z., (2008). Determining erosion indices of cohesive soils with the hole erosion test and jet erosion test. U.S. Department of the Interior, Bureau of Recclamation, Dam Safety Office, Report DSO-08-05.

[19] Wan C.F, Fell R. (2004) Investigation of rate of erosion of soils in embankment dams, *Journal of Geotechnical and Geoenvironmental Engineering* 130(4):373-380.

[20] Wan C.F, Fell R. (2004) Laboratory Tests on the Rate of Piping Erosion of Soils in Embankment Dams, *Geotechnical Testing Journal* 27(3).

EWG-13 The Hole Erosion Test: State of the Art, State of Practise and Open Questions

Your Notes:

EWG-14 A New CSD-Based Filter Retention Criterion

F. Seblany; E. Vincens

Université de Lyon, Ecole Centrale de Lyon LTDS, UMR CNRS 5513, 36 Avenue Guy de Collongue 69134 Ecully, France

C. Picault

Compagnie Nationale du Rhône, CACOH, 4 Rue de Chalon sur Saône 69007 Lyon, France

Internal erosion has long been recognized as a major problem associated with earthen structures such as dams and dikes. This process occurs when soil particles are detached and carried with the water flow through the voids of coarse particles. To avoid the migration of fine particles, filters can be safely used as a preventive or curative measure in the downstream side of the earth structures or in contact with their foundations.

Filter design criteria were first established by Terzaghi [1] throughout laboratory tests and later on modified by several authors. According to these empirical criteria, the filter performance can be controlled by maintaining an adequate ratio between the representative sizes of both filter and base soil materials. However, several recorded cases have demonstrated the weakness of these particle-based criteria, particularly when dealing with broadly graded soils.

Indeed, the design of graded filters cannot only focus on the soil grading as proposed by current guidelines, and has to take into account different parameters including the filter density and the coefficient of uniformity of the filter and the protected soil. Moreover, recent studies have shown that constriction sizes, rather than particle sizes, can better explain the filtering capability of granular media. In particular, the controlling constriction size (also known as the filter opening size) was introduced by Kenney et al. [2] as a characteristic parameter for the retention criterion.

More recently, Indraratna et al. [3] developed a new filter criterion based on the constriction size distribution (CSD), which seemed to be promising. This criterion compares D_{c35}, the constriction size finer than 35%, with a representative base soil particle size, d_{85SA} (the diameter for which 85% by surface area of base particles are finer than this size). D_{c35} is obtained through a mathematical procedure assuming ideal representative particle arrangements.

In an attempt to provide a clear physical interpretation of this characteristic, the discrete element method (DEM) has been used for modelling the behavior of granular media. The DEM study considered spherical particles and different gradation (uniformly graded, well-graded and gap-graded) with different coefficients of uniformity. The samples are prepared by deposit under gravity and two density states are envisaged (loose and dense).

Then, the weighted Delaunay tessellation was performed to derive the void characteristics of the numerical samples including the pore and constriction sizes. However, this technique suffers from an over-segmentation of the void space and thus, adjacent tetrahedra have been merged using an appropriate criterion as highlighted in Seblany et al. [4]. Accordingly, the analytical models for CSD have been properly revised.

In our previous work [5], an analytical method that includes the grading and the density of the granular filter has been developed to quickly estimate the filter opening size, d_{OS}. The formula was inspired by the revised analytical model for CSD and was obtained through a statistical analysis over different sets of numerical filtration tests.

Hereafter, the analytical formula has been validated using a series of experimental filtration tests involving uniformly and widely-graded filters compacted to high densities. The equivalent opening sizes of these filters have been computed and are presented against D_{15} (particle size in filter for which 15% by weight of particles are smaller) in Fig. 1. This figure also includes the equivalent opening sizes of the numerical filters investigated in this study. It can be noted that, for higher density states, the analytical calculations agree with the controlling constriction sizes ($D_{15}/4$ or 5) given in past studies [1, 2]. However, different d_{OS} values can be obtained at different compaction levels. This correlation is then sensitive to the degree of compaction which has not been taken into account previously.

Based on these findings, an improved design criterion is proposed on the basis of the filter opening size. The criterion can be written as following: $d_{OS}/d_{85SA} \leq 1$. The applicability of this criterion has been validated against experimental data from the literature and a very good agreement has been found. This CSD-based retention filter criterion represents a valuable tool for assessing the filtration efficiency of granular soils irrespective of their density

and can successfully address the gaps in existing filter design methods. Undoubtedly, further investigations will be required to extend the current criterion to non-spherical filter materials.

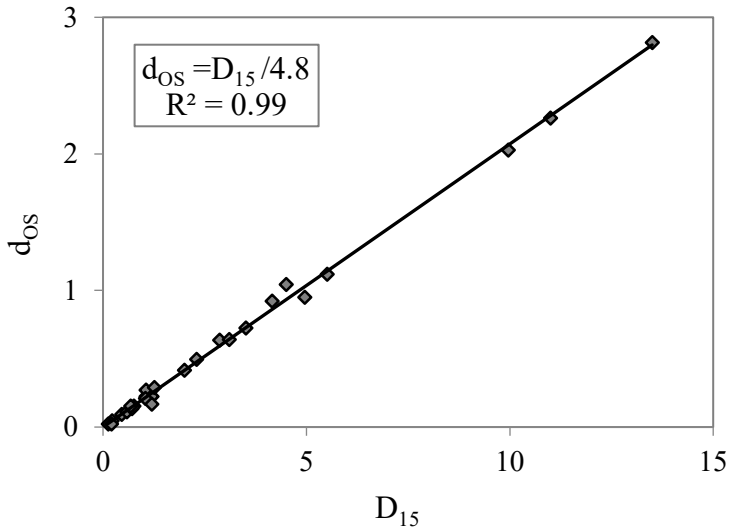

Figure 1. Relation between the equivalent sieve opening size dOS and the representative filter size D15

References

[1] Terzaghi, K. (1922). Failure of dam foundations by piping and means for preventing it (in German). *Die Wasserkraft*, 17(24):445-449.

[2] Kenney, T., Chahal, R., Chiu, E., Ofoegbu, G., Omange, G., and Ume, C. (1985). Controlling constriction sizes of granular filters. *Canadian Geotechnical Journal*, 22(1):32-43.

[3] Indraratna, B., Raut, A. K., & Khabbaz, H. (2007). Constriction-based retention criterion for granular filter design. *Journal of Geotechnical and Geoenvironmental Engineering*, 133(3):266-276.

[4] Seblany, F., Homberg, U., Vincens, E., Winkler, P., and Witt, K. J. (2018). Merging criteria for defining pores and constrictions in numerical packing of spheres. *Granular Matter*, 20(3):37.

[5] Seblany F., Vincens E., Picault C. Simplified estimation of some main characteristics of pores and constrictions in granular materials. *In: Bonelli S., Jommi C., Sterpi D. (Ed.) Internal Erosion in Earth dams, Dikes and Levees (EWG-IE 2018, Milano). Lecture Notes in Civil Engineering*, 17:189-199. Springer, Cham

EWG-14 A New CSD-Based Filter Retention Criterion

Your Notes:

EWG-15 Creation of a Flow Barrier *In-Situ* by Shear-Controlled Direct Aluminum-Organic Matter Floc Injection

J. Zhou; T. J. Heimovaara
Delft University of Technology, The Netherlands
S. Laumann
Delft University of Technology, The Netherlands
Tauw, bv, The Nertherlands

Keywords: building with nature, flow barrier, *in-situ* permeability reduction, shear-controlled direct floc injection

Being able to control and reduce the permeability of a dike body can effectively prevent internal erosion since highly permeable sand layers often result in excessive seepage flow, which results in the translocation of sand grains and triggers piping. In a previous study, we showed that reaction and precipitation of aluminum (Al) and organic matter (OM) *in-situ* can effectively reduce the permeability (Zhou et al., 2019). Hereby, we want to introduce the further development of this technique, namely shear-controlled direct floc injection. The direct floc injection makes use of the shear-dependent size of Al-OM flocs (Yu et al., 2010) and the linear correlation between Darcy velocity and shear (Tosco and Sethi, 2010). During the injection, and therefore under high-flow and high-shear conditions, the Al-OM flocs are small and mobile enough to be transported through the soil. As soon as the injection stops and low-shear conditions prevail, the Al-OM flocs re-grow in size and subsequently deposit in the porous medium. The deposition of Al-OM flocs ultimately leads to a reduction in soil permeability.

The new approach was applied for the first time in a dike section that is surrounding a water reservoir in the Netherlands. At the pilot location, unwanted seepage is spotted at the toe of the dike, which is caused by the high water level in the dike body (Figure 1 a)). The high water level is the result of a high water level maintained in the water reservoir. Direct injection of Al-OM flocs is applied to create a continuous 70 m long and 7 m tall flow barrier that covers the entire aquifer in this section. According to modeling results, a vertical flow barrier with a 50-times reduced permeability will lower the groundwater table in its downstream direction by 25 cm and thus mitigate the surface seepage at the toe of the dike.

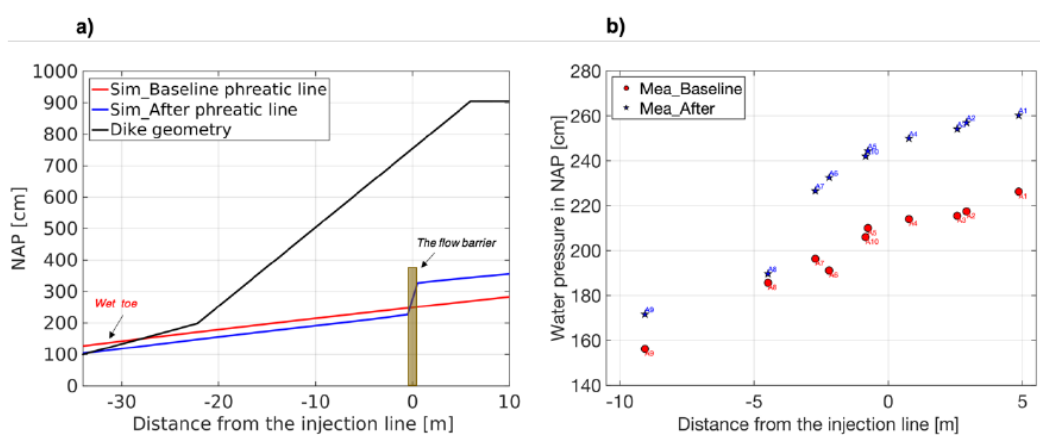

Figure 1. Hydraulic gradient before and after the injection a): simulated results that used for the design and b) is the field measured results from zone A.

For the implementation it was chosen to apply two different Al-OM floc concentrations, 3 g/l OM in zone A (covers 30m) and 5 g/l OM in zone B (covers 40m). The injection was carried out using a fully-automated direct-push system. In order to complete the flow barrier 70 injections were performed. Each of the injection was executed with a bottom to top sequence consisting of 14 injection intervals. To monitor the process 21 monitoring wells were distributed in the two zones and equipped with pressure, temperature, and electrical conductivity sensors (the well arrangement is

illustrated in Figure 2). Pumping and infiltration tests were carried out before and after the injection to quantify the permeability reduction and determine the location of the flow barrier.

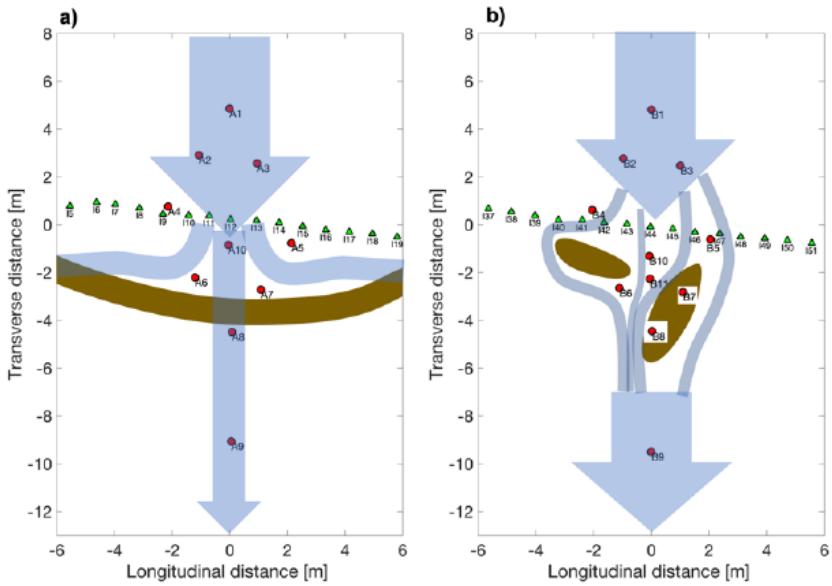

Figure 2. Schematic illustration of the distribution of Al-OM flocs in zone A(a) and B(b). Green triangles denote the injection points; blue arrow represents the background flow, its width reflects the seepage level; brown colour gives the locations of Al-OM precipitates, which are derived from pumping/infiltration tests.

Measurements of the hydraulic head in zone A (Figure 1 b)) show that the hydraulic gradient between monitoring wells A6/7 and A8 is steeper after the injection, while the gradient in the rest of the domain is comparable to the measurements before the injection. This corresponds with the model results and therefore indicates the presence of a continuous flow barrier in the area with a steeper gradient (Figure 2 a)). The results of the pumping tests revealed that the permeability is reduced by a factor 13. The elevated water table after the injection is a result of dredging activities in the water reservoir which led to a change of the hydraulic boundary conditions.

In zone B, little difference in hydraulic gradient before and after the injection was detected. This implies that no (continuous) flow barrier is formed. Additional results from pumping tests in zone B demonstrate that the permeability has been reduced locally by up to 500 times. Due to the discontinuity of the flow barrier, groundwater can circumvent these low-permeable areas. This results in little impact on the overall hydraulic head and no reduced water table at the toe of the dike (Figure 2 b)).

This field experiment proves the viability of the technique, shear-controlled direct Al-OM flocs injection, in reducing soil permeability *in-situ*. A continuous flow barrier was successfully created on site with the permeability reduced by over 1 order of magnitude. However, this field experiment also demonstrates the challenges in the process control. The adaptation of a higher concentration (zone B) might have reduced the mobility of Al-OM flocs, thus led to a spot-wise distribution of reduction in permeability. Also controlling the spatial distribution of Al-OM flocs is proven to be difficult. A better understanding in the interplay between the kinetics of flocs breakage and regrowth and the flow field induced by the injection is needed for further development.

References

Tosco, T. and Sethi, R. (2010). Environmental Science & Technology, 44(23):9062–9068.

Yu, W. Z., Gregory, J., and Campos, L. (2010). Environmental Science and Technology, 44(16):6371–6376.

Zhou, J., Laumann, S., and Heimovaara, T. J. (2019). Science of the Total Environment, 662:99–109.

This work is part of the research programme Water2014 with project number 13883, which is financed by the Netherlands Organization for Scientific Research (NWO)

EWG-15 Creation of a Flow Barrier *In-Situ* by Shear-Controlled Direct Aluminum-Organic Matter Floc Injection

Your Notes:

EWG-16 Enzyme Treatment of Soil for Erosion Control

A. Shidlovskaya
shidanna2018@tamu.edu
I. Shafii; J. Briaud

Enzymes provide a non-toxic alternative to toxic products used in soil improvement and are economically attractive. For example, enzymes have been used in road construction to improve the durability of the base and the subbase of pavements. Would enzyme-treated soils exhibit higher resistance to erosion than untreated soils? That is the question. Erosion Function Apparatus (EFA) tests (Fig. 1) were conducted to provide an answer. The EFA is a laboratory device used to measure the erosion function of a soil defined as the relationship between the soil erosion rate and the water velocity or the water shear stress. In this study three different types of enzymes are used to treat two different types of soils. For each sample, the selected water content is the optimum value from the Proctor compaction test. For each enzyme, two different concentrations and two different treatment periods are considered. The measured erodibility of the enzyme treated soils is compared with the measured erodibility of the untreated soils.

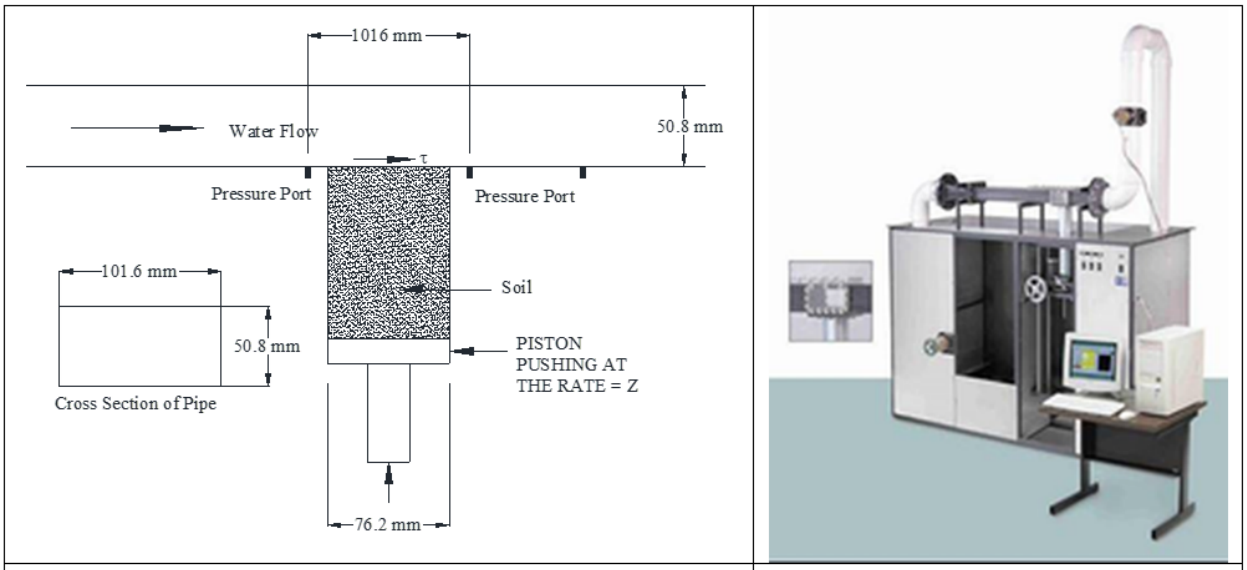

Schematic diagram of the EFA | EFA photograph

Figure 1. Erosion Function Apparatus: EFA test

The enzymes used are: Terrazyme, Road Ferment, and Urease. The two different types of soils are treated: a gap graded low plasticity silt classified as ML and a silty clayey sand classified as SC-SM. Two values for the enzyme concentration in the pore fluid were used: 0.2% and 1 %. Also two curing periods were used: 7 days and 21 days. A total of 18 Erosion Function Apparatus tests, 18 Pocket Erodometer Tests, and 14 mini vane tests were performed. The results show that all three enzymes increased the resistance to erosion of the SC-SM soil (up to 1380% increase in critical shear stress, 390% increase in critical velocity, 50% increase in erosion category, 90% decrease in Ev and Eτ, e.g.) (Fig. 2 and 3), but did not increase the erosion resistance of the ML soil significantly (no change in erosion category but up to 30% increase in critical velocity and 65% increase in critical shear stress). Therefore, the magnitude of the improvement brought about by enzymes on the erosion resistance of a soil seems to be soil specific. As such it is recommended that, if enzymes are to be used on a project to improve the soil resistance to erosion, preliminary tests on the soil samples be conducted to optimize the solution. For the SC-SM, both the higher concentration and the longer curing period tended to increase the erosion resistance but not in all cases. The clay content of SC-SM and ML samples was 1.5% and 2.6% respectively, which indicates that even such low clay content samples were affected by the enzymes in this study. Note that all samples were thoroughly mixed with the enzyme solution so that any field

application should include thorough mixing much like what is done with shallow treatment of soils using lime for pavements. Such field applications are needed to further develop the use of this technique. If successful, the applications include increasing the erosion resistance of levees surfaces, minimizing the erosion at construction sites, slopes of highway embankments, and minimizing the internal erosion of earth dams when compacting the core. One unanswered question is how long the improvement will last.

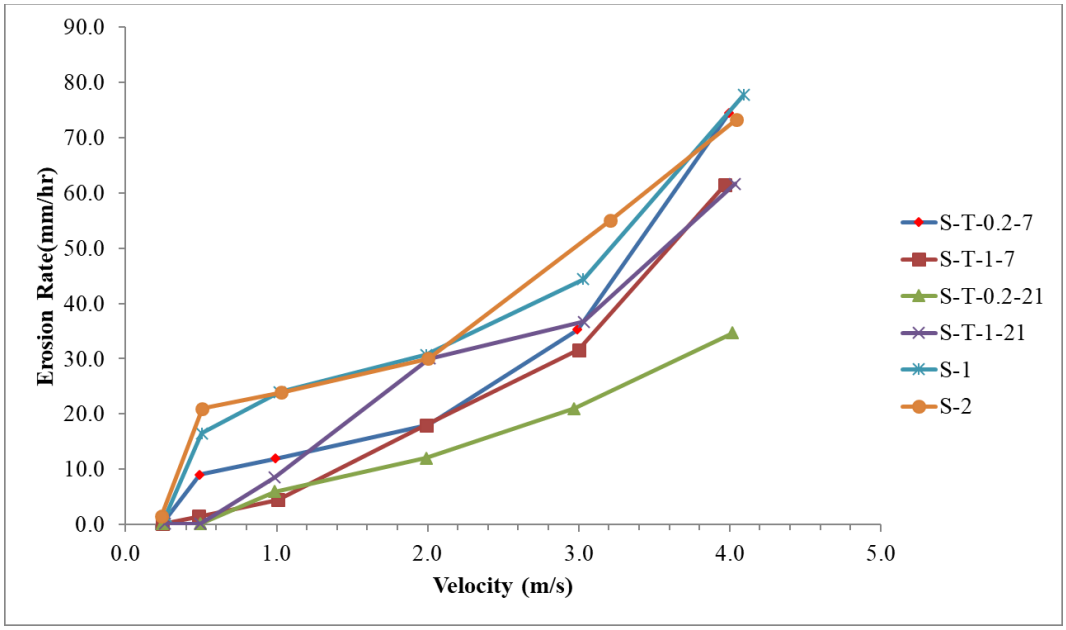

Figure 2. EFA results on SC-SM treated with "Terrazyme" (0.2 % and 1 %) in 7 and 21 days in form of erosion rate-velocity

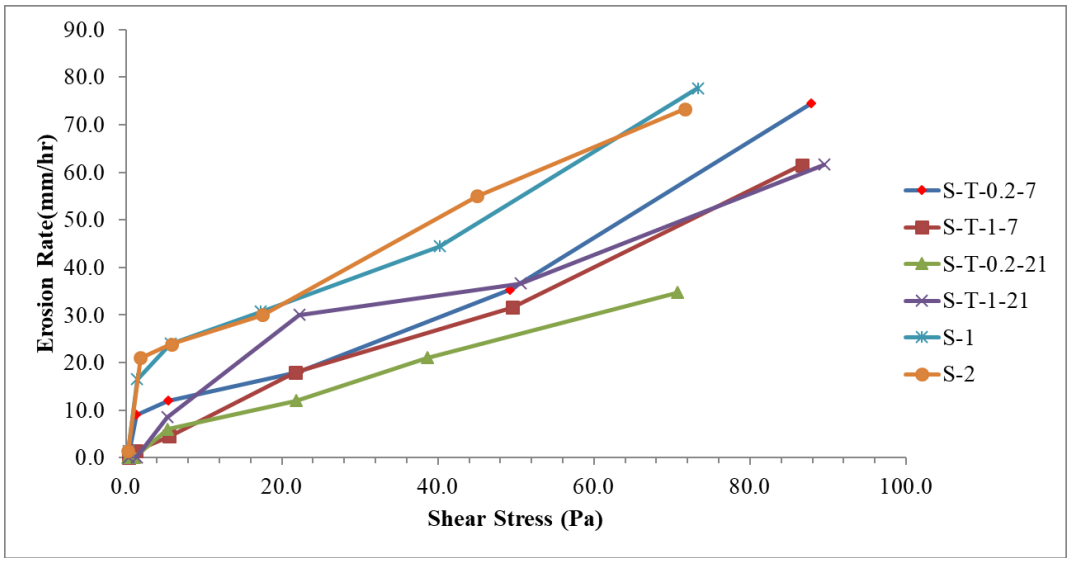

Figure 3. EFA results on SC-SM treated with "Terrazyme" (0.2 % and 1 %) in 7 and 21 days in form of erosion rate-shear stress

EWG-16 Enzyme Treatment of Soil for Erosion Control

Your Notes:

EWG-17 Monitoring Seepage-Induced Internal Erosion Using Acoustic Emission

T. Biller*; A. Smith; N. Dixon
School of Architecture, Building and Civil Engineering, Loughborough University, UK
** Email: t.biller@lboro.ac.uk*

Introduction

A long-standing problem with the longevity of water-retaining earth structures is their vulnerability to internal erosion (IE). Currently available warning systems have technological limitations or prohibitive costs (or both), which impede the deployment of reliable systems to detect seepage-induced IE in its early stages, or before serious damage has occurred. IE is largely invisible from the surface of such structures and significant deterioration has likely already occurred when visible signs are present. Technologies for early detection of IE processes are urgently needed to enable targeted and timely interventions.

Proportions of the energy dissipated during deformation of, and seepage through, particulate materials are converted to heat and sound. The high-frequency (>10kHz) component of this sound energy is called acoustic emission (AE) and its monitoring offers the potential to sense particle-scale behaviours that lead to macro-scale responses of soils (Koerner et al., 1981; Smith & Dixon, 2019). AE is widely used in many industries for non-destructive testing and evaluation of materials and systems (e.g. pipe networks and pressure vessels); however, it is seldom used in geotechnical engineering, despite evidence of the benefits (e.g. Smith et al., 2014, 2017), because AE generated by particulate materials is highly complex and difficult to measure and interpret. AE is generated by seepage-induced IE mechanisms through frictional interactions between particles, friction due to fluid flow through the soil, collisions of migrating particles, and collapse of fabric (e.g. suffosion) (Smith et al., 2019).

This project aims to develop strategies to interpret and quantify seepage-induced internal instability phenomena from AE measurements, enabling early detection of IE processes and hence targeted and timely interventions.

Methodology

Seepage-induced internal erosion experiments are being performed using large permeameter apparatus to investigate the AE generated from internally unstable soils subjected to a range of hydraulic regimes. Figure 1 shows a cross-section of the permeameter apparatus used for preliminary experiments, which employs a waveguide, installed perpendicular to the direction of flow, to transmit AE to the sensor.

A new, bespoke, rigid-wall permeameter has been designed and built to incorporate: vertical load application and a reaction frame; volume change measurement; mass loss measurement; seven total pressure transducers for hydraulic gradient measurements with higher spatial resolution; load cells at the top and base of the permeameter to determine the effective stress distribution across the specimens; and a height-adjustable water tank to enable precise control over the heads applied across the specimens. The permeameter apparatus described in Moffat & Fannin (2006) and Moffat et al. (2011) formed the basis for this design. A suite of AE measurement systems will comprise both piezoelectric sensors and hydrophones. This new apparatus will allow significantly greater control over, and measurement of, hydromechanical behaviour; for example, interpretation in hydraulic gradient-vertical effective stress space and identification of specific internal instability phenomena (e.g. 'suffusion' and 'suffosion') by monitoring the evolution of hydraulic conductivity, mass loss and volume change (Fannin & Slangen, 2014).

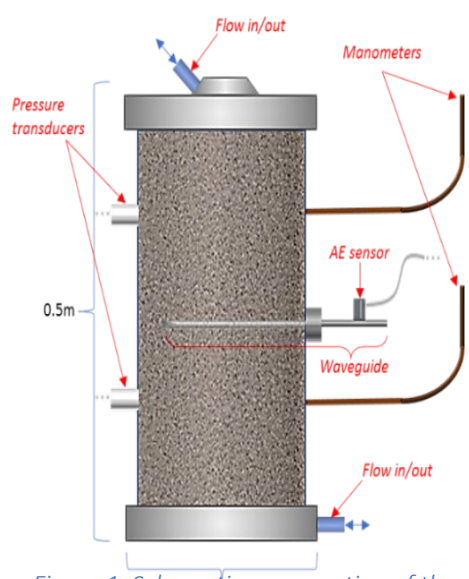

Figure 1. Schematic cross-section of the permeameter apparatus (specimen of 160 mm diameter and 400 mm tall)

Preliminary Results

The permeameter apparatus shown in Figure 1 was used to perform preliminary experiments on a Leighton Buzzard Sand (LBS) and Gravel mix (Figure 2). The LBS and Gravel mix is classed as internally unstable under several geometric criteria (e.g. Chang & Zhang, 2013). The soil was pluviated under a head of water to form the specimen. A constant head of approximately 1.1 m was applied throughout the test.

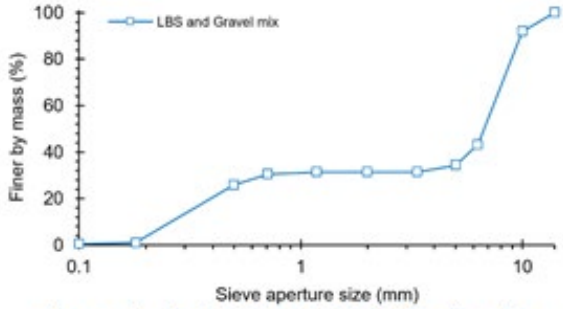

Figure 2. Particle size distribution for the gap-graded LBS and Gravel mix

Figure 3 shows example time series measurements of hydraulic gradient and AE rate. AE generation began rapidly at the onset of head application, and varied with the measured hydraulic gradient, which controlled the soil internal stability conditions. The specimen was under self-weight only, with no additional normal stress applied, and hence fluidisation (i.e. the particles were forced apart, volumetric increase) in addition to the migration of particles (observed during the experiment) caused AE generation.

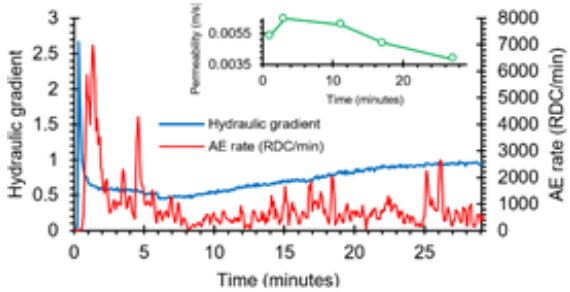

Figure 3. Hydraulic gradient and AE rate vs time

Summary and Future Work

This project aims to develop strategies to interpret and quantify seepage-induced internal instability phenomena from AE measurements, enabling early detection of internal erosion processes and hence targeted and timely interventions. Results from preliminary experiments demonstrate that AE generation is related to seepage-induced internal instability phenomena. A new, bespoke, large rigid-wall permeameter has been designed and built to enable a range of internally unstable soils and hydromechanical behaviours to be investigated and used to establish quantitative interpretation of the AE generated by internal erosion processes. Plans are in progress with project collaborators to perform full-scale field-testing with in-service assets, which will demonstrate performance and benefits in intended applications and environments.

Acknowledgements

The authors acknowledge the excellent technical assistance provided by Mr Lewis Darwin. Tiago Biller gratefully acknowledges the support of a Loughborough University School of Architecture, Building and Civil Engineering studentship for his doctoral work, and Alister Smith gratefully acknowledges the support of an EPSRC Fellowship (Listening to Infrastructure, EP/P012493/1).

References

Chang, D.S. and Zhang, L.M. (2013) Extended internal stability criteria for soils under seepage. *Soils and Foundations*, 53 (4): 569–583. doi:10.1016/J.SANDF.2013.06.008.

Fannin, R.J. and Slangen, P. (2014) On the distinct phenomena of suffusion and suffosion. *Géotechnique Letters*, 4 (4): 289–294. doi:10.1680/geolett.14.00051.

Koerner, R.M., McCabe, W.M. and Lord Jr, A.E. (1981) *Acoustic Emission Behavior and Monitoring of Soils*. ASTM STP 750. Gray, R.E. and Drnevich, V.P. (eds.). West Conshohocken, PA, USA: ASTM International.

Moffat, R., Fannin, R.J. and Garner, S.J. (2011) Spatial and temporal progression of internal erosion in cohesionless soil. *Canadian Geotechnical Journal*, 48 (3): 399–412. doi:10.1139/T10-071.

Moffat, R.A. and Fannin, J. (2006) A Large Permeameter for Study of Internal Stability in Cohesionless Soils. *Geotechnical Testing Journal*, 29 (4): 273–280.

Smith, A., Biller, T., Dixon, N., et al. (2019) "Acoustic emission monitoring in geotechnical element tests." In *XVII ECSMGE-2019*. Reyjavik, 2019.

Smith, A. and Dixon, N. (2019) Acoustic emission behaviour of dense sands. *Géotechnique*, pp. 1–16. doi:10.1680/jgeot.18.P.209.

Smith, A., Dixon, N. and Fowmes, G.J. (2017) Early detection of first-time slope failures using acoustic emission measurements: large-scale physical modelling. *Géotechnique*, 67 (2): 138–152. doi:10.1680/jgeot.15.P.200.

Smith, A., Dixon, N., Meldrum, P., et al. (2014) Acoustic emission monitoring of a soil slope: Comparisons with continuous deformation measurements. *Géotechnique Letters*, 4 (4): 255–261. doi:10.1680/geolett.14.00053.

EWG-17 Monitoring Seepage-Induced Internal Erosion Using Acoustic Emission

Your Notes:

EWG-18 On Specimen Reconstitution and Commissioning a Triaxial Permeameter

V. McClelland[1]; J. Fannin[2]

Dept. of Civil Engineering, Univ. of British Columbia, 6250 Applied Science Lane, Vancouver BC, Canada
[1] *E-mail: vmcclell@mail.ubc.ca*
[2] *E-mail: jonathan.fannin@ubc.ca*

Introduction

A triaxial permeameter (TX-P), with the ability to measure volume change and mass loss during seepage, has been developed at The University of British Columbia (UBC). The apparatus will be used to study the mechanical consequences of internal erosion of internally unstable gap-graded materials, in an effort to establish a mechanics-based understanding of the phenomenon. It is necessary, prior to beginning a comprehensive test program, to ensure that the device is generating accurate and repeatable test results. It is also necessary to ensure that reconstituted gap-graded test specimens used in the triaxial-permeameter test program are homogeneous, so that the effects of different test variables (e.g. confining stress, density, gradation, etc.) can be properly characterized. With these two objectives, a study has been undertaken at UBC to (i) commission the triaxial-permeameter and (ii) evaluate the homogeneity of reconstituted gap-graded specimens.

Commissioning a Triaxial Permeameter:

The newly developed device (Fig. 1) will be primarily used to test sand-sized material from the South Moraine borrow source of the Bennett Dam. The stress-strain response of the borrow materials has not been extensively characterized in any previous research work. Therefore, the commissioning tests were performed on Fraser River Sand (FRS) – a uniformly graded sand for which there is a wealth of data from previous research studies on liquefaction at UBC (see for example Eliadorani 2000, Sivathayalan 2000, and Thomas 1992). The test program consisted of eight isotropically-consolidated triaxial-shear tests – four undrained tests and four drained tests, each on a test specimen that was reconstituted using two different methods. Results were compared to those obtained in previous FRS research studies, with consideration given to the following: (i) repeatability of test results, (ii) similarity of the stress-strain response and related strength parameters, and (iii) effect of data extrapolation on the position of the critical state or steady state locus.

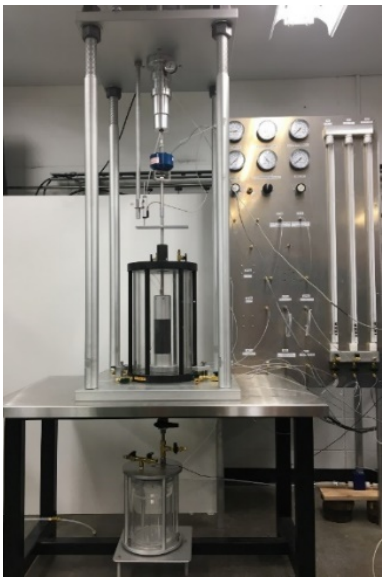

Figure 1. Newly developed UBC TX-P Device

Specimen Reconstitution:

Zoned embankment dams have two fabrics of interest: the body of the dam is a compacted fill, and the dam foundation and/or abutments, which typically includes significant alluvial deposits. Prior research (e.g. Mulilis et al. 1975, Vaid et al. 1999, Verdugo 1992) reveals the fabric of a reconstituted soil has a (sometimes significant) effect on mechanical response of the test specimen. Internally unstable gradations susceptible to internal erosion are not limited to the body of an embankment dam, but also can be present in the abutments and/or foundation. Witness for example the historic issues with the East Abutment of the Cleveland Dam upon first-filling of the reservoir in 1954, or the foundation issues that led to decommissioning of the Coursier Dam in 2003. Kuerbis and Vaid (1988) note that a suitable reconstitution method should "simulate the mode of soil deposition commonly found in the soil being modeled". Thus, in our study of internal instability in zoned embankment dams, we have a need to replicate the fabric of (i) a compacted fill and (ii) an alluvial deposit (Fig. 2).

Moist tamping is widely accepted to model the fabric of a compacted soil (Kuerbis and Vaid 1988), while water-pluviated specimens have been shown to closely replicate undisturbed samples of uniformly graded alluvial deposits (Vaid et al. 1999). However well-graded and gap-graded specimens cannot be reconstituted by water pluviation, due to a tendency for particle segregation. Thus, the slurry deposition method (Kuerbis and Vaid 1988) is used here, because yields fabric that is comparable to water-pluviated specimens.

A reconstituted test specimen should be homogeneous in terms of void ratio. In the case of gap-graded specimens, it should also be homogeneous in with respect to spatial variation of finer fraction content. The variation in void ratio within uniformly-graded moist-tamped specimens has been documented by several researchers (e.g. Frost and Park 2003, Mulilis et al. 1975), however the variation in finer fraction content pre- and/or post-saturation for gap-graded specimens does not appear to have been reported in the literature. Slurry deposition has been shown to create uniform, gap-graded specimens for an angular sand-silt mixture by Kuerbis and Vaid (1988). A modified method has also been shown to create uniform gap-gradations of glass beads by Slangen (2015). The current study examines the homogeneity of gap-graded test specimens reconstituted by moist tamping and slurry deposition, for both a rounded material (glass beads) and for a predominantly sub-angular material (the sands of the South Moraine borrow source). The homogeneity was examined by exhuming reconstituted test specimens in layers and measuring variations in void ratio and finer fraction content.

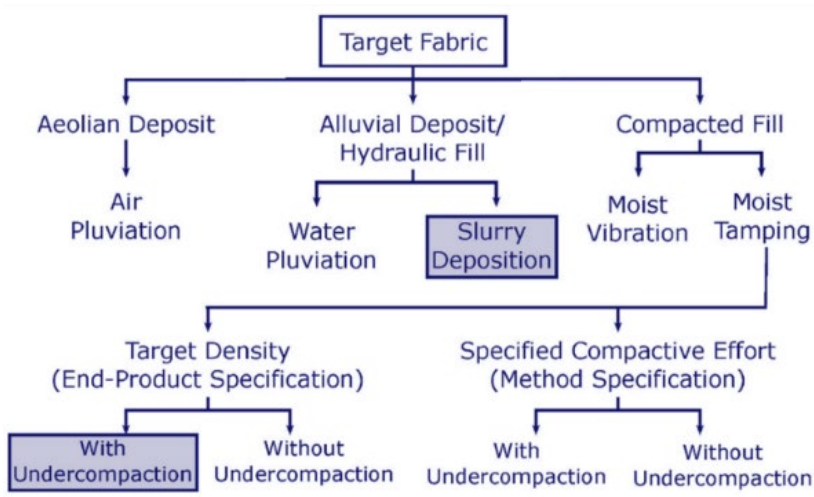

Figure 2. Selected methods of specimen reconstitution: slurry deposition for alluvial deposits, and moist-tamping with undercompaction for embankment fills

Acknowledgements

We acknowledge, with thanks, a series of very informative conversations with Prof. Emeritus Yogi Vaid, on the research findings of his graduate students relating to the fundamental behavior of Fraser River Sand.

References

Eliadorani, A. A. (2000). The response of sands under partially drained states with emphasis on liquefaction (Doctoral dissertation, University of British Columbia), 221 pages.

Frost, J. D., & Park, J. Y. (2003). A critical assessment of the moist tamping technique. Geotechnical Testing Journal, 26(1), 57-70.

Kuerbis, R., & Vaid, Y. P. (1988). Sand sample preparation-the slurry deposition method. Soils and Foundations, 28(4), 107-118.

Mulilis, J. P., Chan, C.K. and Seed, H.B. (1975). The effects of method of sample preparation on the cyclic stress-strain behaviour of sands. Technical Report, Univ. of California at Berkeley, 75p.

Sivathayalan, S. (2000). Fabric, initial state and stress path effects on liquefaction susceptibility of sands (Doctoral dissertation, University of British Columbia), 307 pages.

Slangen, P. H. H. (2015). On the influence of effective stress and micro-structure on suffusion and suffosion (Doctoral dissertation, University of British Columbia), 246 pages.

Thomas, J. (1992). Static, cyclic and post liquefaction undrained behaviour of Fraser River sand (Doctoral dissertation, University of British Columbia), 117 pages.

Vaid, Y. P., Sivathayalan, S., & Stedman, D. (1999). Influence of specimen-reconstituting method on the undrained response of sand. Geotechnical Testing Journal, 22(3), 187-195.

Verdugo, R. (1992). Characterization of sandy soil behavior under large deformation (Doctoral dissertation, 東京大学), 455 pages.

EWG-18 On Specimen Reconstitution and Commissioning a Triaxial Permeameter

Your Notes:

EWG-19 Influence of Flow Direction on Suffusion Development

D. Marot

University of Nantes, Institute GeM, 58 rue Michel Ange, Saint-Nazaire, France
Email: didier.marot@univ-nantes.fr

D. M. Tran*; F. Bendahmane

University of Nantes, Institute GeM, 58 rue Michel Ange, Saint-Nazaire, France
**University of Danang, 54 Nguyen Luong Bang, Da Nang, Vietnam*

Introduction:

This paper focuses on suffusion which is a selective erosion of fine particles under the effect of seepage flow within the matrix of coarser particles. It is recognized that suffusion may induce important modifications in the hydraulic and mechanical characteristics of the soil. Thus to ensure the safety assessment of hydraulic earth structures, it is important to characterize the suffusion susceptibility. Most of tests were performed under vertical flow, whereas the flow in earth structures can be horizontal as well. To study the potential influence of the flow direction, a new apparatus allows the specimen tests under vertical or horizontal flow.

Testing Apparatus and Tested Soils

The general configuration of the testing apparatus is shown in Fig. 1. It is composed of an acrylic cylinder cell, a piston for applying axial strength, a soil collection system with an effluent tank, a water supply system, instrumentation and a data acquisition system. Within the effluent tank, a rotating system contains 8 beakers with linen bags for the sampling of eroded particles carried with the effluent. The water supply system includes upstream and downstream reservoirs, both equipped with an overflow and their relative elevation that can be manually modified. The device is configured to allow performing tests of undisturbed specimen, directly in the tube of core samples (Patent, 2018). However, for this study, specimens were prepared by moist tamping to prevent soil segregation and per layers of 5 cm in height in order to limit the heterogeneity and to reach a total specimen height of 350 mm.

Two cohesionless soils were selected with gap graded and widely graded grain size distributions, named B and R2, respectively (see Fig. 2). According to grain size based criteria proposed by Kenney and Lau (1985), soils B and R2 are internally unstable. Chang and Zhang's (2013) method assessed soil B as internally stable and R2 as unstable. Finally, no clear classification can be drawn thanks to the used criteria. Therefore, the erodibility characterization needs suffusion tests.

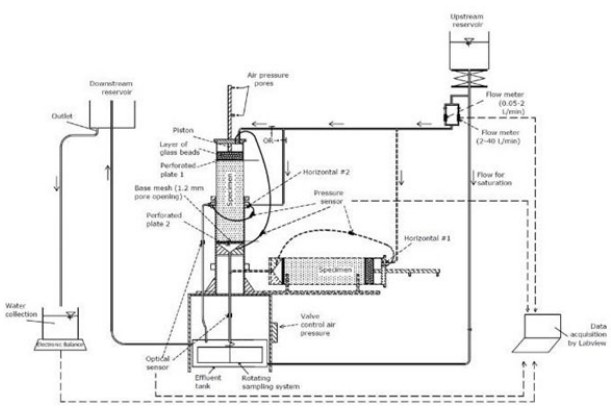

Figure 1: Schematic diagram of the used device

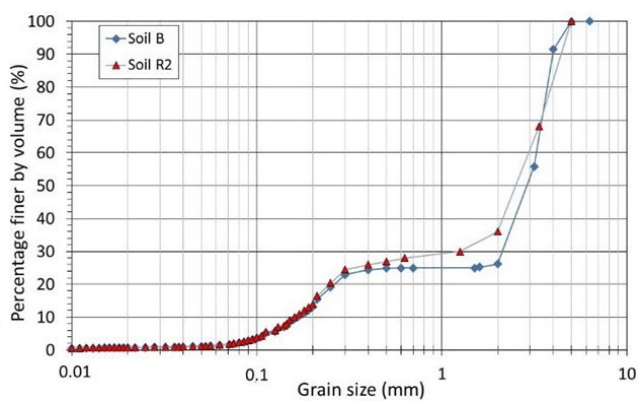

Figure 2: Grain size distribution of tested soils

All specimens were subjected to an axial pressure of 200 kPa through the piston and the pore opening size of the downstream mesh is 1.2 mm in order to allow the erosion of all fine particles. Specimens were subjected to a seepage flow in the downward direction or horizontal direction under multistage hydraulic gradients.

Test Results and Discussion

The time evolution of hydraulic conductivity and erosion rate are shown in Figures 3 and 4, respectively. Both soils appear more permeable under horizontal flow.

It is worth stressing that for specimen of soil B under horizontal flow, the hydraulic conductivity rapidly exceeds 5 10^{-3}m.s^{-1}, even if the erosion rate is lower than 10^{-4} kg.s^{-1}.m^{-2}. Whereas under vertical flow, an erosion rate higher than 4 10^{-4} kg.s^{-1}.m^{-2} appears necessary to observe an increase of the hydraulic conductivity. After tests, specimens were divided in several layers in order to measure the post suffusion gradation. These measurements showed that under vertical flow, the loss of fine particles is larger in the top part (i.e. upstream part) of the specimens in comparison with the middle and downstream parts. Under horizontal flow, the loss of fine particles appears larger in the top part of specimens, but in the bottom part of specimens, the percentage of fine exceeds the initial percentage of fine.

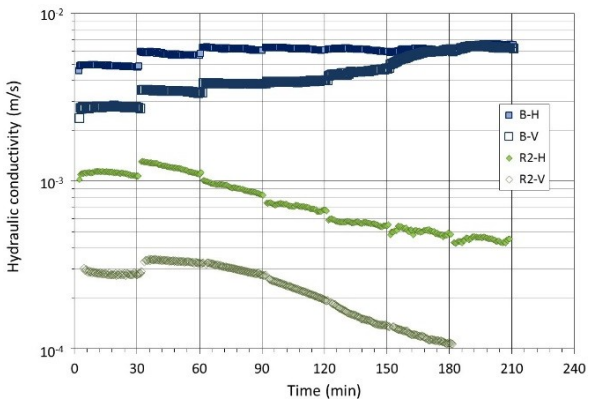

Figure 3: Evolution with time of hydraulic conductivity

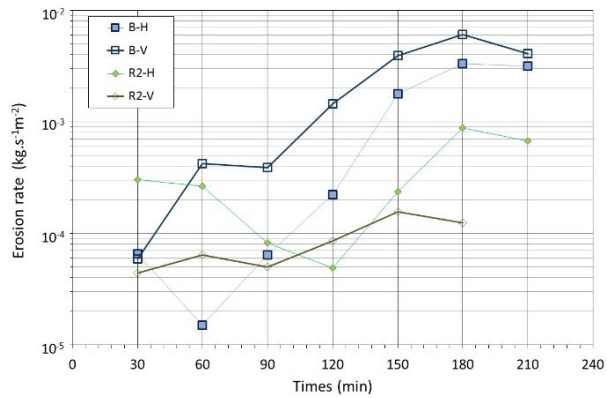

Figure 4: Evolution with time of erosion rate

The instantaneous power dissipated by the water seepage is measured and by time integration, the expended energy is computed until reaching the steady state (i.e. when hydraulic conductivity tends to stabilize and the erosion rate tends to decrease). For a same test duration the cumulative eroded dry mass and the erosion resistance index I_α are determined (Marot et al. 2016). For soil B under vertical flow, I_α is equal to 3.8, whereas I_α is equal to 4 under horizontal flow. For soil R2 under vertical and horizontal flows, I_α is equal to 4.3 and 4.4, respectively. In consequence these soils appear slightly more resistant under horizontal flow.

Two specimens composed of a layer of soil R2 above a layer of soil B were also tested under both flow directions. For the test under horizontal flow, inlet and outlet ports are positioned at the layer of soil B. Figure 5 shows the cumulative dry loss mass versus the cumulative expended energy. It can be noted that under horizontal flow, the evolution for the two layer specimen is quite similar to the soil B under horizontal flow ($I_\alpha = 4$). On the contrary, under vertical flow, the evolution for the two layer specimen is quite similar to soil R2 and $I_\alpha = 4.6$.

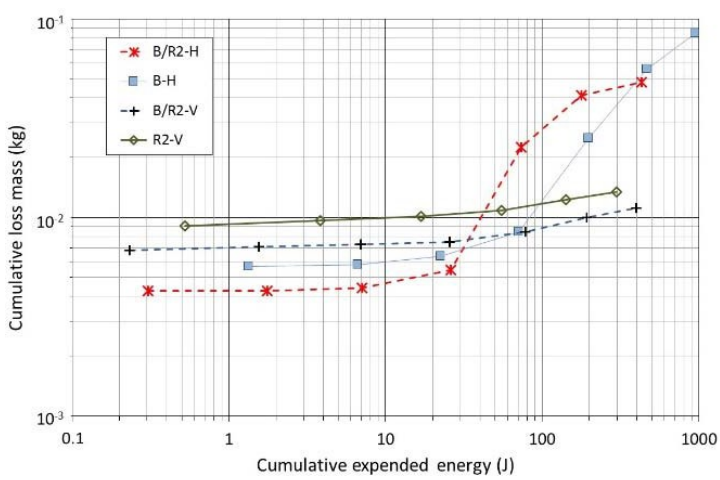

Figure 5: Cumulative dry loss mass versus cumulative expended energy

Conclusion

All these results show that suffusion induces heterogeneities in specimens which depend on the flow direction. Finally the opportunity provided by the apparatus to select the flow direction permits to avoid an overestimation of the soil resistance.

Acknowledgments

The authors thank the company IMSRN, the Ministry of Education and Training of Vietnam, the University of Danang, Vietnam, for providing financial support for this work.

References

Chang D.S., Zhang L.M. (2013). Extended internal stability criteria for soils under seepage. Soils and Foundations, 53(4): 569-583

Kenney T. C., Lau D. (1985). Internal stability of granular filters. Canadian Geotechnical Jal, 22(2): 215-225.

Marot D., Rochim A., Nguyen H.H., Bendahmane F., Sibille L. (2016). Assessing the susceptibility of gap graded soils to internal erosion: proposition of a new experimental methodology. Nat. Hazards, 83(1): 365-388. DOI 10.1007/s11069-016-2319-8.

Patent (2018). System and process of soil erosion measurement. 18209007.6. – 1001. European Patent Office.

EWG-19 Influence of Flow Direction on Suffusion Development

Your Notes:

EWG-20 Numerical and Experimental Investigations of the Mechanical Contribution of Fine Particles in Soils in Relation with Suffusion

A. Wautier[1*]; T. K. Nguyen[1]; R. A. Hosn[1 3]; C. D. Nguyen[1]; N. Benahmed[1]; St. Bonelli[1]; F. Nicot[2]; P. Philippe[1]

1. Université Aix Marseille, Irstea UR RECOVER, Aix-en-Provence, France
2. Université Grenoble Alpes, Irstea UR ETGR, Grenoble, France
3. Université Grenoble Alpes, L3SR, Grenoble, France
* antoine.wautier@irstea.fr

Keywords: suffusion, mechanical stability, fine particles, triaxial test, suffusion permeameter, DEM, second order work criterion

Abstract

Suffusion is the selective erosion of the finest particles of a granular material subjected to an internal flow. Among the four types of internal erosion and piping processes identified today, suffusion still needs further research efforts. Indeed, the driving mechanisms at the microscale are still poorly understood as well as the consequences of microstructure changes on the overall mechanical behaviour. This communication summarizes some of the recent outcomes of four PhD theses focusing on the role of fine particles with respect to the mechanical behaviour of soils subjected to suffusion [1, 6, 7, 11]. Among those four doctoral works, two were only experimental, one was purely numerical and one includes both experiments and numerical simulations. These theses were done in collaboration with L3SR-Grenoble, Ecole Centrale de Nantes and IUSTI Marseille.

Following a flooding episode on the Rhone River in France, the mechanical behavior of silty sand samples collected close to a dike breach has been investigated experimentally by means of triaxial test. The obtained results suggest that a strong contractive behavior of the material is a necessary condition for the existence of mechanical instability. In addition, it has been shown that sample failure is only observed when an appropriate direction of stress increment is considered [6]. These experimental observations are consistent with the concept of bifurcation domain intimately linked to the second order work introduced by Hill [5]. A material characterized by its stress and microstructure state is in its bifurcation domain if at least one incremental loading direction leading to the vanishing of the second order work exists. For such a material, failure (in the sense that the sample cannot withstand the prescribed boundary conditions) will occur only for specific incremental loading direction. Additional test results obtained on mixtures of sand with fines show that a removal of fine particles possibly caused by suffusion favors the occurrence of instability in dikes provided that the inter-granular void ratio (i.e. the void ratio computed only on the coarse particles) remains constant [3].

These results conducted on non-eroded samples have been confirmed thanks to a recently developed suffusion permeameter used to carry out suffusion tests on widely-graded cohesionless soils under controlled hydraulic conditions [7,8]. Drained and undrained triaxial tests of eroded and non-eroded soils confirmed that, when suffusion does not involve significant settlement (i.e. when the inter-granular void ratio remains fairly constant), or the fines removal is not compensated by the settlement, a peak stress reduction is observed for drained and undrained triaxial tests. Conversely, it has been shown that a reduction in the inter-granular void ratio, can lead to a non-modification or less reduction in the peak stress [2, 7]. As a result, the mechanical consequences of suffusion may not always be detrimental for the material.

These same results have also been investigated numerically with the use of discrete element modelling (DEM). With use of the second order work criterion, the particular role played by rattlers has been investigated in detail. It has been shown that rattlers contributed to the mechanical stability of granular materials by controlling the intensity of the plastic deformation and by controlling the non-associated direction of the flow rule in granular materials [9]. Thanks to a recent fluid/grain pore scale finite volume (PFV) coupling scheme [4], the suffusion process has been investigated numerically at the representative elementary volume scale. Based on a simplified one-way coupling scheme, a particle removal was first used to mimic the effect of suffusion on the microstructure of granular materials [2]. The mechanical

behavior of such eroded samples was assessed in drained triaxial tests. As in the experiments, the equivalent void ratio was shown to control the mechanical response. For less widely graded samples, two way coupling DEM/PFV simulations were conducted and micromechanical analyses demonstrated that clogging and erosion have respectively a stabilizing and destabilizing effect in granular materials [10].

Overall, these recent studies proposed a change in paradigm in the sense that the concept of mechanical stability was preferred to the concept of internal stability to analyze the consequences of an internal fluid flow in granular materials. Both the experimental and numerical work demonstrated ambivalent consequences of suffusion depending whether settlement or clogging occur, due to a competition between fine erosion and settlement . It has also been shown, that post suffusion failure requires an incremental loading in some very specific directions.

References

[1] Aboul Hosn R., 2017. Suffusion and its effects on the mechanical behavior of granular soils: numerical and experimental investigations. PhD thesis, Université Grenoble Alpes.

[2] Aboul Hosn R., Sibille L., Benahmed N. and Chareyre B., 2018. A discrete numerical model involving partial fluid-solid coupling to describe suffusion effects in soils. Computers and Geotechnics, 95:30–39.

[3] Benahmed N., Nguyen T. K., Hicher P. Y. and Nicolas M., 2015. An experimental investigation into the effects of low plastic fines content on the behaviour of sand/silt mixtures. European Journal of environmental and civil engineering, 19(1), 109-128.

[4] Chareyre B., Cortis A., Catalano E., Barthélemy E., 2012, Pore-scale modeling of viscous flow and induced forces in dense sphere packings. Transp. Porous Media 94(2), 595–615.

[5] Hill R., 1958. A general theory of uniqueness and stability in elastic-plastic solids. Journal of the Mechanics and Physics of Solids, 6(3):236–249.

[6] Nguyen K. T., 2014, Experimental study of the unstable behavior of silty sand: application to flood protection dikes. PhD thesis, Aix-Marseille Université.

[7] Nguyen C. D., 2018. Experimental study of the impact of suffusion erosion on the physical and mechanical properties of soils. PhD thesis, Aix Marseille Université.

[8] Nguyen C. D., Benahmed N., Andò E., Sibille L., Philippe P. 2019. Experimental investigation of microstructural changes in soils eroded by suffusion using X-ray tomography, Acta Geotechnica, 14(3), 749-765.Wan R., Nicot F. and Darve F., 2016. Failure in Geomaterials, a contemporary treatise. ISTE/Elsevier.

[9] Wautier A., Bonelli S. and Nicot F., 2019. Rattlers contribution to granular plasticity and mechanical stability. International Journal of Plasticity, 112:172–193.

[10] Wautier A., Bonelli S. and Nicot F., 2018 Flow impact on granular force chains and induced instability. Physical Review E, 98(4):042909.

[11] Wautier A., 2018. Micro-inertial analysis of mechanical instabilities in granular media, application to internal erosion. PhD thesis, Aix Marseille Université.

EWG-20 Numerical and experimental investigations of the mechanical contribution of fine particles in soils in relation with suffusion

Your Notes:

EWG-21 Internal Instability Testing of Widely-Graded Materials with Oversize Particles

V. Ganapathiraman[1]; J. Fannin[2]

Dept. of Civil Engineering, Univ. of British Columbia, 6250 Applied Science Lane, Vancouver BC, Canada
[1] *E-mail: gv1134@mail.ubc.ca*
[2] *E-mail: jonathan.fannin@ubc.ca*

Introduction

The phenomenon of internal instability is poorly understood, both with reference to the principles of mechanics, and with regard to our ability to model the consequent material behaviour. It is necessary to acquire good quality laboratory data, at the element scale, to inform our understanding of the phenomenon. Current experimental studies have focused on select gap-graded materials that are susceptible to internal instability. However, the materials used in construction of earth dams, and present in the foundations of those dams, are generally widely-graded with a particle size range from cobbles/boulders to silt/clay. This study explores the challenges in testing widely graded materials for internal instability in a laboratory setting, with specific reference to minimum size of test specimen and the maximum permissible grain size.

Minimum specimen size for laboratory testing

The test specimen needs to be sufficiently large, relative to the size of its largest particles, to avoid any significant influence of size-scale effects on the specimen response. In general, the minimum specimen size is determined with reference to the type of test (eg. as the permeability of the soil depends on its porosity, the specimen size for permeability test should be chosen such that the porosity is uniform throughout the cross-section of the specimen). The minimum specimen size for testing soils is generally expressed as a ratio (D/d) of the diameter of the specimen (D) to the maximum size of the particles (d). For example, ASTM standards specify that the D/d ratio should be kept above 6 for shear tests and permeability tests with flexible wall device, and 8 to 12 for permeability tests with rigid wall (ASTM D2434-68, 2006; ASTM D5084-16a, 2016; ASTM D7181-11, 2011). These ratios are stipulated largely from past experiences of previous researchers, and are generally accepted by the engineering community.

The main concern in testing soils with flow of fluids is the non-uniformity of specimen porosity. In a cylindrical specimen there is a region of larger porosity at the circumferential boundary wall. The extent of this region, with respect to the specimen size, diminishes as the D/d ratio increases. Experiments conducted on mono-sized spheres in rigid-walled cylindrical containers reveal that the porosity, and consequently the permeability, become almost equal to that of a container of infinite diameter when the D/d ratio is more than 10 (Chu and Ng, 1989). However, it is impossible to completely eliminate the region of higher porosity near the wall, as observed by Dudgeon (1967): interpretation of test data with separation of flow through a central core region, from flow through the wall region, established an error of 15% to 5% in the measured hydraulic conductivity as the D/d ratio increases from 5 to 250. These observations are pertinent to uniform gradations, and a lower D/d ratio can be adopted for widely-graded soils, such as those used in earth dams. However, the literature is still lacking a well-accepted criterion for minimum specimen size for such soils.

Since internal instability testing involves flow of water through the soil specimen, it is necessary to minimize this wall effect. In the absence of a relevant criterion for specimen size, it seems reasonable to restrict the maximum size of the particles to approximately 1/10th of the diameter of the specimen. The approach warrants verification by experimentation, in the expectation that a smaller D/d ratio may be permissible for widely-graded soils in a flexible wall permeameter.

Modifying the gradation for internal instability testing

It is challenging to test widely-graded materials in a laboratory because of the presence of what may be termed 'oversize' particles. The specimen size can be increased, but not beyond a practical range. Adopting a flexible boundary reduces the wall effects, but not completely, because during specimen reconstitution the boundary remains rigid and thus it may introduce some degree of order to the otherwise random assembly of particles. Therefore, modifying the gradation of the material appears to provide a pragmatic approach for internal instability testing. The

following three methods are available to modify the particle size distribution of a test material: (i) parallel gradation, (ii) scalping, and (iii) scalping-and-replacement. The average gradation of the zoned Bennett Dam transition material (Morgan and Harris, 1967), and the resulting curves obtained with each of these three methods, is depicted in Figure 1.

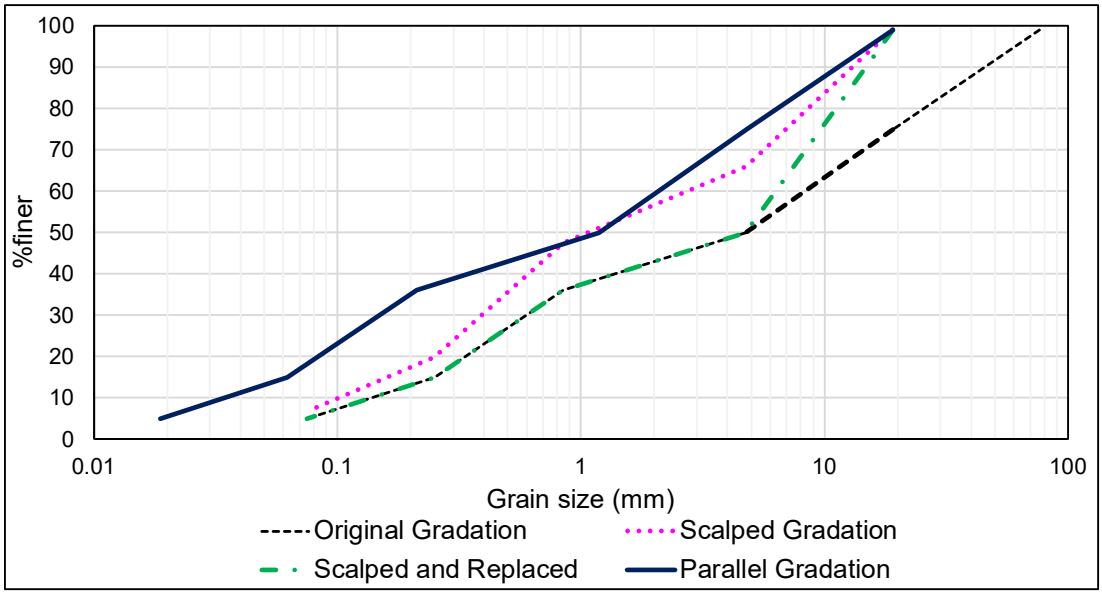

Figure 1. Original and modified gradations of W.A.C. Bennett Dam transition material from Morgan and Harris (1967)

Internal instability testing involves testing for two constraints: (i) a geometric constraint, and (ii) a hydromechanical constraint (Li and Fannin, 2012). The geometric constraint determines whether the soil has the potential for internal instability. This generally depends on the shape of the gradation curve. The parallel gradation method would appear the most appropriate for evaluating the potential for internal instability, because the shape of the gradation curve is preserved in its entirety. However, the introduction of a significant fines content, for a widely-graded test material, renders the approach unacceptable.

In the scalping method, 'oversize' particles are simply removed from the soil. This action modifies the entire shape of the gradation curve, rendering it unsuitable for internal instability testing. Thus, the method that appears best-suited for testing widely-graded materials is the scalp-and-replace method. It involves removing the 'oversize' particles, and replacing them with relatively smaller particles in a select sieve-size range. The action of replacement maintains the original shape of the gradation curve over a significant portion of the size-range. It is appealing for internal instability testing because the 'controlling constriction size' that influences the migration of finer particles depends more on the fine-fraction component than the coarse-fraction of the soil (Kenney et. al.1985). As a qualifying comment, some inherent limitations of the scalp-and-replacement method are recognized and discussed.

References

ASTM D7181-11 (2011). Method for Consolidated Drained Triaxial Compression Test for Soils. West Conshohocken, PA; ASTM International. doi: https://doi.org/10.1520/D7181-11

ASTM D5084-16a (2016). Standard Test Methods for Measurement of Hydraulic Conductivity of Saturated Porous Materials Using a Flexible Wall Permeameter. West Conshohocken, PA; ASTM International. doi: https://doi.org/10.1520/D5084-16A

ASTM D2434-68 (2006). Standard Test Method for Permeability of Granular Soils (Constant Head) (Withdrawn 2015). West Conshohocken, PA; ASTM International. doi: https://doi.org/10.1520/D2434-68R06

Chu, C. F., and Ng, K. M. (1989). Flow in packed tubes with a small tube to particle diameter ratio. *American Institute of Chemical Engineers Journals*, *35*(1), 148-158.

Dudgeon, C. R. (1967). Wall effects in permeameters. *Journal of the Hydraulics Division*. *93*(5), 137–148.

Kenney, T. C., Chahal, R., Chiu, E., Ofoegbu, G. I., Omange, G. N., & Ume, C. A. (1985). Controlling constriction sizes of granular filters. *Canadian Geotechnical Journal*, *22*(1), 32-43.

Li, M., and Fannin, R. J. (2012). A theoretical envelope for internal instability of cohesionless soil. *Géotechnique*, *62*(1), 77-80.

Morgan, G. C., and Harris, M. C. (1967). Portage Mountain dam: II. Materials. *Canadian Geotechnical Journal,* 4(2), 142-166.

EWG-21 Internal Instability Testing of Widely-Graded Materials with Oversize Particles

Your Notes:

EWG-22 Hydro-Mechanical Commissioning of a Novel Large-Scale Triaxial Permeameter (TX-P) for Testing of Widely-Graded Embankment Soils

K.A. Crawford-Flett,
Quake Centre, University of Canterbury, New Zealand.
Email: kaley.crawford-flett@canterbury.ac.nz
M.E. Stringer; S.D. Rees
Department of Civil and Natural Resources Engineering, University of Canterbury, New Zealand

Introduction

This extended abstract summarises the design and commissioning of a novel dynamic triaxial permeameter (TX-P) device for the testing of widely-graded embankment soils under a range of mechanical and hydraulic loading conditions. Increasingly, research needs of the dam engineering community focus on the hydromechanical manifestation of internal instability, in addition to an existing understanding of geometric (gradation-based) susceptibility of soils (e.g. Garner and Fannin, 2010; Crawford-Flett and Haskell, 2016). Specifically, internal erosion mechanisms do not manifest in all susceptible soils, including many operational dams that do not meet modern geotechnical design criteria by virtue of state-of-practice at the time of construction. Rather, the onset and progression of erosion is understood to be a function of combined hydraulic and mechanical (hydromechanical) factors as well as material susceptibility factors. In terms of mechanical factors, a significant knowledge gap concerns the cumulative impact of seismic events on the manifestation of internal erosion in aging dams.

The University of Canterbury (UC) TX-P was assembled on-site in August 2018. The TX-P enables hydraulic, mechanical, and hydromechanical testing of challenging New Zealand embankment materials including widely-graded soils of volcanic, glacial and alluvial origins. The device has been designed for investigations concerning: (1) hydromechanical factors governing the onset and progression of internal erosion mechanisms, including simulated seismic loading, and (2) the mechanical and hydraulic behaviour of soils modified by internal erosion processes. Initial testing programmes will focus on mechnisms of internal instability, specifically suffusion and suffosion; however, the authors acknowledge that other mechanisms of internal erosion (e.g. backward erosion, filter compatibility, defect erosion, contact erosion) will be implicated in experiments concerning particle migration.

A Triaxial Permeameter for hydromechanical testing: device design and capabilities

The TX-P is a custom device, manufactured by GCTS in Arizona, USA, based on a modified STX-600 Large Scale Dynamic/Stress Path Soil Triaxial System. The University of Canterbury TX-P provides a specialised seepage testing facility (Figure 1a), accommodating: (1) large-diameter (300 mm) test specimens, (2) monotonic triaxial and dynamic (simulated seismic) loading capability, (3) conventional permeameter (seepage) capability, (5) volume change measurements in unsaturated or transient flow conditions using a double-walled cell configuration and Volume Change Device (VCD), (6) performance testing of internally unstable soils under downward seepage flow conditions, using a base pedestal design that permits transportation of potentially mobile soil fractions from the bottom specimen boundary.

Prior to specific hydromechanical testing, specimens are reconstituted using a moist-tamping method, to a maximum height to diameter ratio of 2:1 (Figure 1b). Following reconstitution, specimens are installed in the triaxial cell, saturated using backpressure methodology (including CO2 dosing, where required), and consolidated incrementally over a period of hours to weeks depending on soil properties.

Triaxial mechanical loading (steady-state triaxial and/or user-defined dynamic axial loading) and unidirectional hydraulic loading can be imposed sequentially or concurrently. The TX-P device permits direct servo-control of stress and strain (axial deformation and volume change) via transducer feedback. Seepage can be imposed using head-control or volume-control principles. Eroded particles released from the base of the specimen can be collected at the completion of the testing sequence.

Commissioning and verification of the TX-P device

Commissioning and verification of the novel TX-P device involves three distinct phases, using specific materials and loading conditions to ensure independent verification of device capabilities. Firstly, the permeameter capability will be verified through testing of uniform glass bead specimens, providing measurements of seepage flow rate to enable the derivation of hydraulic conductivity. Secondly, conventional triaxial testing capabilities will be verified through monotonic and cyclic testing of washed New Brighton sand, using standard triaxial testing procedures established for smaller triaxial devices in the UC laboratory. Finally, the verification of hydromechanical testing capability for internally unstable soils will be undertaken using gap-graded glass bead specimens, initially, the 'GB-40' glass bead gradation reported in a number of comprehensive international studies (e.g. Moffat and Fannin, 2006; Sail et al. 2011). All commissioning materials have been selected to replicate, or compare against, descriptive test programmes reported in the international literature.

Figure 1. (a) Main TX-P laboratory (High Pressure Unit not shown) and (b) reconstituted specimen under vaccum prior to installation in cell.

Conclusions and future work

A new and novel large triaxial permeameter (TX-P) has been designed and manufactured specifically to address concerns of the seismic dam engineering community in New Zealand, while complementing and extending existing international research on the hydromechanical factors governing internal erosion mechanisms. Following commissioning and verification of the TX-P device, experimental testing will focus on widely-graded dam fill materials. Parametric outputs will serve as a basis for understanding the hydromechanical factors governing performance of earth dam materials in New Zealand's unique geologic and geomorphic (seismic) environment. The aims of the experimental research are intended to enhance local and international understanding of the performance of earthfill soils subject to seepage flows in both steady-state and non-static conditions.

Acknowledgements: The authors gratefully acknowledge the support of the University of Canterbury Quake Centre and industry partners, along with the Department of Civil and Natural Resources Engineering at the University of Cantebury. Guidance from dam owners' engineers (particularly Genesis Energy, Meridian Energy, Mighty River Power, and Trustpower) has been crucial to the success of the research to date.

References

Crawford-Flett, K.A., Haskell, J.J.M. (2016). Assessing the risks associated with internal erosion phenomena in aging embankment dams: a New Zealand perspective. International Conference on Scour and Erosion, Oxford, UK.

Garner, S.J. & Fannin, R.J.. (2010). Understanding internal erosion: A decade of research following a sinkhole event. International Journal on Hydropower and Dams. 17. 93-98.

Moffat R., Fannin R.J., (2006). A large permeameter for study of internal stability in cohesionless soils", Geotechnical Testing Journal, 29:4. p. 1-7.

Sail, Y., Marot, D., Sibille, L., & Alexis, A. (2011). Suffusion tests on cohesionless granular matter, European Journal of Environmental and Civil Engineering, 15:5, 799-817.

EWG-22 Hydro-Mechanical Commissioning of A Novel Large-Scale Triaxial Permeameter (TX-P) for Testing of Widely-Graded Embankment Soils

Your Notes:

EWG-23 Inflow Boundary Conditions in Triaxial Permeameter Testing

S. Ataii[1]; J. Fannin[2]

Department of Civil Engineering, Univ. of British Columbia, 6250 Applied Science Lane, Vancouver, BC, Canada

[1] Email: sara.ataii@alumni.ubc.ca

2 Email: jonathan.fannin@ubc.ca

Introduction

Internal instability occurs when seepage flow washes fine particles through the network of pore spaces and associated pore constrictions in a grain assembly. To investigate the mechanical behavior of a test specimen that has experienced internal instability, a triaxial permeameter apparatus was designed and developed at UBC (Fannin et al. 2019). In comparison with the test procedure used in conventional triaxial testing (ie. specimen reconstitution, saturation, consolidation, and shear), the presence of seepage stage(s) prior to shear in triaxial permeameter testing (ie. specimen reconstitution, saturation, consolidation, seepage, and shear) imposes special requirements on the inflow/outflow boundary of the test specimen. More specifically, water enters the specimen through an inflow boundary, and exits the specimen (carrying some fine particles) through an outflow boundary. This study examines the hydraulic performance of a custom-designed inflow boundary for downward seepage testing (top cap), in the UBC triaxial permeameter apparatus (UBC-TX-P).

Inflow Boundary in Downward Seepage Testing

The inflow boundary for downward flow (the top cap) has four functions: (1) to transmit the force of the loading rod as a uniform contact stress on the specimen; (2) to introduce uniform seepage flow to the specimen; (3) to provide for an accurate measurement of pore water pressure at the inflow boundary; and, (4) to prevent any upward movement of fine particles into the top cap. The general design of a top cap, as the inflow boundary for testing with downward seepage, is typically composed of point-source inlet(s), a flow-distributor layer (which can be a hollow-profiled chamber (Ke and Takahashi 2014), a hollow chamber filled with porous medium (Mehdizadeh 2018; Marot et al. 2017), or a layer of geotextile (Chang and Zhang 2011)), and a rigid perforated plate with/without a fine wire mesh in direct contact with the specimen. Informed by previous studies, and with the goal of having a top cap that performs over a wide range of flow rates, a configuration of top cap was designed for the UBC-TX-P (see Fig. 1), and its performance was tested over a wide range of seepage flow (1 to 15 cm^3/s).

UBC-TX-P Inflow Boundary Design

The top cap includes: (1) two primary inlet ports that yield four secondary inlet ports; (2) a flow-conditioning chamber; (3) a primary rigid perforated plate (opening size: 0.8 mm, open area: 20%); (4) a fine wire mesh on the downstream side of the primary perforated plate (with opening size smaller than the finest material particle size); and, (5) a location of pore water pressure measurement at the center of the primary perforated plate. The flow-conditioning chamber comprises an upper hollow chamber, and a lower chamber filled with three layers of 9-mm diameter glass beads, separated by a 5-mm thick perforated plate (opening size: 0.8 mm, open area: 20%). The design concept is based on flow from the four secondary inlet ports mixing in the upper hollow chamber. Thereafter, the flow experiences three stages of conditioning as it passes through the secondary perforated plate, the lower chamber with glass beads, and the primary perforated plate, respectively, before entering the test specimen.

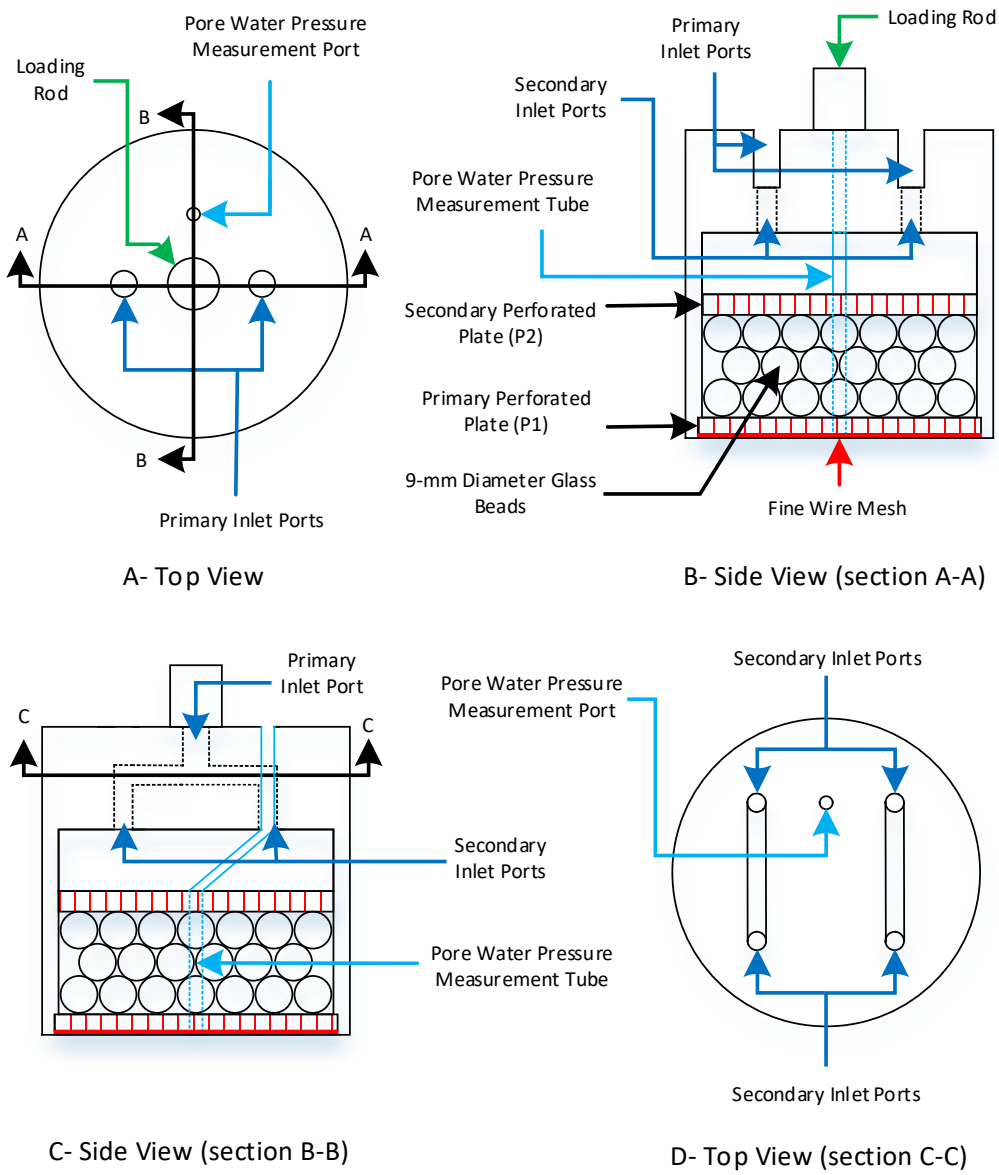

Figure 1. Schematic illustration of UBC-TX-P inflow boundary (top cap)

UBC-TX-P Inflow Boundary Performance

A relatively simple experimental setup was used to evaluate the hydraulic performance of the top cap. The setup enabled colored-water to be introduced to the top cap, at a constant rate of flow (Q) that was varied across a range of interest. Visual observations were made of the flow regime is at the exit of the primary perforated plate, by means of testing a 'dummy' top cap made of acrylic. Illustrative results (see Fig. 2) are presented for a test with Q = 1.25 cm^3/s. Various configurations of flow-conditioning chambers were tested in a parametric study. Results of the study established the suitability of the configuration shown in Fig. 1 for development of a uniform velocity distribution in outflow from the primary perforated plate with fine wire mesh, over the approximate flow range of 1 to 15 cm^3/s. Thus, it is proposed to adopt this design for the main test program.

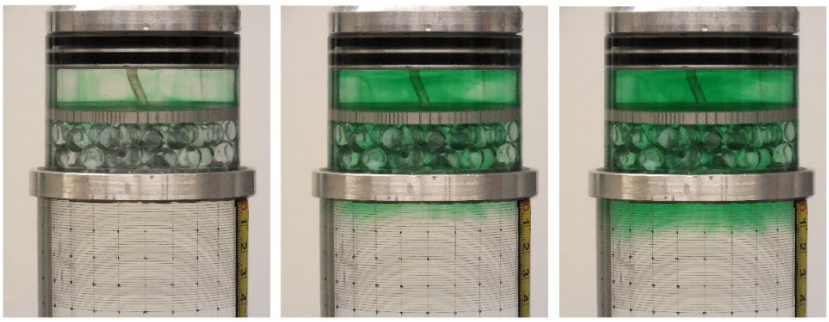

Figure 2. Development of the flow through top cap and at the exit of the primary perforated plate (Q = 1.25 cm3/s)

References

Chang, D. S., & Zhang, L. M. (2011). A stress-controlled erosion apparatus for studying internal erosion in soils. Geotechnical Testing Journal, 34(6), 579-589.

Fannin, J., Slangen, P., Ataii, S., McClelland, V., & Hartford, D. (2018, September). Erosion of zoned earthfill dams by internal instability: laboratory testing for model development. In European Working Group on Internal Erosion, Milan, Italy, 34-49. Springer, Cham.

Ke, L., & Takahashi, A. (2014). Triaxial erosion test for evaluation of mechanical consequences of internal erosion. Geotechnical Testing Journal, 37(2), 347-364.

Marot, D., Bendahmane, F., Andrianatrehina, R., & Gelet, R. (2017). Large triaxial device for suffusion erodibility and mechanical behavior characterization of coarse soils. European Working Group on Internal Erosion in Embankment Dams & their Foundations, Delft, Netherlands, 123-132.

Mehdizadeh, A. (2018). Multi scale investigation of post-erosion mechanical behaviour of granular material (Doctoral dissertation, Swinburne University of Technology, 350 pp.).

EWG-23 Inflow Boundary Conditions in Triaxial Permeameter Testing

Your Notes:

EWG-24 Experimental Development for Multi-Plane Access to Investigate Local Suffusion within Internally Erodible Granular Media

E. T. Bowman
University of Sheffield, Sheffield, United Kingdom
Email: e.bowman@sheffield.ac.uk
N. Sanvitale; J. A. Black
University of Sheffield, Sheffield, United Kingdom

Introduction & Methodology

Internal erosion in granular soils is a complex phenomenon representing one of the greatest hazards for water retaining structures such as embankment dams and levees. When soils are subject to internal instability, fine particles are detached from the granular skeleton under seepage flow and eroded away within the porous media. In this study we describe preliminary tests from a transparent soil permeameter that has been developed to study the fundamental particle scale mechanisms that occur during internal erosion in granular materials.

The experimental apparatus consists of a 100mm square rigid walled permeameter cell in which flow is directed upward via a constant head applied at the base using an adjustable header tank (Hunter & Bowman, 2018) in a similar set up as used to investigate suffusion by Skempton & Brogan (1994). Flow from the top of the cell is recirculated back into a reservoir and then pumped back into the header tank. An immersion fluid is used that is refractively matched to the borosilicate glass particles used in the experiments. A laser sheet can be applied to the side of the permeameter to illuminate a plane within it at a selected depth. A high speed camera and lens are used to record particle and fluid movements within the plane in question. Both the laser and camera are mounted on micrometer stages so that specific planes of interest can be accessed and returned to with precision over long-running tests conducted at increasing hydraulic gradient (Figure 1).

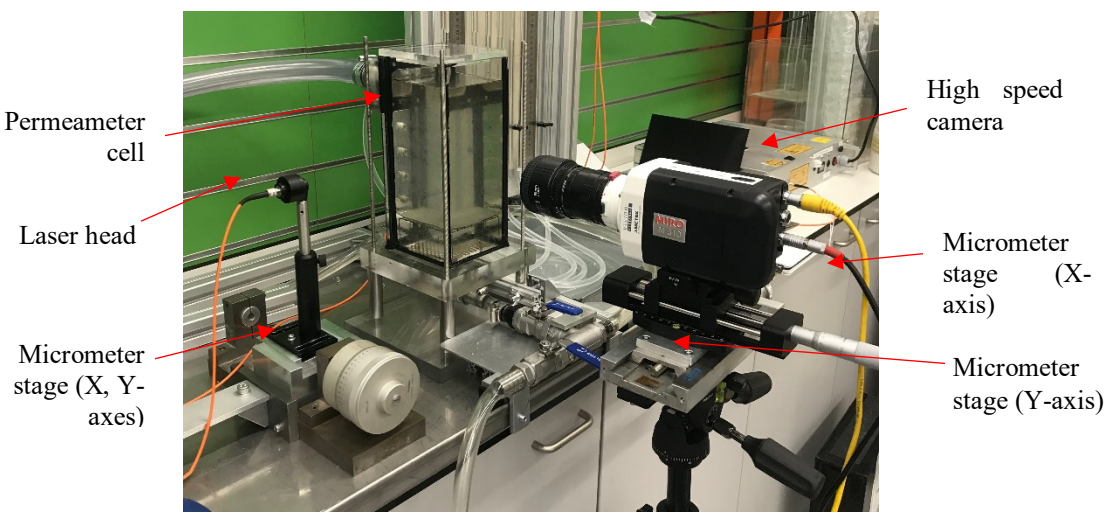

Figure 1. Transparent permeameter set up with micrometer stages for camera and laser

The physical properties of the granular mixture have been selected such that the behaviour matches that of soil particles and water (Table 1). In these experiments, in order to measure the fluid velocity field in a vertical plane, glass microspheres, with very small particle size and specific gravity similar to that of the fluid are seeded into the fluid.

Table 1: Solid and fluid properties

	Refractive index	Kinematic viscosity	Specific gravity	Particle size
Immersion oil	1.4715 (at 25 °C)	16 (at 25 °C)	0.846	-
Borosilicate glass	1.4718 (at 21 °C)	-	2.23	1-25mm (3mm, 15.5mm here)
Glass microspheres	1.4718 (at 21 °C)	-	0.75	5-30μm

Validation for flow velocity

Here we present results of validation tests for the velocity field measured using Particle Image Velocimetry, PIV (PIVLab software) for a purely fluid system (no particles except microsphere seeds) to give confidence to the approach and enable direct comparison with numerical models. These tests were conducted by examining the whole field of the permeameter (100 mm width) with fluid under upward flow through a dispersal screen and a filter at the base. The overall steady flow rate was determined using a measuring cylinder and stopwatch.

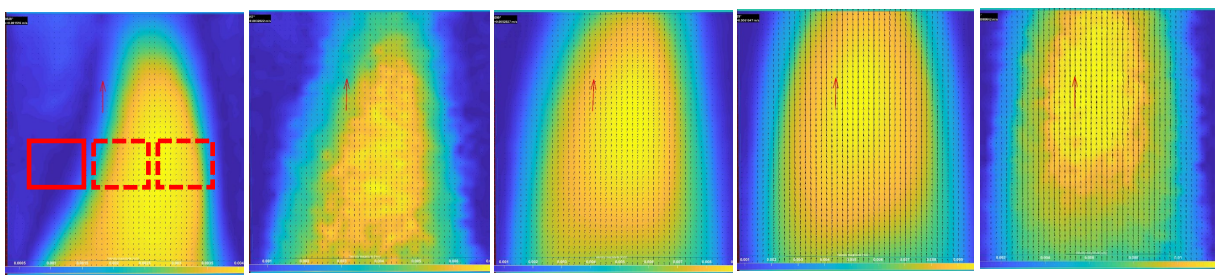

(a) 10mm **(b) 20mm** **(c) 30mm** **(d) 40mm** **(e) 50mm**

Figure 2. Velocity profiles under upward flow from (a) close to the front of the permeameter to (e) the mid-plane. Fluid velocity magnitude (a) to (e) is colour coded from blue (V = 0m/s) to yellow: (a) V = 0.004m/s, (b) V = 0.007m/s, (c) V = 0.009m/s, (d) V = 0.010, (e) V = 0.012m/s.

Results from the PIV analyses were integrated using data obtained over the five slices for a given steady flowrate, and assuming zero velocity at the front and back walls. The comparison of the measured flowrate from the cylinder and that using PIV resulted in a 5% difference. This, coupled with initial outcomes on local fluid velocities determined within stable granular packings (Sanvitale et al, 2018) gives confidence that image analysis can be meaningfully applied to local velocities.

Local flow within internally unstable mixtures

First results for experiments on internally unstable mixtures are presented here. Figure 3 presents three close-up images taken on the left hand side of the permeameter (see inset red square Figure 2a, other positions given as dashed) at depths of 25mm, 37.5mm and 50mm from front face, for an internally unstable mixture of borosilicate particles (70% 15.5mm; 30% 3mm diameter) within a stable flow field. The edges of the particles can seen due to small imperfections on their surfaces, while the tracers are visible as points of light. Images for analysis are taken at three precise locations (left, middle, right) and at these three depths under increasing hydraulic gradient until instability occurs. The influence of the hydraulic gradient on the internal velocity field and hence on the onset of fine movements and detachment are currently the subject of examination.

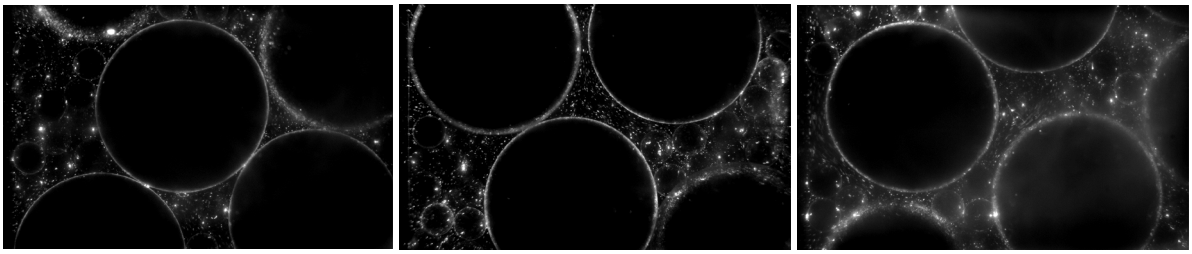

(a) 25mm **(b) 37.5mm** **(c) 50mm**

Figure 3: Images at increasing depth for internally unstable particle packing and fluid tracers. Material is stable under the hydraulic gradient applied.

References

Hunter, R.P. & Bowman, E.T. (2018) Visualisation of seepage induced suffusion and suffosion within internally erodible granular media, *Géotechnique* 60(10), 918-930

Skempton, A. W. & Brogan, J. M. (1994) Experiments on piping in sandy gravels. *Géotechnique* 44(3):449-460.

Sanvitale N., Bowman E.T., Black J.A. (2019) Viewing Fluid Flow Inside a Granular Medium. In: Bonelli S. et al (eds) Internal Erosion in Earthdams, Dikes and Levees. EWG-IE 2018. Lecture Notes in Civ. Eng., 17. Springer.

EWG-24 Experimental Development for Multi-Plane Access to Investigate Local Suffusion within Internally Erodible Granular Media

Your Notes:

EWG-25 Grain Size and Shape in the Glacial Moraine Borrow Source for the Bennett Dam

A. M. Antunes[1]; J. Fannin[2]
The University of British Columbia, Vancouver, Canada
[1] Email: anaysma@mail.ubc.ca
[2] Email: jonathan.fannin@ubc.ca

This study addresses the various grain shapes found in the borrow source for the W.A.C. Bennett Dam. The W.A.C. Bennett Dam is a zoned embankment dam on the Peace River, British Columbia, Canada. Characteristic grain size distribution curves for three of the zoned fill materials are shown in Figure 1 (after Morgan and Harris, 1967). Like many embankment dams in Canada, and other similar northern-climate countries, the zoned fill materials were taken from a borrow location of glacial origin, in this case the Portage Mountain South Moraine.

The geological history of the Portage Mountain South Moraine is described in detail by Rutter (1977). The moraine formed during the last glaciation, around 11.6 thousand years B.P, when a glacier advanced along the Peace River from the Rocky Mountains to the west and terminated between Portage Mountain and Bullhead Mountain. The Peace River used to flow between the two mountains, and at the time of that glacial advance, it was dammed to the east by Laurentide Ice, creating a lake in that area. The glacier is believed to have deposited materials in a glaciolacustrine environment. After it retreated, it left behind the end moraine deposit that would later serve as the borrow source for the Bennett Dam.

The soil of the south moraine is a naturally gap-graded material, a common feature of such glacial deposits. XRD analysis (Kabel et al. 2019) established a low content of clay minerals, comprising kaolinite and illite, which is consistent with the non-plastic fines of the borrow source. The finding suggests the finer fraction of the gradation is a consequence of mechanical processes of degradation, rather than chemical processes of weathering.

The effects of grain shape on the macro-scale mechanical response of soils are extensively reported in the literature, primarily from testing of uniformly graded sands and glass beads. Grain shape has been shown to influence the min-max void ratio, the position of the critical state line, the peak and critical state friction angle of soil, and the susceptibility of a gradation to seepage-induced internal instability (see for example, Cho et al. 2006, Slangen 2015, Yang and Luo 2015, Chang et al. 2018, and Xiao et al. 2018).

The Internal Erosion Research Group at the University of British Columbia (UBC) undertook a field sampling program in October 2018, and collected approximately 2.5 m^3 of soil from the South Moraine borrow area. The sampled materials were in the size range up to 3” (76mm). The material was trucked to UBC, where it has been processed, sieved, and washed for use in the research program using the newly designed and commissioned UBC triaxial permeameter (Fannin et al. 2019).

A grab sample of the South Moraine soil was taken for purposes of grain shape analysis. It was sieved into 9 different sieve-fractions (see Fig. 1), in the size range passing the ¼" and retained on the #200 sieve. The characteristic shape of each fraction was quantified at Imperial College London, using a QICPIC device manufactured by Sympatec GmBH. The device allows for grains to fall freely, with a random orientation, while a series of images are acquired for analysis. The output is a series of values for the sphericity (ratio between the perimeter of a circle with equivalent area of the projection and the perimeter of the projection), the aspect ratio (ratio between minimum and maximum Feret diameter), and the convexity (ratio between the area of the projection and the area of the convex hull) of the grains. One of the perceived advantages of this device, over common microscopy photography coupled with image

analysis, is the random orientation of the grains that is believed to yield a better statistical representation of the grain shape.

The data obtained in this investigation indicate a trend of increasing roundness of the grain shape with increasing size. These objective measurements are consistent with subjective visual assessments of the companion optical microscope images, and digital photographs, of the grains (see Figure 2). A comparison with other standard research sands, and their qualitative description, was made with reference to the findings of Altuhafi et al. (2012). A qualitative assessment of the results indicates the soil of the South Moraine borrow source is angular in the finest fraction and, as the grain size increases, the shape changes to subangular and then to subrounded (see Figure 1).
The results indicate that there is a relation between grain shape and grain size in this soil, which is attributed to geological processes that formed it. The crushing and abrasion suffered by the fragments of bedrock during its transportation by the glacier may be the cause of both the gap-graded characteristic of the soil, and the increase in particle roundness with size. This attribute of the soil will likely have implications for (i) microstructure of the grain assembly (ii) susceptibility to internal erosion of select finer fractions, (iii) critical state parameters and stress-strain behavior of the soil upon shearing, and more generally (iv) numerical analyses, particularly in discrete element modelling of similar glacial materials.

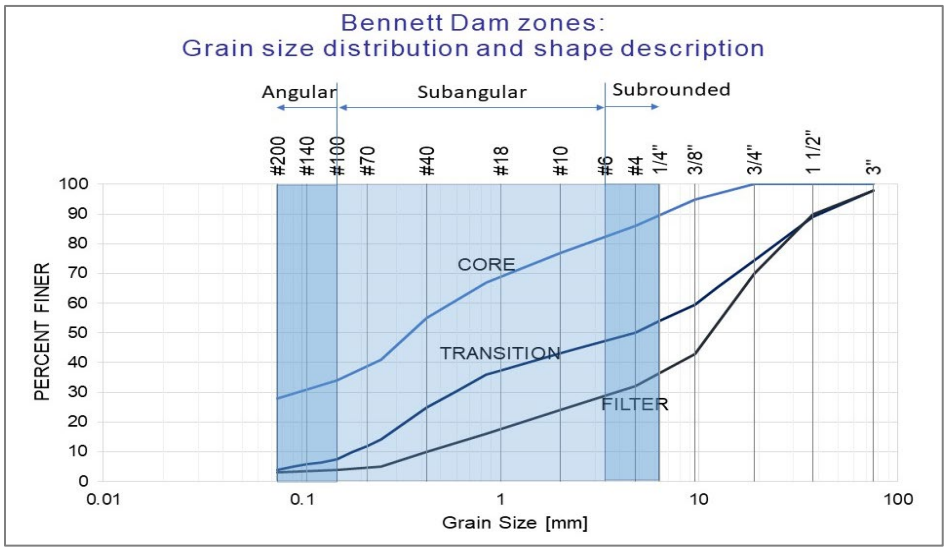

Figure 1. Representative grain size distribution curves for three zones of the W.A.C. Bennett Dam (after Morgan and Harris, 1967).

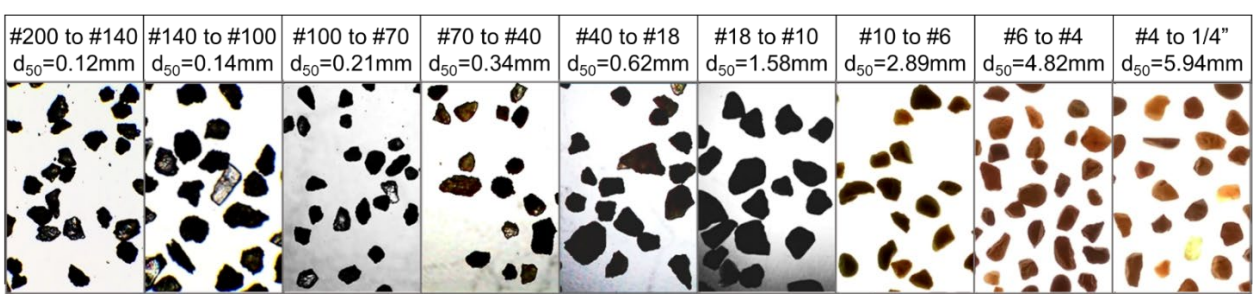

Figure 2. Photographs of samples with different grain sizes obtained with an optical microscope (the six smallest sizes) and a digital camera (the three largest sizes).

Acknowledgements:

The authors would like to express their gratitude to Catherine O'Sullivan, the Imperial College London, for kindly providing access and user support on the QICPIC device.

References

Altuhafi, F., O'Sullivan, C., and Cavarretta, I. 2012. Analysis of an image-based method to quantify the size and shape of sand particles. Journal of Geotechnical and Geoenvironmental Engineering, **139**(8): 1290–1307. doi:10.1061/(asce)gt.1943-5606.0000855.

Chang, C.S., Meidani, M., and Deng, Y. 2018. Role of morphologic indices on the variation of limiting void ratios for uniform sands. Géotechnique Letters, **8**(4): 248–255. doi:10.1680/jgele.18.00087.

Cho, G.-C., Dodds, J., and Santamarina, J.C. 2006. Particle shape effects on packing density, stiffness, and strength: natural and crushed sands. Journal of Geotechnical and Geoenvironmental Engineering, **132**(5): 591–602. doi:10.1061/(ASCE)1090-0241(2006)132:5(591).

Fannin, J., Slangen, P., Ataii, S., McClelland, V., and Hartford, D. 2019. Erosion of zoned earthfill dams by internal instability: laboratory testing for model development. *In* Internal Erosion in Earthdams, Dikes and Levees. *Edited by* S. Bonelli, C. Jommi, and D. Sterpi. Springer International Publishing, Cham. pp. 34–49.

Kabel, J., Pani, E., Czech, E., Lai, J., and Kato, L. 2019. Quantitative phase analysis of two powder samples using the Rietveld Method and X-Ray powder diffraction sata. Report from Dept. of Earth, Ocean & Atmospheric Sciences, The University of British Columbia.

Morgan, G. C., and Harris, M. C. (1967). Portage Mountain dam: II. Materials. Canadian Geotechnical Journal, 4(2), 142-166.

Rutter, N.W. 1977. Multiple glaciation in the area of Williston Lake, British Columbia. Geological Survey of Canada. Bulletin 273,. Available from http://publications.gc.ca/collections/collection_2016/rncan-nrcan/M42-273-eng.pdf.

Slangen, P.H.H. 2015. On the influence of effective stress and micro-structure on suffusion and suffosion. PhD thesis, University of British Columbia, 218p.

Xiao, Y., Long, L., Matthew Evans, T., Zhou, H., Liu, H., and Stuedlein, A.W. 2018. Effect of particle shape on stress-dilatancy responses of medium-dense sands. Journal of Geotechnical and Geoenvironmental Engineering, **145**(2): 04018105. doi:10.1061/(asce)gt.1943-5606.0001994.

Yang, J., and Luo, X.D. 2015. Exploring the relationship between critical state and particle shape for granular materials. Journal of the Mechanics and Physics of Solids, **84**: 196–213. Elsevier. doi:10.1016/j.jmps.2015.08.001.

EWG-25 Grain Size and Shape in the Glacial Moraine Borrow Source for the Bennett Dam

Your Notes:

EWG-26 A Description of Suffusion Kinetics Inspired from Experimental Data

G. Rachel[1*]; K. Alaa[1,2]; M. Didier[1]; N. Nguyen[1]; A. Fino[2]
[1]University of Nantes, Institute GeM, 58 rue Michel Ange, Saint-Nazaire, France
[2]Faculty of Sciences, Lebanese University, Faculty of Sciences, Department of Mathematics, Tripoli, Lebanon.
*rachel.gelet@univ-nantes.fr

Keywords: Internal erosion, Suffusion, Erodimeter, Erosion resistance index

Suffusion is characterized by a migration of the fine particles within a soil under the effect of flow. This complex phenomenon involves simultaneous detachment, transport and possible filtration of the fine fraction. The stakeholder needs in terms of risk management of embankment structures urge researchers to model suffusion at the laboratory scale and at the structure scale. This urge requires relationships that can reproduce the whole development of the suffusion process and that uses suitable parameters in terms of modeling implications.

With the objective to reproduce the kinetics of the suffusion process, three relationships are compared. A new energy-based law, inspired from the energy-based approach (Marot et al. 2012) is proposed that relates the volumetric cumulative eroded mass $\bar{m}_{cum}(\mathrm{t})$ and the volumetric cumulative expended energy $\bar{E}_{cum}(t)$,

$$\frac{\bar{m}_{cum}(\mathrm{t}) - \bar{m}_{sat}}{\bar{m}_{max} - \bar{m}_{sat}} = \left(\frac{\bar{E}_{cum}(t)}{\bar{E}_{max}}\right)^{b(t)} \tag{1}$$

in which $\bar{m}_{sat}$ is the mass lost during saturation phase per unit volume and $b(t)$ is a new parameter that controls the kinetics of suffusion. Small values of $b(t)$ indicate a fast kinetics and conversely. Aside from $\bar{m}_{sat}$ which is initially measured and from $b(t)$ which will be introduced below, the above relationship uses two parameters: the volumetric maximum cumulative expended energy $\bar{E}_{max}$ and the suffusion resistance index I_α by use of the relation $\bar{m}_{max} = 10^{-I_\alpha}\,\bar{E}_{max}$. This relation characterizes the end of suffusion at which the volumetric maximum cumulative eroded mass is measured $\bar{m}_{max}$ (Marot et al. 2012). Since b(t) describes the kinetics of suffusion, it may be related to the power dissipated by the flow which is a key variable to fully describe the hydraulic loading. By looking at eq. (1), the determination of $b(t)$ is constrained by two restrictions:

- First, $b(t)$ should be a dimensionless variable that describes a fast kinetics at the beginning of each loading step, rapidly decreasing towards the end of the step. In that essence, $b(t)$ may be defined as a function of the instantaneous power dissipated by flow $P_{flow}\,(t)$ and of a smoothed value of this power determined based on a moving average method $P_{smoothed}(t)$,

$$b(t) = \frac{P_{smoothed}(t)}{P_{flow}\,(t)} \tag{2}$$

- Second, the volumetric cumulative eroded mass $\bar{m}_{cum}(\mathrm{t})$ should never decrease to remain physically admissible which brings an additional constraint on $b(t)$ to satisfy $\bar{m}_{cum}(t_n) \geq \bar{m}_{cum}(t_{n-1})$ at all times.

It is a common practice to evaluate the relevance of relationship (1) by comparing its prediction with experimental data (Sibille et al., 2015). Moreover, this energy-based law is also compared with two other laws inspired from the shear stress-based approach (Wan and Fell, 2004) and the power-based approach (Sibille et al., 2015). These three relationships are compared against suffusion tests previously performed on seven specimens issued from two cohesionless gap-graded soils (Zhong et al., 2018). For each soil, various seepage lengths and different histories of hydraulic loading are tested. Due to the saturation phase and to the distinctive characteristic of each apparatus, the initial microstructure of each tested specimen differs so that an individual set of parameters is measured for each

specimen. With this individual set of parameters, the shear stress based approach tackles well the initiation of the suffusion process but overestimates the development of the process. On the other hand, both the energy-based law and the power-based law can reproduce reasonably well the evolution of the cumulative eroded mass. Figure 1 presents these results for specimen 4-O.

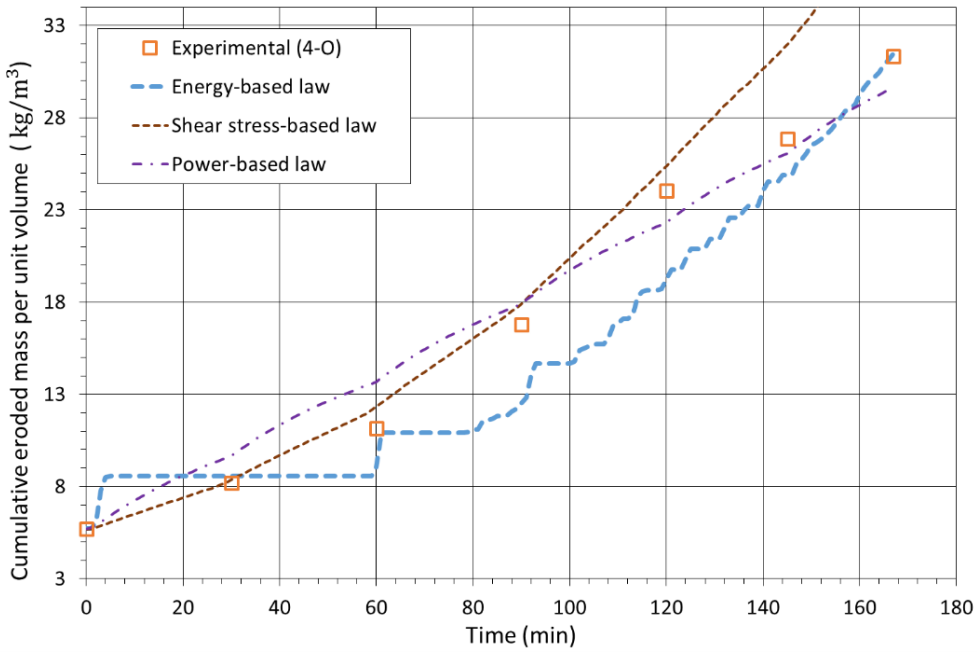

Figure 1: Comparison of the cumulative eroded mass predicted using the shear stress-based law, the energy-based law, and the power based law with the collected mass measured during the experimental test of specimen 4-O.

Finally, the intrinsic quality of each parameter is examined, advantages and drawbacks of each approach are also highlighted. Regarding the shear stress based approach, both introduced parameters are characterized by a noticeable dispersion of their relative error with the flow length. In terms of modeling implication, the use of the power-based approach is complicated by a history term ΔE_v because its computation requires the knowledge of the beginning and the end of each loading step. Although this knowledge is fairly obvious for laboratory specimens tested under multi-stage hydraulic gradient conditions, it can become unclear when considering hydraulic loading conditions in the field. This observation is at the root of the development of the energy-based law. Regarding the energy-based approach, the relative error on the erosion resistance index remains below 18% ensuring that I_α is fairly independent with respect to the flow length and seems to be intrinsic to a soil, at least at the laboratory scale; while the volumetric maximum cumulative dissipated energy $\bar{E}_{max}$ seems to increase linearly with the flow length. This latter trend along with the robustness of eq. (2) towards various loading patterns should be further investigated to validate the relevance of eq. (1) for modelling purposes.

References

Marot, D., Le, V. D., Garnier, J., Thorel, L. and Audrain, P., 2012. Study of scale effect in an internal erosion mechanism: centrifuge model and energy analysis. *European Journal of Environmental and Civil Engineering*, 16(11), 1-19.

Sibille, L., Marot, D. and Sail, Y., 2015. A description of internal erosion by suffusion and induced settlements on cohesionless granular matter. *Acta geotechnica*, 10(16), 735-748.

Wan, C. F., and Fell, R., 2004. Investigation of rate of erosion of soils in embankment dams. *Journal of geotechnical and geoenvironmental engineering*, 130(14), 373-380.

Zhong, C., Le, V. T., Bendahmane, F., Marot, D., Yin, Z.-Y., 2018. Investigation of spatial scale effects on suffusion susceptibility. *Journal of Geotechnical and Geoenvironmental Engineering*, 144(19).

EWG-26 A Description of Suffusion Kinetics Inspired from Experimental Data

Your Notes:

EWG-27 Description of the Pore Network in Granular Media Using the Delaunay Triangulation

N. Nguyen[1*]; H. Taha[1;2]; D. Marot[1]; A. Hijazi[2]; K. Abou-Saleh[2]

[1]GeM Institute, University of Nantes, 58 rue Michel Ange, BP 420, 44606, Saint-Nazaire Cedex, France
[2]MPLAB-Multisciplinary Physics Laboratory, Faculty of Sciences, Lebanese University, Hadat-Baabda, Lebanon
[*]Email: ngocson.nguyen@univ-nantes.fr

Key words: granular filters, pore network, discrete element method, Delaunay triangulation, merging procedure

Abstract

Granular filters are used in earth-filled structures to retain finer base particles that are detached and transported by seepage flow. The effectiveness of a filter depends on several factors, mainly on the geometry of the pore network, in particular the sizes of constrictions, on the sizes of the base particles and on hydraulic loadings. Granular filters are usually designed by using empirical retention criteria that have been developed based on laboratory tests. Many empirical criteria have been proposed, each of which has been developed for a particular range of soils tested in the laboratory [1]. They lack consideration of the micro-structure of the filter material and of main mechanisms at the particle scale such as the transport of base particles through the pore network of the filter and the retention of base particles by constrictions.

Models based on the pore network have been then introduced with the aim to remedy limitations of empirical rules. Most of them make use of idealized pore network inside the filter. Kenney et al. [2] modeled a filter as a stack of plates containing holes which are randomly distributed on a regular grid. According to this pore network, base particles can move along vertical lines but they cannot move laterally. Locke et al. [3] and Shire et al. [4] used a regular cubic network for which each cylindrical connection between two neighboring pores represents a constriction and each pore has six connections with its neighbors. In this model, base particles can move not only vertically but also laterally and the sizes of cylindrical connections are randomly specified according to a constriction size distribution curve. However, the pore network of granular media is far from being this idealized regular cubic one.

We aim to advance this kind of approaches by using the pore network constructed from a virtual granular sample simulated with the Discrete Element Method. To simplify our model, we consider only spherical particles for both base soil and filter. The void space in the filter is partitioned into individual pores and two adjacent pores share a constriction which is defined as the narrowest section of the channel between them. Spherical base particles whose sizes follow a base particle size distribution are inserted to the entrance pores of the network. A base particle is moved from one pore to a neighboring one according to some rule until it is blocked by a constriction whose diameter is smaller than its diameter or until it reaches an exit pore. The key point in this model is the construction of the pore network of the filter.

Different methods have been developed to define the pore network in a granular material such as method based on imaging technique or method based on Delaunay triangulation. The latter one is adopted in our work since the Weighted Delaunay Triangulation (WDT) is very efficient to partition an assembly of spherical particles into tetrahedra, each of which joins four centers of neighboring particles. However, a single pore might be over-subdivided into several smaller pores by the WDT, so adjacent tetrahedra need to be merged together with some criterion to form single pores. To identify adjacent tetrahedra to be merged, an inscribed void sphere is defined for each tetrahedron, which is the largest sphere contained within its void space. Al-Raoush et al. [5] merged two adjacent tetrahedra if the center of the inscribed sphere of a tetrahedron is located inside the inscribed sphere of the other tetrahedron, while Reboul et al. [6] merged two adjacent tetrahedra if their inscribed spheres touch each other. For the latter criterion, the number of merged tetrahedra is limited to avoid the formation of flow paths. Criteria for merging tetrahedra still diverge and need further investigation.

We propose in this presentation a new method for merging adjacent tetrahedra. This method consists in partitioning a granular sample into polyhedral subdomains whose vertices are particle centers. Each subdomain comprises then

neighboring solid particles and the void between them. A void sphere is defined for each subdomain, which minimizes its distance to the solid particles. Each sub-domain must satisfy the following conditions: (i) its void sphere does not intersect adjacent solid particles; (ii) the center of its void sphere is located inside it; and (iii) its void sphere is sufficiently separated from the neighboring ones. We start by using the WDT to subdivide the granular sample into tetrahedra, each of which is considered as a subdomain. We proceed to identify all the sub- domains which do not fulfill the conditions (i) and (ii) and then merge them to their neighboring ones. Whenever two adjacent subdomains are merged, a new void sphere is identified for the newly created subdomain. This pro- cedure, called primary merging procedure, is repeated until all the sub-domains fulfill the two first conditions. It allows us to eliminate all the flat tetrahedra issued from the WDT. However, many void spheres resulting from this procedure still overlap greatly their neighbors, meaning that they might be not sufficiently separated from their neighbors. The spacial separation between two adjacent void spheres i and j with respective diameters di and dj is quantified by a relative overlap γij defined as $\gamma ij = \delta ij / \min(di, dj)$ where δij is the overlap between them. Two void spheres are considered to be sufficiently separated from each other if their relative overlap γij is smaller than a threshold value γth. Otherwise, the sub-domains containing them are considered to be interconnected and then are merged to form a new subdomain for which a new void sphere is identified. We iteratively identify every couple of interconnected subdomains and merge them until all the resulting void spheres are sufficiently separated from their neighbors. The threshold value γth for the above separation criterion can be chosen between 0.5 (partial separation according to Al-Raoush et al.) and 0 (complete separation according to Reboul et al.). Every couple of adjacent subdomains share a constriction that is composed of one or several triangular faces. The constriction size is defined as the diameter of the largest sphere that can pass through this constriction and is identified by a minimization procedure.

Figure 1 shows the pore diameter distribution (PSD) and the constriction diameter distribution (CSD) obtained with the proposed merging method, compared to that issued from the WDT. After the primary merging procedure (PM), the PSD et CSD are greatly shifted to the left. When the separation criterion with different threshold values γ_{th} is applied, the PSD and CSD continue to change; however they change slightly when $\gamma_{th} < 0.3$. It is interesting to note that this method allows us to impose a complete separation between the void spheres ($\gamma_{th} = 0$) without giving rise to subdomains having shape of flow paths.

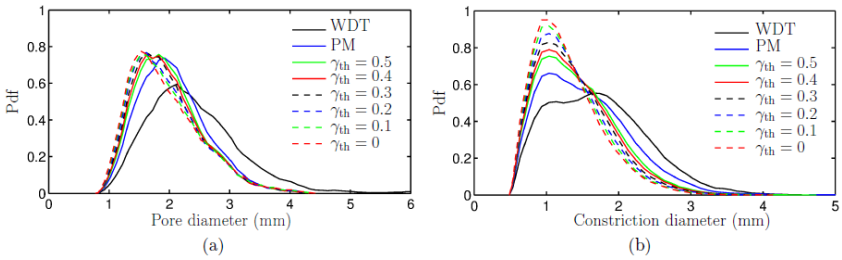

Figure 1. (a) Pore size distribution and (b) constriction size distribution obtained with the pro- posed merging method.

References

[1] Lafleur, J., Mlynarek, J. and Rollin, A.L., Filtration of broadly graded cohesionless soils. Journal of Geotechnical Engineering, 115(12), pp.1747–1768 (1989).

[2] Kenney, T.C., Chahal, R., Chiu, E., Ofoegbu, G.I., Omange, G.N. and Ume, C.A., Controlling constriction sizes of granular filters. Canadian Geotechnical Journal, 22(1), pp.32–43 (1985).

[3] Locke M, Indraratna B, Adikari G., Time-dependent particle transport through granular filters. Journal of Geotechnical Engineering, 127(6), pp.521–529 (2001).

[4] Shire, T. and O'Sullivan, C., A network model to assess base-filter combinations. Computers and Geotechnics, 84, pp.117-128 (2017).

[5] Al-Raoush, R., Thompson, K., Willson, C.S., Comparison of network generation techniques for unconsolidated porous media. Soil Science Society of America Journal 67(6), pp.1687–1700 (2003)

[6] Reboul N., Vincens E., Cambou B., A stastistical analysis of void size distribution in a simulated narrowly graded packing of spheres, Granular Matter, 10 (6), pp.45–468 (2008)

EWG-27 Description of the Pore Network in Granular Media Using the Delaunay Triangulation

Your Notes:

EWG-28 Application of Pore Network Models to Investigate Internal Erosion in Gap-Graded Soils

A. Sufian[1*]; C. Knight[1]; C. O'Sullivan[1]; B. van Wachem[2]; D. Dini[3]

[1]Department of Civil and Environmental Engineering, Imperial College London, United Kingdom.
[2]Chair of Mechanical Process Engineering, Otto-von-Guericke-Universit¨at Magdeburg, Magdeburg, Germany
[3]Department of Mechanical Engineering, Imperial College London, United Kingdom
[*]Corresponding Author (Email: a.sufian@imperial.ac.uk)

The migration of soil particles due to internal erosion is a complex process originating at the particle-scale. Understanding the fundamental mechanisms requires consideration of how an assembly of discrete particles interacts with a flowing fluid field. This is typically achieved by coupling the Discrete Element Method (DEM) to model individual particles with Computational Fluid Dynamics (CFD), which models fluid flow at the continuum. There are two main categories for CFD-DEM: (i) fully-resolved, and (ii) unresolved or coarse-grained.

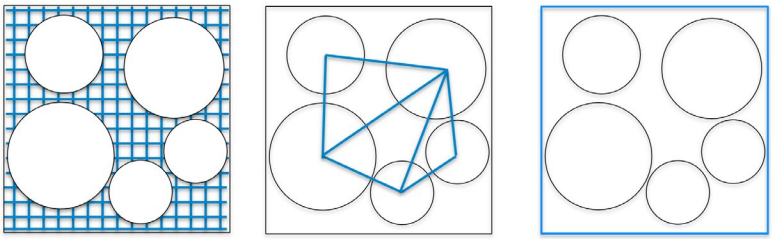

Figure 1: (Left) Sub-particle spatial resolution in fully-resolved CFD-DEM simulations; (Right) Fluid cell in an unresolved or coarse-grained CFD-DEM comprising several particles; (Middle) Fluid cells in the PNM which are at an intermediate length scale

In fully-resolved simulations, the fluid mesh has a sub-particle resolution, while in coarse-grained simulations each fluid mesh comprises several particles (Figure 1). Fully resolved simulations provide high resolution data in regards to the local flow and particle drag force, but at the cost of high computational resources and small sample sizes. In contrast, coarse-grained simulations can consider can consider large sample sizes but the ability to capture local behaviour is dependent on the fluid mesh size and empirical drag force expressions. This is particularly an issue with gap-graded soils which comprise coarse and fine particles with no intermediate sizes. The fluid mesh must be very small to perform fully resolved simulations, or there will be a large number of fine particles within each fluid mesh of the coarse-grained simulations and consequently local behaviour cannot be accurately captured.

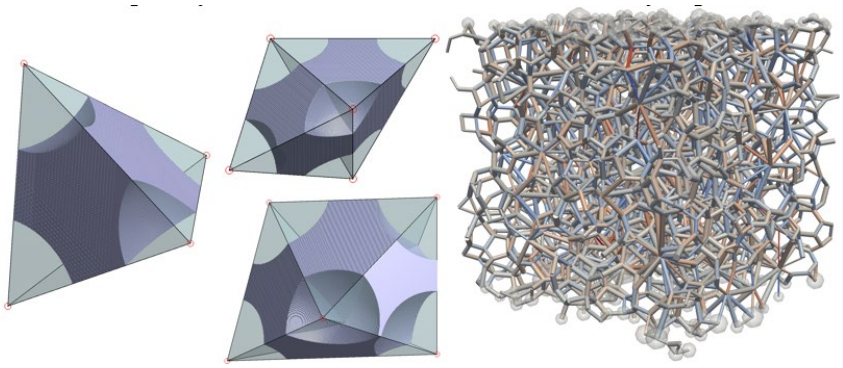

Figure 2: (Left) Examples of individual pores in the MDT where the faces of the polyhedral cells are the constrictions connecting pores; (Right) Network representation of the pore space.

An alternate approach is to employ Pore Network Models (PNM). PNM provides a network representation of the pore space, where individual pores are taken as nodes of the network and are connected by constrictions which are edges

of the network. In assemblies of spheres, this network representation is often achieved using Delaunay-based tessellation methods (Figure 2). Fluid flow is simulated in the network model using a Stokes flow algorithm which solves for continuity (conservation of mass) for each node in the network using a local conductivity model. The seepage induced drag forces can be obtained from the resulting flow field and geometric properties of the pores and constrictions.

PNM models fluid flow at an intermediate length-scale to fully resolved and coarse-grained CFD-DEM (Figure 1). While PNM is computationally efficient and can handle large sample sizes, there is a simplification of the pore space geometry and governing fluid equations. To better understand these assumptions, the local flow field and seepage induced drag obtained from PNM is compared to fully-resolved Immersed Boundary Method (IBM) simulations. The comparative study was conducted for a range of linear graded and bimodal samples. PNM were generated using a weighted Delaunay Tessellation (DT), along with the Modified Delaunay Tessellation (MDT) which considers the merging of tetrahedral Delaunay cells to provide a more physical representation of the pore space. Two local conductivity models were compared in simulating fluid flow in the PNM.

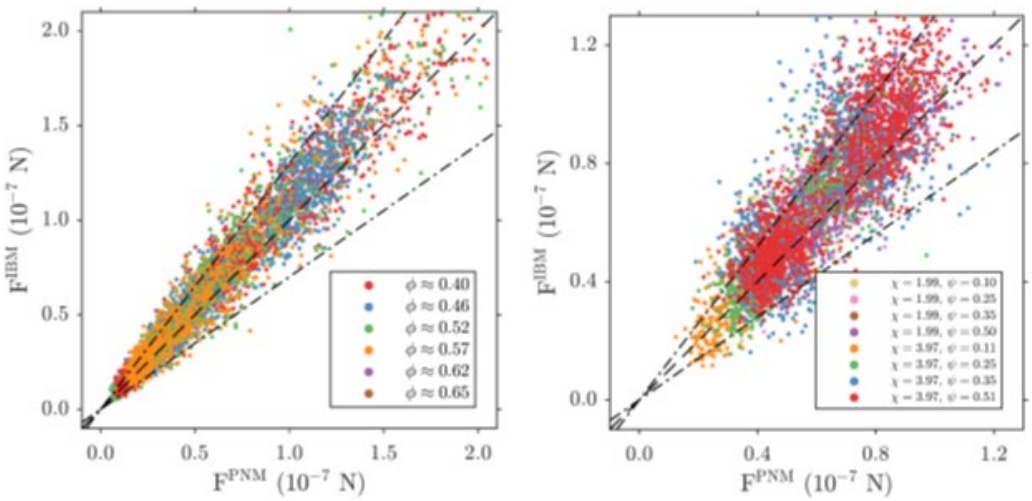

Figure 3: Comparison of the drag force obtained from the PNM and IBM simulations for the linear graded (left) and bimodal (right) sample.

The local pressure field was very accurately captured for both the linear and bimodal samples with Pearson correlation coefficients above 0.98. The local flow rate exhibited slightly more scatter and sensitivity to the choice of the local conductance model. PNM based on the MDT clearly provided a better correlation with the IBM. In addition, there was close similarity in the network shortest paths, indicating that the PNM captures dominant flow channels. Comparison of streamline profiles demonstrated that local pressure drops coincided with the pore constrictions. Following a rigorous validation of the drag force calculation, the comparison showed that linear graded samples were able to calculate the force with reasonable accuracy (Figure 3), while the bimodal samples exhibited slightly more scatter. This suggests that the PNM is a viable option to investigate the local behaviour of seepage induced migration of particles but further research is required to improve the accuracy of the method, and this is subject of ongoing research.

References

[1] Sufian A., Knight C., O'Sullivan C., van Wachem B., and Dini D. *Ability of a pore network model to predict fluid flow and drag in saturated granular materials*. Computers and Geotechnics 110, p.344-366 (2019).

[2] van der Linden J.H., Sufian A., Narsilio G.A., Russell A.R., and Tordesillas A. *A computational geometry approach to pore network construction for granular packings*. Computers and Geosciences 112, p.133-143 (2018).

[3] Sufian A., Russell A.R., Whittle A.J., and Saadatfar M. *Pore shapes, volume distribution and orientations in monodisperse granular assemblies*. Granular Matter 17(6), p.727-742 (2015).

EWG-28 Application of Pore Network Models to Investigate Internal Erosion in Gap-Graded Soils

Your Notes:

EWG-29 Factors that Determine Fluid Particle Interaction Forces in Dams and Flood Embankments

C. Knight; C. O'Sullivan; D. Dini; B. van Wachem

In saturated sand filters and transition zones in dams and flood embankments subject to seepage the relation between the fluid-particle interaction forces and the contact forces acting on individual grains determines the point at which internal erosion initiates. Understanding of the relationship between applied stresses, packing density, and particle size distribution has been advanced by use of discrete element method (DEM) simulations. The fluid-particle interaction forces are more difficult to establish. This contribution gives an overview of the challenges associated with determining these forces.

The first point to establish is that numerical simulations are essential in any general study of fluid- particle interaction. Useful experimental work has been carried out; for example Ergun (1952) considered the pressured drop across beds of particles and developed a drag expression by considering the Kozeny-Carmen equation. While the Ergun equation has been widely used it is based on an indirect approach to determining the fluid particle interaction force generated that relies on a number of hypotheses and approximations. More recently, use of transparent soil and particle tracking in experiments has the potential to advance understanding of the flow field, however measurement of the forces on the individual grains is intractable.

To accurately determine the force acting on the grains using a numerical model the flow in the void space must be resolved. This poses a particular problem for geomechanics applications as the particles are relatively tightly packed and the geometry of the void space close to the particle is highly complex. Options available include computational fluid dynamics (CFD) simulations using a fixed (Eulerian) regular Cartesian grid in conjunction with an immersed boundary method (IBM), CFD simulations using an unstructured body-fitted Eulerian mesh, or use of the Lattice Boltzman Method (LBM). The first step in adopting one of these methods is to validate the method, its implementation and understand the influence of grid resolution and model parameters on accuracy; the work of Zick & Homsy (1982) is very useful in this regard.

Knight (2018) considered the influence of particle size distribution (polydispersity) on the fluid-particle interaction force. He prepared isotropic virtual filter samples using DEM simulations and considered linear particle size distributions as well as bi-modal samples; representative samples are illustrated in Figure 1(a). Computational consideration restricted consideration to coefficients of uniformity (Cu)≤

2.5 for the linear-graded samples, while the maximum size ratio for the bimodal samples was 4. Permeameter test simulations were carried out without allowing the particles to move. The fluid flow was simulated using IBM simulations with a regular Cartesian grid; a limited number of simulations were carried out using a more complex body-fitted unstructured mesh to verify the results. The permeability values were compared with experimental data from Taylor (2016).

The IBM-derived data were used to explore the effectiveness of existing expressions to calculate the particle drag forces knowing the porosity and fluid velocity in a representative element of soil. Figure 1(a) shows that the variation in the total fluid particle interaction force, i.e. the sum of the forces on the individual particles in the sample is captured well by the existing expression proposed by Tenneti et al. (2011) which includes correction for polydispersity. However, as illustrated in Figure 1(b) the individual fluid-particle interaction forces are poorly predicted using this approach.

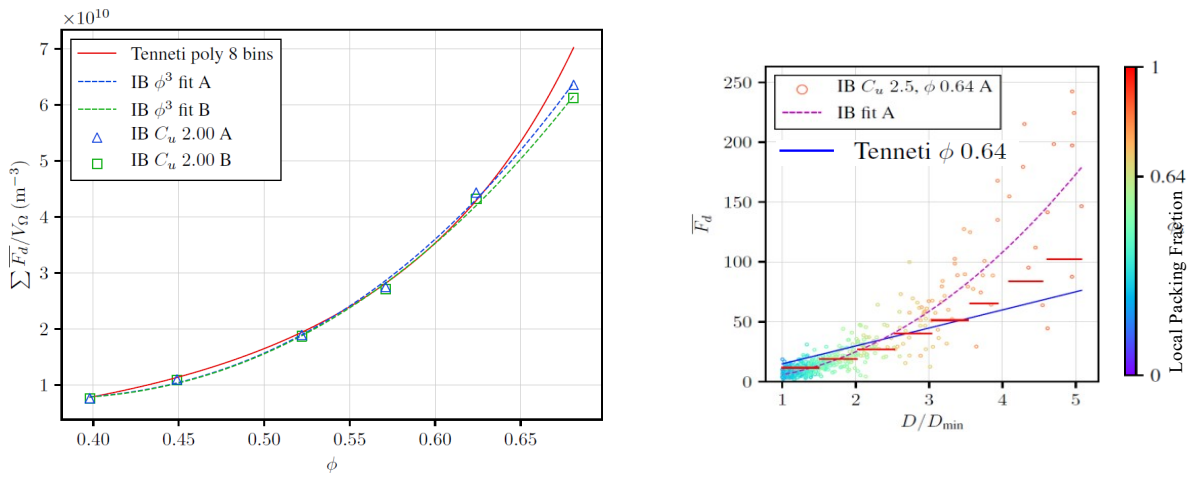

(a) Variation in total fluid-particle interaction force with packing density for samples with Cu=2.0

(b) Variation in fluid-particle interaction force with particle diameter for sample with Cu=2.5 and void ratio=0.553

Figure 1: Fluid particle interaction forces: comparison of IBM derived data and semi-empirical expression by Tenneti

Figure 1(b) illustrates a dependency between the local packing fraction of individual particles and the fluid-particle interaction force. Recognising this link, the drag expressions can be calculated using the local packing density, as calculated using a weighted sum of the volumes of the Voronoi cells surrounding each grain. As illustrated in Figure 2, this approach gives a significant improvement to the predictions of the individual fluid-particle interaction forces. This finding advances understanding of the factors that influence drag on individual sand grains in a saturated granular material subject to seepage flow as often occurs in embankment dams and flood embankments.

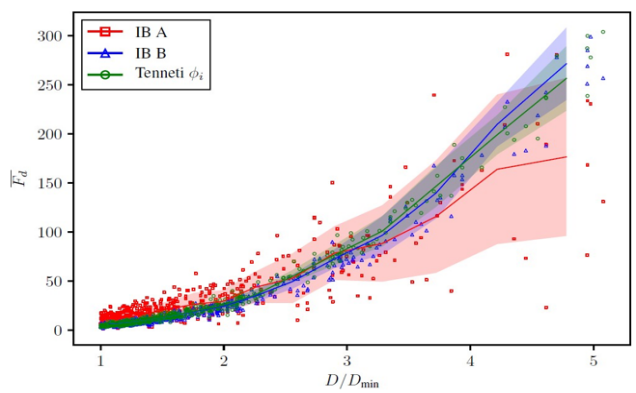

Figure 2: Fluid particle interaction force for sample with Cu=2.5 and void ratio of 0.427, Tenneti expression applied using local particle-scale packing fraction values.

References

Ergun, S., 1952. Fluid Flow Through Packed Columns. *Journal of Chemical Engineering Progress*, 48(2), pp.89–94.

Knight, C.S., 2018. *Fluid flow and drag in polydisperse granular materials subject to laminar seepage flow*. Imperial College London.

Taylor, H., 2016. *Assessing the potential for suffusion in sands using x-ray micro-CT images*. Imperial College London.

Tenneti, S., Garg, R. & Subramaniam, S., 2011. Drag law for monodisperse gas–solid systems using particle-resolved direct numerical simulation of flow past fixed assemblies of spheres. *International Journal of Multiphase Flow*, 37(9), pp.1072–1092.

Zick, A.A. & Homsy, G.M., 1982. Stokes flow through periodic arrays of spheres. *Journal of Fluid Mechanics*, 115(1), p.13.

EWG-29 Factors that Determine Fluid Particle Interaction Forces in Dams and Flood Embankments

Your Notes: